Response to Reviewer's comments

(Manuscript No. ACP-2019-752)

Reviewer #1

SO2 has been significantly reduced in recent years; therefore, the nitrate aerosols become more and more important in China. This study presented a long-time measurement (2016-2017) of water-soluble ions of PM2.5 in Yangtze River Delta (Nanjing), China. They found that the nitrate was a major faction of the PM2.5 mass. From their study, they found the nitrate was mostly produced by the N2O5 heterogeneous uptake under the NH4+-rich condition. This study suggests the studied region is located in HNO3-limit regime and thus the reduction of NOx may be more helpful to mitigate the PM pollution. The results could help the understanding of the heterogeneous formation of NO3- aerosol in East China. This paper is well written, the method is sound, and the results could be important for aerosol chemistry community. I recommend this paper may be published after the following comments be addressed.

1st comment

Line 48: reference is missing here.

Author's response:

As suggested, we have added a reference here (Huang et al., 2018) in the revised manuscript. (line 49 on page 2)

2nd comment

Lines 130-136: QA/QC (ion balance) should be provided.

Author's response:

The results of ion balance has been written in lines 205-211 and shown in Figure S2. Good correlations were found between cations and anions during the various sampling periods. The ratio of cation-to-anion was very close to 1.0 during each season, reflecting good quality of our data in this study.

3rd comment

Line 209: should provide more evidence

Author's response:

Thanks for the reviewer's comment. Previous studies showed that the build-up of nitrate concentrations at the urban site in the early morning was due to enhanced nitrate formation in the residual layer in the mixing troposphere (Baasandorj et al., 2017, ES&T; Prabhakar et al., 2017, ACP). To explain this point, chemical model simulations are needed. However, in this work, we mainly focused on explaining the particulate nitrate behaviors based on observations and we cannot provide more evidence to support the argument as mentioned above. Thus, we have removed the sentence of "The higher nitrate……in the mixing troposphere (Baasandorj et al., 2017; Prabhakar et al., 2017)." in the revised manuscript.

4th comment

Lines254-282: the criterion value should be explained in the very beginning.

Author's response:

Thanks for the reviewer's comment. The criterion value can be calculated as the absolute value of intercept dividing by the slope in each linear regression model. (lines 309-310 on page 12)

5th comment

Lines 328-333: are there any difference between day and night samples?

Author's response:

Thanks for the reviewer's comment. As suggested, we made correlation analysis of Fn vs. Ox and Fn vs. ALWC during the high $PM_{2.5}$ events for daytime and nighttime aerosol samples. The results showed that weak correlations between Fn and Ox were found in both daytime and nighttime. In contrast, Fn correlated very well with ALWC in both daytime and nighttime aerosol samples. This suggested that heterogeneous process played an important role in forming nitrate aerosols during both daytime and nighttime in the high $PM_{2.5}$ episodes. (line 388 on page 15, lines 389-394 on page 16 and Figure 7)

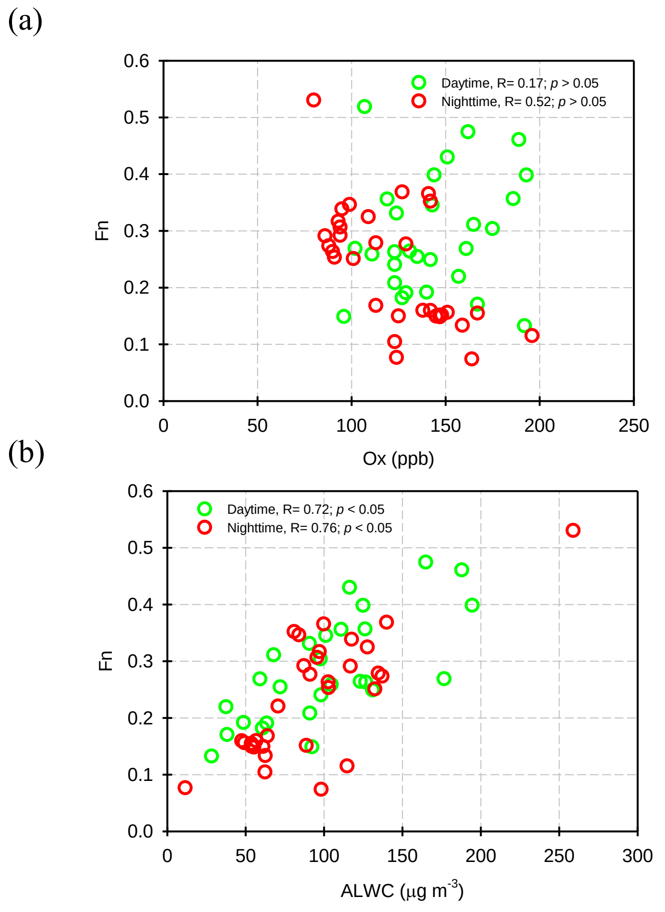

Figure 7 Scatter plots of (a) Fn against Ox and (b) Fn against ALWC in daytime and nighttime aerosol samples during the high hourly $PM_{2.5}$ concentration conditions (hourly $PM_{2.5} \geqq 150$ μg m^{-3}).

6th comment

Lines 360-378: I suggest comparing NO3 increase rate with those reported in other studies.

Author's response:

As suggested, we have compared the production rate of NO_3^- between this work and the previous studies. In this work, the average NO_3^- production rate due to heterogeneous process was 12.6 ± 7.3 % h^{-1} (4.1 ± 3.6 μg m^{-3} h^{-1}). Previous studies showed that heterogeneous process of nitrate formation exhibited rates of 14.4 % h^{-1} (file measurement) and 14.3 % h^{-1} (lab. work). Our value was in accordance with those of the literatures (Calvert and Stockwell, 1983, ES&T; Pathak et al., 2011, ACP). On the contrary, the average growth rate of NO_3^- by gas-oxidation process was 2.5 ± 0.1 % h^{-1} (0.8 ± 0.3 μg m^{-3} h^{-1}). This value was in line with that (2.4 % h^{-1}) in the subtropical polluted urban site where nitrate aerosols were mainly produced by gas-oxidation reaction (Lin et al., 2007). Moreover, we also found some cases in which the elevated NO_3^- might have been from both gas-phase and heterogeneous reactions, and the corresponding growth rate of $NO_3^-$was approximately 7.5 ± 3.0 % h^{-1} (2.5 ± 0.2 μg m^{-3} h^{-1}).(lines 432-440 on page 17 and lines 441-445 on page 18)

7th comment

Lines 388-390： I think the authors should present more details about the Eq2. How to get this equation?

Author's response:

Thanks for the reviewer's comment. In the revised manuscript, we have re-organized the section of "3.7 NH_3/HNO_3 limitation of nitrate aerosol formation". We used the ISORROPIA II model to evaluate whether control of NH_3 or HNO_3 (NO_x) is a better way to reduce particulate NO_3^- concentrations in Nanjing. ISORROPIA II is a thermodynamic equilibrium model which is built based on the Na^+ - Cl^- - Ca^{2+} - K^+ - Mg^{2+} - SO_4^{2-} - NH_4^+ - NO_3^- - H_2O aerosol system (lines 140-143 on page 6). The input of this model includes the concentrations of total ammonium (NH_3 + NH_4^+), total chloride (HCl + Cl^-), SO_4^{2-}, Na^+, K^+, Mg^{2+} and Ca^{2+} along with ambient T and RH. In addition to ALWC and pH, ISORROPIA II model can also fit the observed SIA species very well (lines 462-466 on page 18 and Figure S7). Thus, we used this model to predict the concentrations of particulate nitrate under different total nitrate and ammonium conditions (lines 469-491 on page 19) and we deleted Eq. 2 in the revised manuscript.

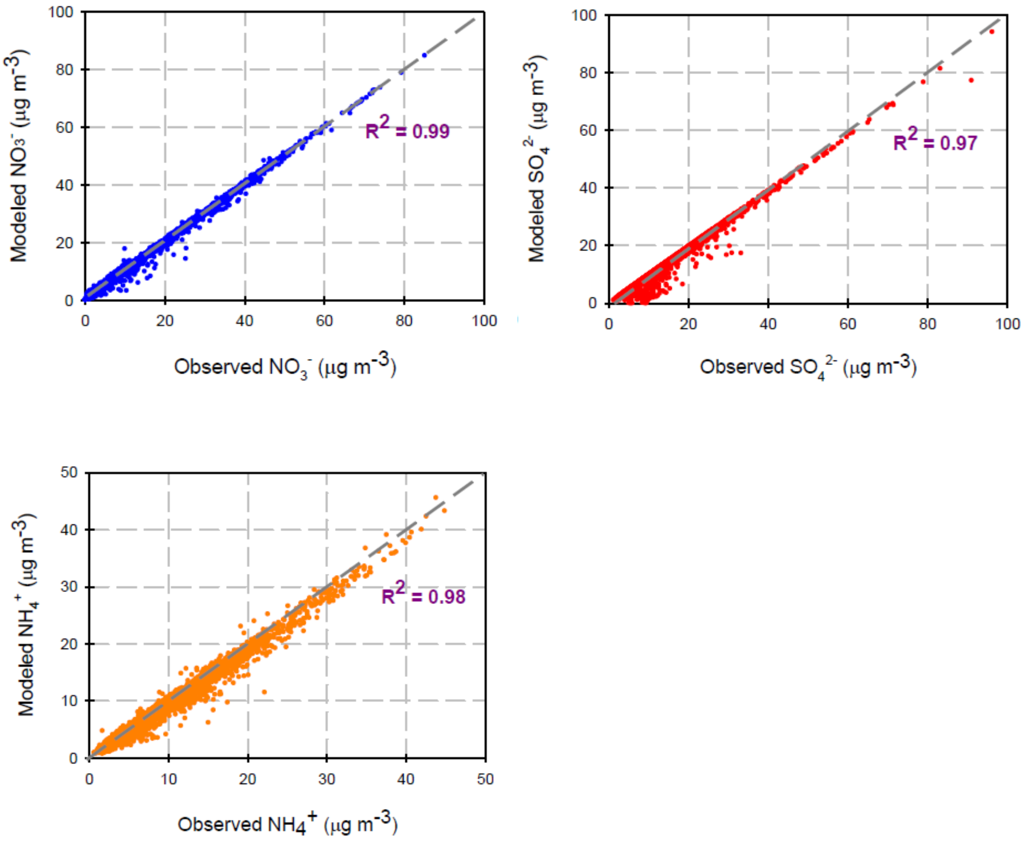

Figure S7 Scatter plots of modeled results vs. observations of NO_3^-, SO_4^{2-} and NH_4^+ in $PM_{2.5}$ in Nanjing during the sampling periods.

Reviewer #2

1st comment

This manuscript "Heterogeneous Formation of Particulate Nitrate under Ammonium rich Regime during the high PM2.5 events in Nanjing, China" by Lin et al. investigates the formation of nitrate under polluted conditions. The conclusion on the importance of the heterogeneous formation of nitrate is drawn from the good linear relationship between the nitrogen conversion ratios (Fn) and aerosol liquid water (ALW), in contrast to the poor correlation between nitrate and Ox. However, good linear relationship does not necessarily correspond to a causal relationship between the two variables. This is particularly true for the semi-volatile nitrate, the partitioning of which between gas and particle-phases is also associated with other factors such as temperature and RH. The morning peak of nitrate as reported in this manuscript (Fig. 4) could be caused by the photo-chemical production of nitrate after sun rise and the subsequent condensation on pre-existing particles before the temperature increases and RH decreases afterwards. Also, regional transport should be considered. In particular, the evaporation and re-condensation of nitrate during transport could also result in an increase of nitrate in the morning, coinciding with increase of ALW. Apart from the major issues mentioned above, there are several parts of the manuscript that need better interpretation or clarification as can be seen below.

Author's response:

Thanks for the reviewer's comment. In terms of this comment, we gave the responses as follows:

(1) Gas-phase oxidation (step1: $NO_{2(g)}+OH_{(g)} \rightarrow HNO_{3(g)}$, step2: $HNO_{3(g)} + NH_{3(g)} \rightarrow NH_4NO_{3(s,aq)}$) and heterogeneous reaction ($N_2O_{5(g)} + H_2O_{(g)} \rightarrow 2HNO_{3(aq)}$) are important mechanisms of particulate nitrate formation. In gas-phase oxidation, the reaction rate constant of step 1 is $2.4 \times 10^{-11} (T/300)^{-1.3}$, which depends on ambient temperature (T)

(Seinfeld and Pandis, 1998). Assuming the concentrations of NO_2 and OH are, respectively, 100 ppb and 10^6 molecules cm^{-3} (the typical values in the atmosphere in China), we then obtain the production rate of HNO_3 in a range of 4.5-5.2 ppb h^{-1} as the T is between 0°C (273°K) and 30°C (303°K) (see the figures in this response). However, assuming NO_2 concentration is 100 ppb and T is 25°C, we can find that the HNO_3 formation rate increased from 0.9 ppb h^{-1} (OH=2×10^5 molecules cm^{-3}) to 23.8 ppb h^{-1} (OH=8×10^6 molecules cm^{-3}). Obviously, OH seems to be the major factor affecting on HNO_3 production rather than T in step 1 in gas-phase oxidation reaction. In step 2, the production of nitrate particles is very sensitive to T and RH (Lin et al., 2007). For heterogeneous process, ALWC is an important factor to induce formation of liquid HNO_3 (Brown and Stutz, 2012, Chem. Soc. Rev.).

Without modeling and isotope techniques, the correlation analysis between nitrogen conversion ratio (Fn or nitrogen oxidation ratio, NOR) and other parameters (Ox, RH and ALWC) were commonly used to discuss whether gas-oxidation or heterogeneous process is a possible formation mechanism of particulate nitrate (Kohder, 2002, AE; Jansen et al., 2014, AE; Quan et al., 2015, AE). Fn is defined as the conversion ratio of NO_2 to HNO_3 (total nitrate in the text). As mentioned above, the conversion from NO_2 to HNO_3 is mainly influenced by OH, and ALWC. Therefore, we employed correlation analysis between Fn and Ox (proxy of OH) and ALWC to study the potential pathways of nitrate production; the result showed that Fn correlated well with ALWC. Apart from correlation analysis, we also selected twelve $PM_{2.5}$ episode cases to explore the variations of the concentrations of nitrate, Ox and ALWC. We found most of enhanced nitrate coincided with increasing ALWC and decreasing Ox. Thus, we concluded that heterogeneous process might be a major formation mechanism of nitrate formation in Nanjing during the high-$PM_{2.5}$ events (lines 382-388 on page 15, lines 389-394 on page 16, lines 399-414 on page 16, lines 415-440 on page 17 and lines

441-448 on page 18)..

(2)We agreed the reviewer's comment, that is, the partition of NH_4NO_3 (semi-volatile-nitrate) between gas- and particle-phase is very sensitive to T and RH. However, Fn means the formation ratio of NO_2 to total nitrate. In other words, Fn is used to evaluate the capability of NO_2 to HNO_3 prior forming nitrate particles. As mentioned above, Fn is mainly affected by OH and ALWC through different production processes. Consequently, we used the correlation analysis between Fn vs. Ox and Fn vs. ALWC to explore the formation mechanisms of HNO_3 (also reflected the pathway of nitrate aerosol formation).

(3)As our observed data, high nitrate concentrations were found between 3 a.m. and 7 a.m.. The high nitrate concentrations in the early morning might be caused by the nitrate formation via heterogeneous reaction in the dark, and gas-phase oxidation after sunrise and the subsequent condensation on pre-existing particles before the temperature increased and RH decreased afterwards. Moreover, the lower planet boundary layer (PBL) might be another reason for enhanced nitrate in the early morning. In the revised manuscript, we have rephrase the sentences in lines 239-244 on page 10.

(4) Regional transported air pollution would induce haze formation in China and is an important scientific issue. Nevertheless, it is very difficult to differentiate local and regional transported nitrate based on observations. The potential source contribution function (PSCF) is a method for identifying source region of air pollutants based on the HYSPLIT model. It is also commonly used to differentiate long-range transported air pollution from local air pollution based on observations combining with backward trajectories (Zhang et al., 2013, ACP; Hui et al., 2018, AE). The details of definition and calculation of PSCF are written in lines 158-179.. To compute PSCF, the 80 percentile value of nitrate concentration was selected as the "high nitrate pollution" threshold. The results showed that the hotspots (red color) of nitrate are shown in the

vicinity of Nanjing, suggesting that high nitrate pollution at the receptor site might not be contributed by long-range transported air pollution, but was likely contributed by local emissions (lines 275-284 on page 11 and lines 285-287 on page 12). In this work, the influences of ambient T, RH and long-range transported nitrate on Fn can be neglected (mentioned above). Consequently, we still used the correlation analysis between Fn and Ox (ALWC), and the variations of concentrations in NO_3^-, O_x and ALWC to investigate the formation mechanisms of particulate nitrate during the high $PM_{2.5}$ events.

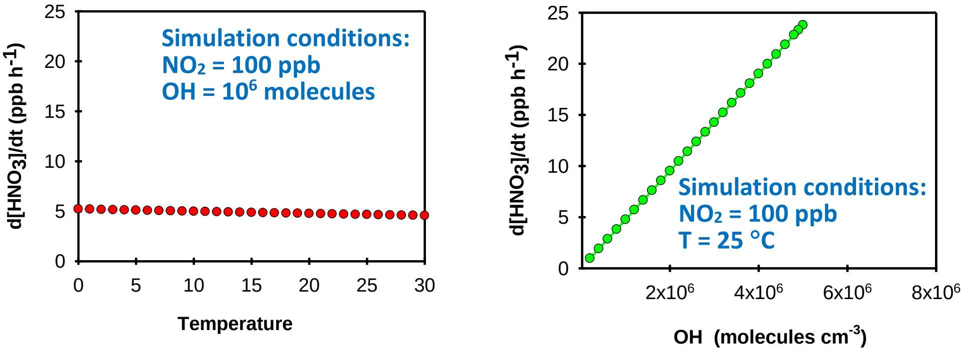

Figure The HNO_3 production rate of gas-oxidation depending on temperature and OH concentrations.

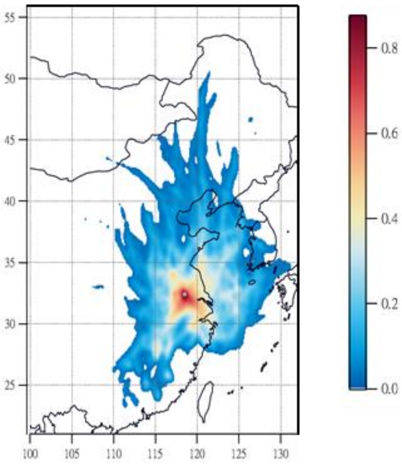

Figure 4 The PSCF maps of high nitrate pollution.

Specific comments:

2^{nd} comment

Line 33-35. What is the absolute production rate? Please provide both μg m^{-3} h^{-1} and % h-1.

Author's response:

As suggested, we have provided the production rate of particle nitrate in both units of μg m^{-3} h^{-1} and % h^{-1} in the revised manuscript. During the sampling periods, a total of twelve high $PM_{2.5}$ events were found. Seven episodes suggested that heterogeneous processes were the major pathway of nitrate formation and two episodes indicated that gas-oxidation was the dominant formation mechanism of nitrate. On average, the production rate of nitrate aerosols via heterogeneous reaction was 12.6 ± 7.3 % h^{-1} (4.1 ± 3.6 μg m^{-3} h^{-1}), which was 5 times higher than that by gas-oxidation reaction (2.5 ± 0.1 % h^{-1}, 0.8 ± 0.3 μg m^{-3} h^{-1}). (lines 34-36 on page 2, lines 448-450 on page 18 and Table S1)

3rd comment

Line 146-148. It is not clear what are the inputs for the ISORROPIA II model. Why use "forward" instead of "backward" mode? One should acknowledge the uncertainty of this model. Specifically, is organics causing uncertainty in the model?

Author's response:

Thanks for the reviewer's comment. ISORROPIA II is one of models to estimate aerosol liquid water content (ALWC) and has been widely used in many studies (Fountoukis and Nenes, 2007, ACP; Bian et al., 2014, ACP; Guo et al., 2015, ACP; Liu et al., 2017, GRL). The input of ISORROPIA II includes the concentrations of the observed total nitrate (HNO_3+NO_3^-), total ammonium (NH_3 + NH_4^+), total chloride (HCl + Cl^-), SO_4^{2-}, Na^+, K^+, Mg^{2+} and Ca^{2+} along with measured ambient T and RH.

Two modes, such as "forward" and "reverse", can be selected under the different input conditions. "forward" problem is always used when the quantity of ambient temperature and relative humidity along with the total concentrations (gas + aerosol) of NH_4^+, Cl^-, NO_3^-, and aerosol concentrations of SO_4^{2-}, Na^+, Ca^{2+}, K^+ and Mg^+ are known. On the contrary, ISORROPIA II also offers the ability to solve the "reverse problem", in which known quantities are the concentrations of NO_3^-, SO_4^{2-}, Cl^-, Na^+, NH_4^+, K^+, Mg^{2+} and Ca^{2+} in the aerosol phase together with ambient T and RH. In this work, we employed an online MAGAR instrument to monitored water-soluble inorganic ions in the aerosol phase and SO_2, HNO_3, HCl and NH_3 concentrations. We also obtained the data of ambient T and RH. Therefore, we selected the "forward" mode in ISORROPIA II model; the observed concentrations of total nitrate (HNO_3+NO_3^-), total ammonium (NH_3 + NH_4^+), total chloride (HCl + Cl^-), SO_4^{2-}, Na^+, K^+, Mg^{2+} and Ca^{2+} along with measured ambient T and RH served as input of this model (lines 143-155 on page 6 and line 156 on page 7). The earlier study suggested that ISORROPIA II model can fit ALWC very well with the uncertainty of 13-20 % (Fountoukis and Nenes, 2007, ACP; Bian et al., 2014, ACP; Guo et al., 2015, ACP; Liu et al., 2017, ACP). Organic aerosols are not taken into account in ISORROPIA II model and some organic species contribute water content in aerosols. According to the results by Bougiatioti et al. (2016, ACP), ALWC would be underestimate about 28 % without considering organic aerosols. (lines 143-148 on page 6)

4th comment

Line 179-180. Please provide correlation coefficient here.

Author's response:

The correlation coefficients between cation and anion were in a range of 0.98-0.99. As suggested, we have provided correlation coefficient in the revised manuscript. (lines

207-208 on page 9)

5th comment

Line 198-200. It is not clear how the theoretical equilibrium constants were derived? I saw large disagreement between the theoretical and observed values in every season in Fig. S3.

Author's response:

Thanks for the reviewer's comment. The reaction of $HNO_3 + NH_3$ is one of the pathway to produce particulate NH_4NO_3. In the reaction of $HNO_{3(g)} + NH_{3(g)} \rightarrow NH_4NO_{3(s,\ aq)}$, the theoretical equilibrium constant between gaseous HNO_3 and NH_3 and particle NH_4NO_3 (k_2 in the main text) can be calculated as (Mozurkewich, 1993, AE):

$$\ln(k_2) = 118.87 - \frac{24084}{T} - 6.025\ln(T)$$

where T is ambient temperature with a unit of °K. As the relative humidity (aw=RH/100) is greater than the deliquescence relative humidity of NH_4NO_3, the influence of RH on k_2 should be considered. Thus, k_2 should be replaced by k_2', namely:

$$k_2' = (P_1 - P_2(1-a_w) + P_3(1-a_w)^2) \times (1-a_w) \times (1-a_w)^{1.75} \times k_2$$

where

$$\ln(P_1) = -135.94 + \frac{8763}{T} + 19.12\ln(T)$$

$$\ln(P_2) = -122.65 + \frac{9969}{T} + 16.22\ln(T)$$

$$\ln(P_3) = -182.61 + \frac{13875}{T} + 24.46\ln(T)$$

Using an appropriate expression for the temperature and relative humidity dependence of NH_4NO_3 thermodynamic properties, the equilibrium constant can be calculated at a specific temperature and relative humidity. Apart from theoretical equilibrium constants, we also have observed equilibrium constants which were derived by the products of observed total nitrate (HNO_3 + NO_3^-) and total ammonium (NH_3 + NH_4^+). If the observed equilibrium constants were higher than the theoretical ones, indicating NH_4NO_3 would be produced (see in *supplementary S1*), otherwise the nitrate and ammonium should be partitioned into gas-phase. As shown in Figure S4b, most of the observed equilibrium constants were higher than the theoretical ones, suggesting that NH_4NO_3 was formed during the most sampling periods. However, the lower observed and higher theoretical equilibrium constants were found during the summer periods. This could partly explain the lower nitrate (or lower NH_4NO_3) concentrations during the hot seasons (lines 229-232 on page 9 and lines 233-235 on page 10).

6th comment

Line 266-268. Negative values of excess NH_4+ means deficit instead of excess. Please reword here.

Author's response:

As suggested, we have changed the sentence of "The results revealed that ………… and only 1 % of the excess-NH_4^+ data were lower than zero, reflecting…." to "The results revealed that ………… and only 1 % of data showed deficit-NH_4^+ conditions, reflecting….." in line 318 on page 13.

7th comment

Line 257-259. It is not clear how the criteria values were derived from the linear regression model. Is it the intercept or slope?

Author's response:

Thanks for the reviewer's comment. The criteria value can be calculated as the absolute value of intercept dividing by the slope in each linear regression model (He et al., 2012).

(lines 309-310 on page 12)

8th comment

Line 302-306. Why not correct for background values for the calculation of Fn. Background values could have a big effect on Fn, leading to large uncertainties. Also, the diffusion rate or the distribution of gas and particles are different.

Author's response:

Thanks for the reviewer's comment. Actually, Fn means nitrogen conversion ratio during each aerosol sampling duration time. Thus, we used the concentrations of NO_3^-, HNO_3 and NO_2 obtained in each sample to calculate the Fn values.

9th comment

Line 310-312. Please explain why they are comparable, and why higher than other sites rather than just comparison of values.

Author's response:

Thanks for the reviewer's comment. In this work, the conversion ratio of nitrogen (Fn) was 0.14, which was comparable to that (0.17) in Taichung city of Taiwan where both gas-oxidation and heterogeneous reaction were dominant formation mechanisms of atmospheric HNO_3 (or NO_3-). However, our Fn value was 2.3 time higher than that (0.06) in Dokki, Egypt (Khoder, 2002, AE). The reason of significant discrepancy of Fn between this work and that in Dokki was not clearly understood, but it might be attributed to different formation processes of HNO_3. In Dokki, gas-phase oxidation was the dominant pathway of HNO_3 production while heterogeneous process (R3) played an important role in HNO_3 formation in addition to gas-phase oxidation in Nanjing, especially during the high-$PM_{2.5}$ events. The production rate of HNO_3 by heterogeneous process was much higher than that by gas-phase oxidation. Consequently, the Fn value was much higher in this study (lines 360-362 on page 14 and lines 363-371 on page 15).   .

10th comment

Line 318-319. You are saying nitrate was totally formed from gas phase reaction during the day-time. Then, where does nitrate go during the night? It disappears or is transported to downwind sites? If transported, then, the nitrate transported form your upwind site could reach your sampling site in the evening?

Author's response:

Thanks for the reviewer's comment. In this sentence, the total nitrate does not mean nitrate concentration, but means the concentrations of "total nitrate" ($HNO_3 + NO_3^-$). In the atmosphere, gas-phase oxidation ($NO_{2(g)} + OH_{(g)} \rightarrow HNO_{3(g)}$) and heterogeneous process ($N_2O_{5(g)} + H_2O_{(aq)} \rightarrow 2HNO_{3(aq)}$) are potential pathways of HNO_3 formation (Here, the HNO_3 means the nitric acid before forming nitrate and is also called total nitrate in this work). The product, HNO_3, would then reacts with NH_3 (or would be neutralized by NH_4^+) to produce NH_4NO_3 aerosols. In this work, we used correlation analysis between Fn (nitrogen conversion ratio), Ox and ALWC together with cases studies to discuss weather gas-phase oxidation or heterogeneous process was a major formation mechanism of particulate nitrate during the high $PM_{2.5}$ levels. The equation of Fn can be expressed as:

$$F_n = \frac{GNO_3^- + PNO_3^-}{GNO_3^- + PNO_3 + NO_2}$$

As seen, the numerator of Fn is the concentrations of total nitrate. The denominator is the total NO_2 concentrations. The results showed that there were two peaks of Fn. In the first peak, the elevated Fn coincided with increasing ALWC, suggesting heterogeneous reaction since ALWC is one of the key parameters to accelerate the transformation of N_2O_5 to liquid HNO_3. On the contrary, a second peak of Fn was found in the early afternoon when Ox (Ox = $NO_2 + O_3$, an index of the oxidation capacity) concentrations increased, but ALWC decreased. This suggested that the HNO_3 formation might be mainly associated with the gas-phase reaction of NO_2 + OH during the daytime. To avoid misunderstanding for the reader, we have changed "total nitrate " to "HNO_3" in line 379 on page 15 in the revised manuscript.

11th comment

Line 329-331. You mentioned that nitrate could be formed through gas-phase processes. Here, you are saying it is not from gas-phase reactions because of poor linear correlation between Fn and Ox.

Author's response:

Thanks for the reviewer's comment. Both gas-phase oxidation process and heterogeneous reaction are potential formation mechanisms of particulate nitrate. In this work, the good correlation between Fn and ALWC (R = 0.72 and 0.76, $p < 0.05$) in the high $PM_{2.5}$ events. On the contrary, no correlation between Fn and Ox was found under the high $PM_{2.5}$ conditions. Thus, nitrate formation during the high-$PM_{2.5}$ events in Nanjing was likely attributed to heterogeneous reactions rather than gas-phase processes. (lines 388 on page 15 and lines 389-394 on page 16)

12th comment

Line 364-366. It is not clear how to get 70%. What are the absolute values of growth rate here, and in other cases?

Author's comment

During the sampling periods, a total of twelve high $PM_{2.5}$ events were found. The significant enhancements of NO_3^- were observed during all the $PM_{2.5}$ episodes. Seven episodes suggested that heterogeneous process ($N_2O_5 + H_2O$) might be a major pathway for nitrate formation since elevated NO_3^- levels coincided with increasing AWLC and decreasing Ox (or Ox remaining at a constant level). In the heterogeneous-process cases, five of them (Case III, Case IX, Case X, Case XI and Case XII in Table S1) were observed during the nighttime (17:00 – 6:00 on the next day), suggesting that approximately 70 % heterogeneous reaction was observed in the dark (lines 428-432 on page 17). Moreover, the growth rate of nitrate of each high $PM_{2.5}$ case is listed in Table S1. As seen, the growth rate of nitrate was from 2.4 to 26.7 % h^{-1}. On average, the production rate of NO_3^- (12.6 % h^{-1}) by heterogeneous processes was 5 times higher than that (2.5 % h^{-1}) of gas-oxidation reactions. This might explain the abrupt increase of nitrate concentrations during the high $PM_{2.5}$ events (lines 448-451 on page 18).

13th comment

Line384-385. You are assuming HNO_3+NH_3 is the major pathway, but in previous part and in Table S1. Night time N_2O_5+H_2O is the major pathway.

Author's comment

Thanks for the reviewer's comment. In the revised manuscript, we have re-organized the section of "3.7 NH_3/HNO_3 limitation of nitrate aerosol formation". We used the ISORROPIA II model to evaluate whether control NH_3 or HNO_3 (NO_x) is a better way to reduce particulate NO_3^- concentrations in Nanjing since ISORROPIA II model can predict the concentrations of NO_3^-, SO_4^{2-} and NH_4^+ very well (R^2=0.97-0.99 with all slopes of approximately 1.0) under thermodynamic equilibrium in aerosol system (lines 462-466 on page 18, lines 467-468 on page 19 and Figure S7). In this work, we used this model to calculate concentrations of particulate nitrate depending on various total nitrate and total ammonium concentrations under high- and low-sulfate concentrations.

The results showed that nitrate aerosol formation in Nanjing during the high $PM_{2.5}$ events was HNO_3-limited. This also reflected that control NOx emissions can reduce particulate nitrate concentrations. (lines 481-491 on page 19 and Figure 9)

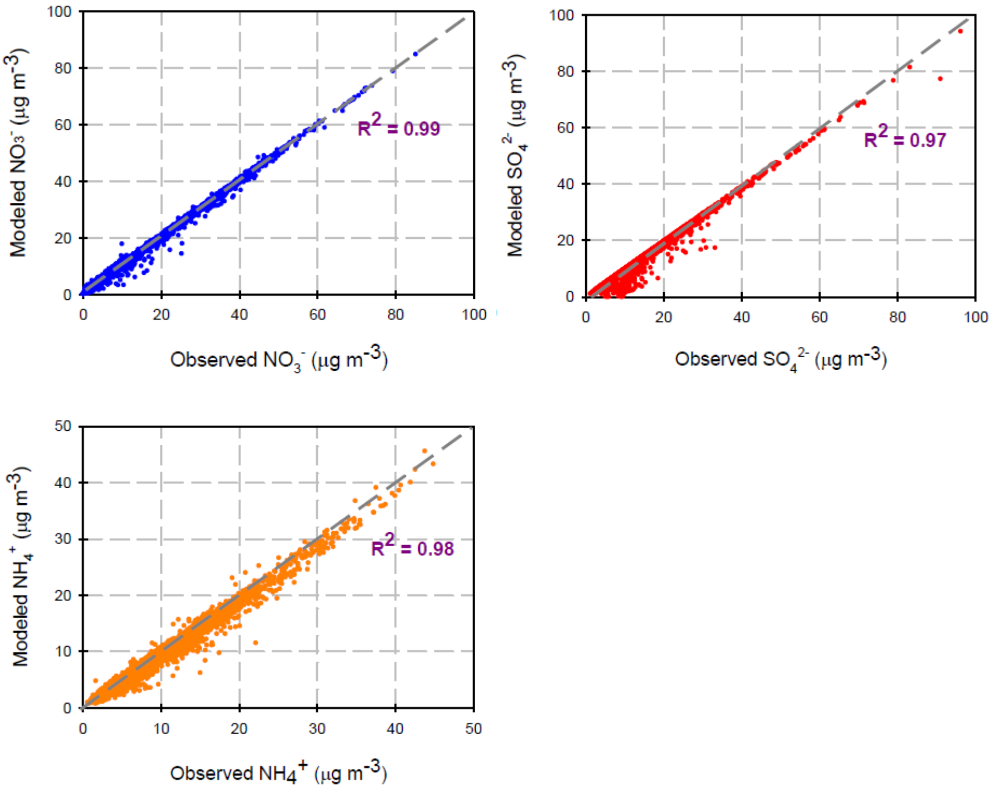

Figure S7 Scatter plots of simulated concentrations of NO_3^-, SO_4^{2-} and NH_4^+ against observed ones in Nanjing during the sampling periods.

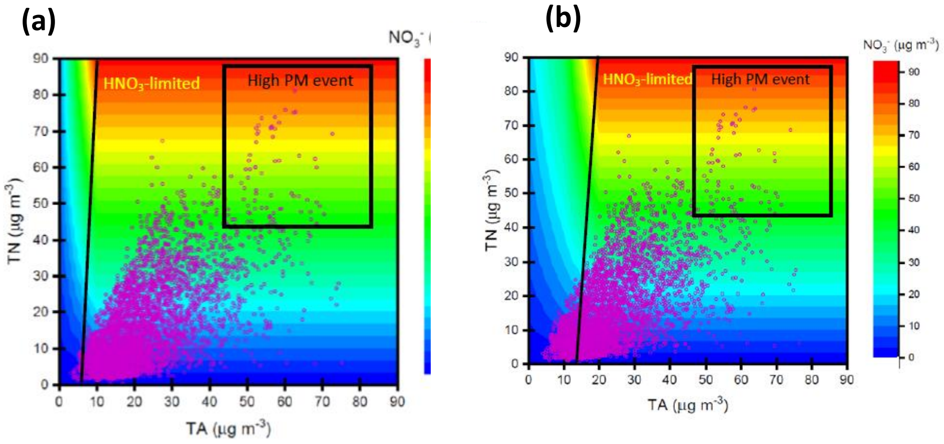

Figure 9 Nitrate concentrations simulated by ISORROPIA II model depending on TA and TN concentrations under (a) SO_42^- = 10 µg m^{-3} and (b) SO_4^{2-} = 60 µg m^{-3}.

14th comment

Figure 1. please provide better resolution. Also, the color bar has repeated 102, and Figure 1 is not discussed in the main text. If the goal of Fig. 1 is to show the location of the sampling site, it should be in supplementary.

Author’s response:

Thanks for the reviewer’s comment. In the revised manuscript, we have replaced the new figure with a better resolution. However, this figure only shows the relative location of the sampling site and therefore we move this figure to the supplementary (Figure S1).

15th comment

Figure 2. Please provide year on the x-axis. Also indicate season and the cases you selected in Table S1 and Fig. 8.

Author’s response:

As suggested, we have provide year on the x-axis in “new Figure 1” . Also, we have indicated the season and used shadows to pointed out the cases we selected in Table S1 and Fig. 8 in the revised manuscript.

Heterogeneous Formation of Particulate Nitrate under Ammonium-rich Regime during the High $PM_{2.5}$ Events in Nanjing, China

Yu-Chi Lin[1,2,3], Yan-Lin Zhang[1,2,3*], Mei-Yi Fan[1,2,3], Mengying Bao[1,2,3]

[1.] Yale-NUIST Center on Atmospheric Environment, International Joint Laboratory on Climate and Environment Change, Nanjing University of Information Science and Technology, Nanjing, 210044, China.

[2.] Key Laboratory Meteorological Disaster; Ministry of Education & Collaborative Innovation Center on Forecast and Evaluation of Meteorological Disaster, Nanjing University of Information Science and Technology, Nanjing, 210044, China.

[3]. Jiangsu Provincial Key Laboratory of Agricultural Meteorology, College of Applied Meteorology, Nanjing University of Information Science & Technology, Nanjing 210044, China.

Corresponded to Yan-Lin Zhang (dryanlinzhang@outlook.com; zhangyanlin@nuist.edu.cn)

ABSTRACT

Particulate nitrate (NO_3^-) not only influences regional climates but also contributes to the acidification of terrestrial and aquatic ecosystems. In 2016 and 2017, four intensive online measurements of water-soluble ions in $PM_{2.5}$ were conducted in Nanjing City to investigate the potential formation mechanisms of particulate nitrate. During the sampling periods, NO_3^- was the most predominant species, accounting for 35 % of the total water-soluble inorganic ions, followed by SO_4^{2-} (33 %) and NH_4^+ (24 %). Significant enhancements of nitrate aerosols in terms of both absolute concentrations and relative abundances suggested that NO_3^- was a major contributing species to high-$PM_{2.5}$ events (hourly $PM_{2.5} \geqq 150$ μg m^{-3}). High NO_3^- concentrations mainly occurred under NH_4^+-rich conditions, implying that the formation of nitrate aerosols in Nanjing involved NH_3. During the high-$PM_{2.5}$ events, the nitrogen conversion ratios (Fn) were positively correlated with the aerosol liquid water content (ALWC, $R > 0.72$, $p < 0.05$). Meanwhile, increasing NO_3^- concentrations regularly coincided with increasing ALWC and decreasing Ox (Ox = O_3 +NO_2). These results suggested that the heterogeneous reaction was probably a major mechanism of nitrate formation during the high-$PM_{2.5}$ events. Moreover, the average production rate of NO_3^- by heterogeneous processes was estimated to be 12.6 % h^{-1} (4.1 μg m^{-3} h^{-1}), which was much higher than that (2.5 % h^{-1}, 0.8 μg m^{-3} h^{-1}) of gas-phase reactions. This can also explain the abrupt increase of nitrate concentrations during the high $PM_{2.5}$ events. Utilization of ISORROPIA II model, we found that nitrate aerosol formation in Nanjing during the high-$PM_{2.5}$ events was HNO_3-limited. This indicated that the control of NOx emissions will be able to efficiently reduce airborne nitrate concentrations and improve the air quality in this industrial city.

Keywords: Nitrate aerosols, nitrogen conversion ratios, NH_4^+-rich regime, Hydrolysis of N_2O_5, Nitrate production rate

1. Introduction

Due to the rapid growth of industrialization and urbanization, particulate matter (PM) pollution has become a severe problem in China in recent years (Chan and Yao, 2008; Zhang and Cao, 2015). Fine mode particles ($PM_{2.5}$, with aerodynamic diameters less than 2.5 μm) exhibit smaller sizes and contain many toxins emitted from anthropogenic emissions (Huang et al., 2018). $PM_{2.5}$ easily penetrates the upper respiratory tract and is deposited into the human body, causing serious threats to human health. Numerous previous studies have proven that people exposed to high

$PM_{2.5}$ concentrations show increased risks of respiratory illness, cardiovascular diseases and asthma (Brauer et al., 2002; Defino et al., 2005), resulting in an increase of mortality (Nel, 2005).

Secondary inorganic aerosols (SIA), including sulfate (SO_4^{2-}), nitrate (NO_3^-) and ammonium (NH_4^+), are major constituents of $PM_{2.5}$, accounting for 25 - 60 % of the $PM_{2.5}$ mass in urban cities of China (Huang et al.,2014a; Wang et al., 2018; Yang et al., 2005; Ye et al., 2017; Zhao et al., 2013; Zhou et al., 2018). Among these species, SO_4^{2-} and NO_3^- are acidic ions which tend to be neutralized by NH_4^+. Previously, many studies suggested that SO_4^{2-} dominated SIA in urban cities of China (Kong et al., 2014; Tao et al., 2016; Yang et al., 2005; Yao et al., 2002; Zhao et al., 2013). In recent years, the Chinese government reduced its anthropogenic emissions by 62 % and 17 % for SO_2 and NOx, respectively (Zheng et al., 2018). This revealed that the reduction efficiency of SO_2 emissions were much higher than those of NOx. Consequently, nitrate has become the dominant species of SIA, especially during PM haze events (Wang et al., 2018; Wen et al., 2015; Zou et al., 2018).

In the atmosphere, ammonium nitrate (NH_4NO_3) is a major form of nitrate aerosols in fine mode particles. NH_4NO_3 is a semi-volatile species which partitions from the particle phase into the gas phase under high-temperature (T) conditions. It deliquesces when the ambient relative humidity (RH) is higher than its deliquescence relative humidity (DRH, nearly 62 % RH at atmospheric standard condition). To produce NH_4NO_3, nitrogen oxides (NO_x) and ammonia (NH_3) undergo a series of chemical reactions. NO_x mostly emits as fresh NO, which is subsequently oxidized to NO_2 and reacts with hydroxyl (OH) radicals to generate nitric acid (HNO_3), and then HNO_3 reacts with NH_3 to yield NH_4NO_3 particles as listed in R1 and R2 (Calvert and Stockwell, 1983). Particulate NH_4NO_3 formation rate is profoundly dependent on the ambient T and RH since both parameters influence the equilibrium constant of NO_3^-

and NH_4^+ between the particle and gas phases, as listed in R2 (Lin and Cheng, 2007).

$$NO_{2(g)} + OH_{(g)} \rightarrow HNO_{3(g)} \qquad k_1 \qquad (R1)$$

$$HNO_{3(g)} + NH_{3(g)} \rightarrow NH_4NO_{3(s,\ aq)} \qquad k_2 \qquad (R2)$$

Here, k_1 and k_2 are the reaction rate and equilibrium constant of R1 and R2, respectively. The equilibrium constant k_2 can be expressed as the product of HNO_3 and NH_3.

Heterogeneous reactions have been considered an important mechanism of nitrate formation during the nighttime. As listed in R3, liquid HNO_3 is produced by the hydrolysis of dinitrogen pentoxide (N_2O_5) on aerosol surfaces (Brown & Stutz, 2012; Chang et al., 2011; Mental et al., 1999; Wahner et al., 1998). Liquid HNO_3 can be neutralized by NH_4^+, which is produced from the conversion of gaseous NH_3. Nitrate aerosols yielded from both R2 and R3 require NH_3, and we can therefore consider these processes of NO_3^- formation to occur under NH_4 -rich conditions. Sometimes, there is not enough NH_3 (NH_4^+) to react (to be neutralized) with HNO_3 (NO_3^-) after complete neutralization by H_2SO_4. Under this condition, HNO_3 tends to react (or to be neutralized) with other alkaline species such as Ca-rich dust ($CaCO_3$), and subsequently, nitrate aerosol is produced under a NH_4^+-poor regime (Goodman et al., 2000).

$$N_2O_{5(g)} + H_2O_{(l)} \rightarrow 2HNO_{3(aq)} \qquad (R3)$$

The Yangtze River Delta (YRD) region is one of the well-known polluted areas in China (Zhang and Cao, 2015). Different from the case of dramatic elevated sulfate aerosol levels in Beijing (Wang et al., 2016), nitrate aerosols seemed to be a major contributing species during haze days in the YRD region (Wang et al., 2015; Wang et al., 2018). The formation mechanisms of nitrate in Nanjing have not yet been well understood, especially during high PM events. In this study, four intensive online measurements of water-soluble ions in $PM_{2.5}$ were conducted in Nanjing City in 2016 and 2017. The data provided information on the hourly evolution of water-soluble inorganic ions (WSIIs) in the industrial city. The NO_3^- distributions under different NH_4^+ regimes (NH_4^+-poor and NH_4^+-rich conditions) were also discussed. Finally, we investigated the potential formation mechanisms of nitrate aerosols and their production rates during high-$PM_{2.5}$ events based on the online measurements.

2. Methodology

2.1 Sampling site

Particulate WSIIs and inorganic gases were continuously monitored at Nanjing University of Information Science and Technology (NUIST) located in the northern part of Nanjing City (see Figure S1). In addition to the contributions from vehicle emissions, petroleum chemical refineries and steel manufacturing plants are situated in the northeast and east direction at a distance of approximately 5 km. Four intensive campaigns were conducted from March 2016 to August 2017. During each experiment, the hourly concentrations of WSIIs in $PM_{2.5}$ and inorganic gases were continuously observed. Meanwhile, the hourly $PM_{2.5}$, NO_2 and O_3 concentrations along with the ambient T and RH were acquired from the Pukou air quality monitoring station which is located to the southwest of the receptor site.

2.2 Instruments

To monitor the hourly concentrations of WSIIs (Cl^-, NO_3^-, SO_4^{2-}, Na^+, NH_4^+, K^+, Mg^{2+} and Ca^{2+}), an online Monitor for Aerosols and Gases (MAGAR, Applikon-ENC, The Netherlands) instrument with a $PM_{2.5}$ inlet was employed. Using this instrument, the WSIIs in $PM_{2.5}$ were collected by a stream jet aerosol collector, while acidic (HCl, HONO, HNO_3 and SO_2) and basic gases (NH_3) were dissolved in a hydrogen peroxide solution on a wet rotation denuder (ten Brink et al., 2007; Griffith, et al., 2015). The liquid samples were then collected with syringe pumps and analyzed by ion chromatography (IC). Before each campaign, a seven-point calibration curve of each species was made, and an internal standard solution (LiBr) was used to check instrumental drifts. The method detection limits (MDLs) of Cl^-, NO_3^-, SO_4^{2-}, Na^+, NH_4^+, K^+, Mg^{2+} and Ca^{2+} were, 0.01, 0.04, 0.06, 0.05, 0.05, 0.07, 0.05 and 0.11 μg m^{-3}, respectively. For gases, the MDLs were 0.07, 0.09, 0.06, 0.02 and 0.08 μg m^{-3} for HCl, HONO, HNO_3, SO_2 and NH_3, respectively.

2.3 ISORROPIA-II model

In this work**,** we used the ISORROPIA-II model to calculate the aerosol liquid water content (ALWC). ISORROPIA II is a thermodynamic equilibrium model which is built based on the $Na^+ - Cl^- - Ca^{2+} - K^+ - Mg^{2+} - SO_4^{2-} - NH_4^+ - NO_3^- - H_2O$ aerosol system (Fountoukis & Nenes, 2007). This model has been successfully used to estimate the liquid water content in aerosols with uncertainty of ~ 20 % compared to the observed ALWC (Bian et al., 2014; Guo et al., 2015; Liu et al., 2017). This underestimation might be due to the missed species in ISORROPIA II, organic aerosols, , which contributed approximately 27 % of the total ALWC (Bougiatioti et al., 2007). Here, the model was computed as a “forward problem”, in which the quantities of aerosol- and gas-phase compositions along with the T and RH were well known. Additionally, the modeled values were determined using the “metastable” mode, which indicated that the aerosol compositions were assumed to be composed of an aqueous solution (Liu et al., 2017). The details of this model can be found elsewhere (Fountoukis and Nenes, 2007). In this work, the observed concentrations of total nitrate (HNO_3+NO_3^-), total ammonium (NH_3 + NH_4^+), total chloride (HCl + Cl-), SO_4^{2-}, Na^+, K^+, Mg^{2+} and Ca^{2+} along with measured ambient T and RH served as input of ISORROPIA II model.

2.4 Potential source contribution function

Potential source contribution function (PSCF) is a method to identify the potential source regions of air pollutants. It has also been widely used to differentiate local emission from long-range transported pollution (Zhang et al., 2013; Hui et al., 2018) based on the trajectory analysis calculated from GDAS (Global Data Assimilation System), which processed by the National Centers for Environmental Prediction (NCEP). The zone of concern is divided into $i \times j$ small equal grid cells and then PSCF in the *i-jth* cell ($PSCF_{ij}$) can be defined as (Polissar et al., 1999):

$$PSCF_{ij} = \frac{m_{ij}}{n_{ij}} \quad (1)$$

where m_{ij} is the number of "high nitrate pollution" trajectory endpoints in the *i-jth* cell and n_{ij} is the total number of trajectory endpoints fallen into the *i-jth* cell. In this study, the 80th percentile value of nitrate concentration was treated as "high nitrate pollution" threshold. To reduce the uncertainty caused by the small values of n_{ij}, the weighting function of W_{ij} has to be considered (Polissar et al., 1999):

$$W_{ij} = \left\{ \begin{array}{l} 1.00;\ 80 < n_{ij} \\ 0.70;\ 20 < n_{ij} \leqq 80 \\ 0.42;\ 10 < n_{ij} \leqq 20 \\ 0.05;\ n_{ij} \leqq 10 \end{array} \right\}$$

In this study, the domain of the study area was in a range of 20-55 °N and 105-135 °E; the resolution of grid cell was 0.5°×0.5°.

3. Results and discussion

3.1 Overview of water-soluble inorganic ions

Four intensive online measurements of WSIIs in $PM_{2.5}$ were carried out in Nanjing City from March 2016 to August 2017. Figure 1a plots the time series of the hourly $PM_{2.5}$ mass concentrations during the sampling periods. As seen, the hourly $PM_{2.5}$ mass concentrations varied from 5 to 252 μg m^{-3} with a mean value of 58 ± 35 μg m^{-3}. Compared with the 24-hour guideline (25 μg m^{-3}) suggested by the World Health Organization (WHO), our average $PM_{2.5}$ concentration (58 μg m^{-3}) was 2.3 times higher. This indicated that PM pollution in Nanjing City was a serious problem. During the campaigns, several high-$PM_{2.5}$ events with hourly $PM_{2.5}$ concentrations of higher than 150 μg m^{-3} were observed in the springtime and wintertime. These high $PM_{2.5}$ levels lasted for more than 3 hours, with obviously elevated NO_3^-. The details of nitrate formation during the high-$PM_{2.5}$ hours will be discussed in the following sections.

Figure 1b shows the time series of the hourly concentrations of SIA species, including SO_4^{2-}, NO_3^- and NH_4^+. The lack of data from March 7 to 14, 2016 was due to a malfunction of the MARGA instrument. During the sampling periods, the NO_3^- concentrations varied from 0.1 to 85.1 μg m^{-3} with a mean value of 16.7 ± 12.8 μg m^{-3}. The SO_4^{2-} concentrations ranged from 1.7 to 96.2 μg m^{-3} and averaged 14.9 ± 9.1 μg m^{-3}. The NH_4^+ concentrations fluctuated between 0.8 and 44.9 μg m^{-3} with a mean value of 10.7 ± 6.7 μg m^{-3}. On average, SIA accounted for 91 % of the total water-soluble inorganic ions (TWSIIs) during the entirety of the sampling periods (see Figure 2a). Among these species, NO_3^- accounted for 35 % of the TWSIIs, followed by SO_4^{2-} (33 %) and NH_4^+ (24 %). The abundances of other ions, including Cl^-, K^+, Ca^{2+}, Na^+ and Mg^{2+}, were 5, 2, 1, 0.7 and 0.3 %, respectively. Figure S2 shows the scatter plot of the equivalent concentrations of the cations (Na^+, NH_4^+, K^+, Mg^{2+} and

Ca^{2+}) and anions (Cl^-, SO_4^{2-} and NH_4^+). As seen, good correlations (R = 0.98 -0.99, with a significance level $p<0.05$) between cations and anions were found during the various sampling periods. The ratio of cation-to-anion was very close to 1.0 during each season, reflecting an ionic balance. This also indicated that our data exhibited good quality and was able to be used for the further analysis of scientific issues.

All SIA species exhibited similar seasonal patterns, with lower concentrations in the summer, especially for NO_3^-. The average concentrations of nitrate were 6.7 and 5.7 μg m^{-3} in the summertime of 2016 and 2017, respectively (see Figure S3). These values were much lower than those observed during other seasons. The local meteorological conditions, which were favorable for the dilution of air pollution, were one of the reasons for the declined NO_3^- concentrations during the hot seasons (Zhang and Cao, 2015). Another important reason for this effect was attributed to the formation process of $PM_{2.5}$ nitrate, which is very sensitive to the ambient T and RH (Lin and Cheng, 2007). Figure S4a depicts the theoretical equilibrium constants of partitioned NO_3^- and NH_4^+ between the particle and gas phase ($HNO_{3(g)} + NH_{3(g)} \rightarrow NH_4NO_{3(s,\, aq)}$ as seen in R2) under different T and RH conditions. The details of calculation approach of the theoretical equilibrium constants are described in *Supplementary S1*. Note that the *Y-axis* is presented on a log scale. The theoretical equilibrium constants increased exponentially with increasing ambient temperature but decreased with increasing RH. This indicated that NH_4NO_3 would be partitioned into the gas phase due to high equilibrium constants under high-temperature and low-RH conditions. Figure S4b illustrates the time series of the theoretical and observed equilibrium constants during the sampling periods. As can be seen, most of the observed equilibrium constants were higher than the theoretical ones, suggesting that NH_4NO_3 aerosols were produced in Nanjing during the sampling periods. Obviously, higher theoretical and lower observed equilibrium constants were found during the summer. This suggested that more NO_3^- and NH_4^+ would tend to be partitioned into the gas phase, resulting in lower particulate nitrate concentrations during hot seasons (Lin and Cheng, 2007).

Apart from seasonal variations, pronounced diurnal patterns were also found for SIA species (see Figure 3). NO_3^- exhibited similar diel cycles during different seasons, with higher concentrations in the early morning (3 a.m. - 7 a.m.) and lower levels between 2 p.m. and 5 p.m. The high nitrate concentrations in the early morning might be caused by the nitrate formation via heterogeneous reaction in the dark, and gas-phase oxidation after sunrise and the subsequent condensation on pre-existing particles before the temperature increased and RH decreased afterwards. Moreover, the lower planet boundary layer (PBL) might be another reason for enhanced nitrate in the early morning. However, the lower concentrations of nitrate during the daytime might be attributed to the higher PBL, and high temperatures, which inhibited the build-up of nitrate, especially during the summertime. In terms of sulfate, higher concentrations were observed between 6 am. and 1 p.m., indicating that the formation rate of sulfate was higher than the removal/dilution rate, leading to an increase of the sulfate concentration during the daytime. The diurnal patterns of NH_4^+ mimicked those of NO_3^-, showing lower concentrations during the daytime. This was explained by the drastic decrease of particulate NH_4NO_3 concentrations under high temperatures and low relative humidity, resulting in lower NH_4^+ levels during the daytime.

3.2 Enhancements of nitrate at high $PM_{2.5}$ levels

Figure S5 shows the scatter plots of NO_3^-, SO_4^{2-} and NH_4^+ against $PM_{2.5}$. As seen, the slopes of NO_3^- (NO_3^- vs. $PM_{2.5}$ mass), SO_4^{2-} and NH_4^+ were 0.30, 0.24 and 0.19, respectively. This suggested that the increasing rate of NO_3^- during the high-$PM_{2.5}$ events was higher than those of other SIA species. At high $PM_{2.5}$ levels ($PM_{2.5} \geq$

150 μg/m^3), NO_3^-, SO_4^{2-} and NH_4^+ contributed 39, 28 and 24 % of the TWSIIs, respectively (Figure 2b). However, the relative abundances of NO_3^-, SO_4^{2-} and NH_4^+ during low $PM_{2.5}$ concentrations (hourly $PM_{2.5}$ < 35 μg/m^3, see Figure 2c) were 29, 37 and 23 %, respectively. In recent years, dramatically enhanced amounts of nitrate aerosols during high-PM events have been observed at many urban sites in China (Wen et al., 2015; Wang et al., 2017; 2018; Zou et al., 2018). For instance, Zou et al. (2018) found that the nitrate concentrations during the occurrence of polluted air in Beijing and Tianjin were almost 14 times higher than those on relatively clean days ($PM_{2.5}$ < 75 μg/m^3), and the enhancement ratio of nitrate was much higher than that (5.3) of sulfate. Wang et al. (2018) noted that the enhancement ratio of NO_3^- (~6) between haze and clear days in Ningbo of the YRD region was much higher than that of SO_4^{2-} (~3). These findings suggested that NO_3^- was a major contributing species to fine particles during haze days since its increasing ratio between haze and non-haze days was much higher than those of other SIA species, such as sulfate and ammonium.

3.3 PSCF result of high nitrate pollution

During the high $PM_{2.5}$ pollution, significant enhanced nitrate aerosols in terms of both absolute concentration and relative abundance to TWSIIs were found. Next, we tried to use PSCF analysis to identify whether local emission or long-range transported pollution was the major source of high nitrate concentrations at the receptor site. In this work, the 80th percentile values of nitrate concentration was selected as "high nitrate pollution" threshold for PSCF analysis. Figure 4 plots the PSCF result of high nitrate pollution in Nanjing during the sampling periods. The region corresponding to high PSCF value grid is a potential source region of nitrate aerosols. As can be seen, the areas with high PSCF value (>0.8) were regularly local areas surrounding by Nanjing while PSCF values from other long-distance areas were lower than 0.2. This suggested that NO_3^- aerosols in Nanjing during the high nitrate pollution were likely from local emissions rather than long-range transported sources.

3.4 Nitrate formation under different ammonium regimes

Ammonium is a major species that neutralizes particulate SO_4^{2-} and NO_3^-. In the atmosphere, SO_4^{2-} competes with NO_3^- for NH_4^+ during their formation processes, and therefore, the relationship between the molar ratios of NO_3^-/SO_4^{2-} and NH_4^+/SO_4^{2-} can give us a hint for understanding the formation of NO_3^- under different ammonium regimes (Pathak et al., 2009; He et al., 2012; Tao et al., 2016). In an ammonium-rich regime, the HNO_3 produced by both gas oxidation and heterogeneous process reacts (or neutralizes) with "excess-ammonium" (excess-NH_4^+) at a NH_4^+/SO_4^{2-} molar ratio > 2 (theoretical value in an NH_4^+-rich regime) when sulfate is completely neutralized by NH_4^+ to form $(NH_4)_2SO_4$ (Squizzato et al., 2013; Ye et al., 2011). In contrast, nitrate can be found under ammonium-poor conditions with a theoretical NH_4^+/SO_4^{2-} value that should be less than 2 (Pathak et al., 2009). Under NH_4^+-poor conditions, HNO_3 reacts with other cations, such as the calcium carbonate frequently found in natural dust.

Figure 5 shows the scatter plot of the molar ratios of NO_3^-/SO_4^{2-} against NH_4^+/SO_4^{2-}. It is found that good correlations exist between NO_3^-/SO_4^{2-} and NH_4^+/SO_4^{2-} under NH_4^+-rich regimes, with a coefficient of determination (R^2) of 0.84 - 0.94 in the different seasons (see in Table 1). Utilizing the linear regression model, we suggested that nitrate aerosols (in NH_4^+-rich regimes) began to form when the NH_4^+/SO_4^{2-} molar ratios exceeded the criterion values of 1.7-2.0 during the different seasons (Table 1). The criterion value can be calculated as absolute value of "intercept" dividing by slope in each linear regression model (He et al., 2012). The criterion values below 2 suggested that part of the sulfate might have existed in other forms, such as ammonium bisulfate. On the other hand, under ammonium-rich conditions, nitrate concentrations should be positively proportional to "excess-NH_4^+" concentrations, a relationship which was defined as [excess-NH_4^+] = (NH_4^+/SO_4^{2-} - criterion value) × [SO_{4-}^{2-}] (Pathak et al., 2009) (sulfate is in the units of nmol m^{-3} here). The criterion values were acquired from the regression models, as listed in Table 1. The results revealed that the excess-NH_4^+ concentrations varied from -283 to 1422 nmol m^{-3} (see Figure 6), and only 1 % of data showed deficit-NH_4^+ conditions, reflecting that NO_3^- formation in Nanjing occurred primarily under the NH_4^+-rich conditions. Moreover, the excess-NH_4^+ had apparent diurnal cycles, with higher concentrations in the early morning and lower concentrations at midday and in the early afternoon (see Figure 3, where we converted the units from nmol m^{-3} to μg m^{-3}). The diurnal patterns of NO_3^- mimicked those of the excess-NH_4^+. This also suggested that particulate NO_3^- formation occurred mainly under NH_4^+-rich conditions. Figure 6 illustrates the relationship between the nitrate and excess-NH_4^+ molar concentrations during the sampling periods. The nitrate molar concentrations correlated linearly with the excess-NH_4^+ molar concentrations with a slope of approximately 1.0, which was consistent with the molar ratio of reaction between HNO_3 and NH_3. Interestingly, some scattered points were found in high ammonium concentrations (excess-NH_4^+ ≧ 900 nmol m^{-3} ~ 16.2 μg m^{-3}), implying that residual NH_4^+ might be presented in another form such as NH_4Cl under high-NH_4^+ conditions. On the contrary, NO_3^- aerosols can be produced without involving NH_3; therefore, NO_3^- did not correlate well with the excess NH_4^+ under a NH_4^+-poor regime.

In this study, high nitrate concentrations were always found under NH_4^+-rich regimes, elucidating that nitrate production during high PM levels in Nanjing had to be involved with NH_3 or NH_4^+. Figure 6 also shows the nitrate concentrations against the excess-NH_4^+ observed in various cities of China during the summertime (Pathak et al., 2009; Griffith et al., 2015). In Beijing and Shanghai, high nitrate concentrations during the summertime were found under NH_4^+-deficient conditions, which was very different from the findings of this work. In these studies (Pathak et al., 2009; Griffith et al., 2015), the high nitrate concentrations associated with NH_4^+-poor conditions might be due to the lower excess-NH_4^+ concentrations under high-SO_4^{2-} conditions at that time since the strict control of SO_2 emissions by the Chinese government started in 2010 (Zheng et al., 2018). In recent years, the reduction of anthropogenic SO_2 emissions decreased the airborne SO_4^{2-} concentrations, resulting in more excess-NH_4^+ and leading to nitrate aerosol formation under NH_4^+-rich regimes. This argument can be supported by the recent results shown in Figure S6, in which high nitrate concentrations in Beijing were always found under NH_4^+-rich regimes.

3.5 Nitrate formation mechanism during high-$PM_{2.5}$ episodes

In this section, we attempted to explore the formation mechanisms of nitrate aerosols during high $PM_{2.5}$ levels. Here, nitrogen conversion ratio (Fn) was used to evaluate the conversion capability of NO_2 to total nitrate (TN, TN=HNO_3 + NO_3^-), and it can be defined as (Khoder, 2002; Lin et al., 2006):

$$F_n = \frac{GNO_3^- + PNO_3^-}{GNO_3^- + PNO_3 + NO_2} \quad (1)$$

where GNO_3^- and PNO_3^- represent the NO_2 concentrations in nitric acid and particulate nitrate, respectively, with the units of μg m^{-3}. The results showed that the Fn values during the sampling periods varied from 0.01 to 0.57 with a mean value of 0.14 ± 0.09 (see Figure 1e). This value was comparable to that (0.17) in Taichung, Taiwan, where both gas-oxidation and heterogeneous reaction were the dominant formation mechanisms of atmospheric HNO_3 (or NO_3^-) (Lin et al., 2006). However, our Fn value was 2.3 time higher than that (0.06) in Dokki, Egypt (Khoder, 2002). The reason of significant discrepancy of Fn between this work and that in Dokki was not clearly understood, but it might be attributed to different formation processes of HNO_3. In Dokki, gas-phase oxidation was the dominant pathway of HNO_3 production while heterogeneous process (R3) played an important role in HNO_3 formation in addition to gas-phase oxidation in Nanjing, especially during the high-$PM_{2.5}$ events (discussed later). The reaction rate of HNO_3 by heterogeneous process was much higher than that by gas-phase oxidation (Calvert and Stockwell, 1983) and therefore, the Fn value was much higher in this study. On the other hand, Fn displayed significant diurnal cycles, with the highest value in the early morning (see in Figure 3). This elevated Fn coincided with increasing ALWC, suggesting heterogeneous reaction since ALWC is one of the key parameters which favors the transformation of N_2O_5 to liquid HNO_3 in this process (also indicated that nitrate formation was associated with heterogeneous process). On the contrary, a second peak of Fn was found in the early afternoon when Ox (Ox = NO_2 + O_3, an index of the oxidation capacity) concentrations increased, but ALWC decreased. This suggested that the HNO_3 formation might be mainly associated with the gas-phase reaction of NO_2 + OH during the daytime; also reflected that nitrate formation was via gas-phase oxidation.

Assuming that long-range transported nitrate can be neglected in this study (in section 3.3), we attempted to analyze the correlations of Fn vs. OH and Fn vs. ALWC to investigate whether gas-phase oxidation or heterogeneous reactions might be the dominant mechanism of nitrate production. In this work, the OH radical concentrations were not measured; hence, we used O_X as a proxy of OH. The ALWC was acquired by computing the ISOPROPIA II model as described in section 2.3. Figure 7 illustrates the scatter plots of Fn against Ox and ALWC in both daytime and nighttime aerosol samples during the high-$PM_{2.5}$ events. Fn correlated well with the ALWC, with a correlation coefficient (R) of 0.72 and 0.76 ($p < 0.05$) at daytime and nighttime samples, respectively. However, a poor correlation was found between Fn and Ox (R was 0.17 and 0.52 for the daytime and nighttime samples, p>0.05). This implied that nitrate formation during the high-$PM_{2.5}$ events in Nanjing was likely attributed to heterogeneous reactions. This result was consistent with recent conclusions reached by oxygen isotope techniques, in which the hydrolysis of N_2O_5 in preexisting aerosols was found to be a major mechanism of NO_3^- formation (Chang et al., 2018).

3.6 Case study and production rate of NO_3^- during $PM_{2.5}$ episodes

Figure 8 shows several high-$PM_{2.5}$ events observed from March 3 to 6 in 2016. In case I, the high $PM_{2.5}$ concentrations started at 6 p.m. on March 3 and ended at 3 a.m. on March 4. During this event, the SO_4^{2-} and NH_4^+ concentrations remained at almost constant levels, but the NO_3^- concentrations revealed a slight enhancement. In the early morning of March 4, the NO_3^- concentrations increased from 39.4 to 47.8 μg m^{-3} within 4 hours, resulting in a nitrate production rate of 2.3 μg m^{-3} h^{-1} (~5.5 % h^{-1}, the calculation of NO_3^- production rate can be seen in the *Supplementary S2*). In case II, high $PM_{2.5}$ concentrations were observed from 8. a.m. to 2. p.m. on March 4. The NO_3^- concentrations were much higher than those of SO_4^{2-}, indicating nitrate-dominated aerosols. In this case, the NO_3^- concentrations increased from 38.1 to 51.2 μg m^{-3} within 6 hours, suggesting that the increasing rate of NO_3^- was 1.0 μg m^{-3} h^{-1} (2.4 % h^{-1}). Since the high NO_3^- concentrations occurred under high-Ox and low-ALWC conditions, this suggested that the gas-phase reaction of NO_2 + OH might be the dominant source of NO_3^- production in this event. In case III, a rapid growth of the $PM_{2.5}$ mass was found around midnight, along with a dramatic increase of NO_3^-

concentrations from 11 p.m. on March 4 (31.0 μg m^{-3}) and maximizing at 1 a.m. the next day (64.5 μg m^{-3}). The increasing rate of NO_3^- was estimated to be 11.4 μg m^{-3} h^{-1} (~19.5 % h^{-1}), which was much higher than those in case I and II. The high-nitrate event was found under increasing ALWC and decreasing Ox concentration conditions, suggesting that nitrate production occurred through heterogeneous processes. In case IV, the enhancements of all SIA species coincided with increasing ALWC and declining Ox concentrations. Again, the enhancement of nitrate was likely attributed to heterogeneous reactions rather than to gas-phase processes. In these events, the NO_3^- production rate was estimated to be 5.0 μg m^{-3} h^{-1} (~ 15.4 % h^{-1}).

Through the sampling periods, a total of twelve high $PM_{2.5}$ events were found, and the NO_3^- concentrations increased significantly during all the episodes (see in Table S1). Seven episodes suggested that heterogeneous processes ($N_2O_5 + H_2O$) might be a major pathway for nitrate formation since elevated NO_3^- levels coincided with increasing AWLC and decreasing Ox (or Ox remaining at a constant level). Among these heterogeneous process events, five cases (Case III, Case IX, Case X, Case XI and Case XII in Table S1) were observed during the nighttime (5 p.m. – 6 a.m. on the next day). This suggested that approximately 70 % heterogeneous reaction of nitrate production was observed in the dark. In these events, the average NO_3^- growth rate was 12.6 ± 7.3 % h^{-1} (4.1 ± 3.6 μg m^{-3} h^{-1}). This value was in agreement with those in the literatures which the production rate of nitrate via heterogeneous reaction were 14.3 % h^{-1} by both field measurements and laboratory works (Calvert and Stockwell, 1983; Pathak et al., 2011). On the contrary, NO_3^- concentrations rose with increasing Ox and decreasing ALWC in two $PM_{2.5}$ episodes, indicating gas-phase processes (NO_2 + OH). As listed in Table S1, these gas-phase reaction cases occurred mainly during the daytime. The average production rate of NO_3^- in the gas-oxidation reaction cases averaged 2.5 ± 0.1 % h^{-1} (0.8 ± 0.3 μg m^{-3} h^{-1}), which was in line with that (2.4

% h^{-1}) in the subtropical polluted urban site that nitrate aerosols were mainly from gas-oxidation process (Lin et al., 2007). Moreover, we also found some cases in which the elevated NO_3^- might have been from both gas-phase and heterogeneous reactions, and the corresponding NO_3^- growth rate was approximately 7.5 ± 3.0 % h^{-1}(2.5 ± 0.2 μg m^{-3} h^{-1}). In conclusion, enhancements of NO_3^- in Nanjing usually occurred under increased ALWC and decreased Ox conditions, indicating that heterogeneous reactions provided the dominant pathway of nitrate formation during the $PM_{2.5}$ episodes. Moreover, the average growth rate of NO_3^- (12.6 % h^{-1}) by heterogeneous processes was 5 times higher than that (2.5 % h^{-1}) of gas-phase reactions. This might explain the abrupt increase of nitrate concentrations during the high $PM_{2.5}$ events.

3.7 HNO_3/NH_3 limitation of nitrate aerosol formation

In Nanjing, high nitrate concentrations occurred mainly under NH_4^+-rich regimes, indicating the involvement of atmospheric NH_3. This also demonstrated that both HNO_3 and NH_3 were crucial precursors for particulate nitrate formation. In this section, we attempted to discuss whether HNO_3 or NH_3 was the limited factor for nitrate formation in Nanjing during the high-$PM_{2.5}$ events. ISORROIPA II model is capable of predicting concentrations of particulate ions in addition to ALWC under thermodynamic equilibrium between gas- and aerosol-phase of these ions (Tang et al., 2016). In section 3.5, we used this model to estimate ALWC. Indeed, the output data also included concentrations of ionic species. Figure S7 illustrates the scatter plots of modeled results against observations of NO_3^-, SO_4^{2-} and NH_4^+ in Nanjing during the sampling periods. Good correlations were found between modeled results and observations (R^2=0.97-0.99 with all slopes of approximately 1.0), suggesting that ISORROPIA II had a good performance in prediction of SIA species. As a result, we can use ISORROPIA II model to test sensitivity of HNO_3 and NH_3 to particulate nitrate concentrations (Guo et al., 2018).

Figure 7 shows the contour plot of the simulated nitrate concentrations depending on the various total nitrate (TN) and total ammonium (TA, TA=NH_3 + NH_4^+) levels under thermodynamic equilibrium conditions computed by ISORROPIA II model. The details of considered chemical reactions in ISORROPIA II model can be seen elsewhere (Fountoukis & Nenes, 2007). Here, sulfate concentrations were assumed to be 10 and 60 μg m^{-3} for the tests of different sulfate conditions. The average concentrations of total chloride (HCl + Cl^-, 1.3 μg m^{-3}), Na^+ (0.2 μg m^{-3}), K^+ (0.8 μg m^{-3}), Mg^{2+} (0.1 μg m^{-3}) and Ca^{2+} (0.5 μg m^{-3}) along with ambient T (20 °C) and RH (62 %) at the receptor site during the sampling period served as input data in this model. The results showed that the lower simulated NO_3^- concentrations was found in the higher SO_4^{2-} case. This was attributed to less NH_4NO_3 formation under higher SO_4^{2-} conditions since SO_4^{2-} would compete with NO_3^- for NH_4^+.

According to the simulated results, we can roughly split the plots into two parts: one is HNO_3-limited area (right), and another is NH_3-limited region (left). The observed TN and TA concentrations (pink circles) in Nanjing are also plotted in this figure. Most of the observed data sets were mainly affected by TN under a low-SO_4^{2-} case. Under a high-SO_4^{2-} condition, the observed data fell into TA-limited under a low-TN and -TA regime, but fell into TN-limited in high-TA and-TN regimes. During the sampling period, high nitrate concentrations always accompanied with high TN and TA levels, highlighting that nitrate aerosol production in Nanjing during the high $PM_{2.5}$ levels was mainly control by HNO_3. Therefore, control of NOx emissions, which reduced HNO_3 concentrations, might be an important way to decrease airborne nitrate concentrations and ameliorate the air quality in Nanjing.

4. Conclusion and remarks

Four intensive online measurements of water-soluble ions in $PM_{2.5}$ were carried out in Nanjing City in 2016 and 2017 to realize the evolutions of SIA and the potential formation mechanisms of particulate nitrate. During the sampling periods, the average concentrations of NO_3^-, SO_4^{2-} and NH_4^+ were 16.7, 14.9 and 10.7 μg m^{-3}, respectively. This indicated that NO_3^- dominated the SIA. Significant seasonal variations and diurnal cycles were found for all SIA species. The low NO_3^- concentrations observed during the summer daytime could be attributed to the enhanced theoretical and declined observed equilibrium constants of NO_3^- and NH_4^+ between gas- and particle-phase. Obvious enhancements of NO_3^- were found in terms of both absolute concentrations and relative abundances during the $PM_{2.5}$ episodes, indicating that NO_3^- was a major contributing species to $PM_{2.5}$. Different from the results obtained in Beijing and Shanghai, high nitrate concentrations always occurred under NH_4^+-rich regimes. The nitrogen conversion ratio, Fn, correlated well with the ALWC but not with Ox during high-$PM_{2.5}$ episodes. These findings indicated that NO_3^- aerosols at the receptor site were mainly produced by heterogeneous reactions ($N_2O_5 + H_2O$) with the involvement of NH_3. The average production rate of NO_3^- from heterogeneous reactions was estimated to be 12.6 % h^{-1}, which was 5 time higher than that of gas-phase reactions. According to the observations and ISORROPIA II simulated results, particulate nitrate formation in Nanjing was HNO_3-limited, suggesting that the control of NOx emissions will be able to decrease the nitrate concentration and improve the air quality in this industrial city.

During the last decade, the mass ratios of nitrate-to-sulfate in $PM_{2.5}$ in the YRD region have been found to range from 0.3 to 0.7 (Lai et al., 2007; Wang et al., 2003; 2006; Yang et al., 2005; Yao et al., 2002), reflecting that the SO_4^{2-} concentration was much higher than the NO_3^- concentration. In the current study, the average mass ratio of nitrate-to-sulfate was 1.1. Indeed, high nitrate-to-sulfate mass ratios of > 1 were also observed in other mega-cities of China recently (Ge et al., 2017; Wei et al., 2018; Ye et al., 2017; Zou et al., 2018). The elevated nitrate-to-sulfate ratio should be due to the dramatic reduction of SO_2 emissions. The enhanced ratio also suggests that we should pay more attention to and develop some strategies for the reduction of NOx emissions, leading to declined nitrate concentrations in the atmosphere and improvement of the air quality in China.

Data availability

All the data used in this paper are available from the corresponding author upon request (dryanlinzhang@outlook.com or zhangyanlin@nuist.edu.cn).

Author contributions

YLZ conceived and designed the study. YCL analyzed the data and wrote the manuscript with YLZ. FM and MB performed aerosol sampling and data analyses with YCL.

Competing interests

The authors declare that they have no conflict of interest.

Acknowledgements

This study was financially supported by the National Key R&D Program of China (Grant No. 2017YFC0212700), the Natural Scientific Foundation of China (Nos. 41761144056, 91644103 and 41977185) and Jiangsu Innovation & Entrepreneurship Team.

References

Baasandorj, M., Hoch, S. W., Bares, R., Lin, J. C., Brown, S. S., Millet, D. B., Martin, R., Kelly, K., Zarzana, K. J., Whiteman, C. D., Bube, W. P., Tonnesen, G., Jaramillo, J. C. and Sohl, J.: Coupling between chemical and meteorological processes under persistent coal-air poor conditions: evolution of wintertime $PM_{2.5}$ events and N_2O_5 observation in Utah's Salt Lake Valley. *Environ. Sci. Technol.*, **51**, 5941-5950, https://doi.org/10.1021/acs.est.6b06603, 2017.

Bian, Y. X., Zhao, C. S., Ma, N., Chen, J., and Xu, W. Y.: A study of aerosol liquid water content based on hygroscopicity measurements at high relative humidity in the Northern China Plain. *Atmos. Chem. Phys.,* **14**, 6417-6426, https://doi.org/10.5194/acp-14-6417-2014, 2014.

Bougiatioti, A., Nikolaou, P., Stavroulas, I., Kouvarakis, G., Weber, A., Nenes, R., Kanakidou, M., and Mihalopoulos, N.: Particle water and pH in the eastern Mediterranean: source variability and implication of nutrient availability. *Atmos. Chem. Phys.,* **16**, 4579-4591, https://doi.org/10.5194/acp-7-4639-2007, 2007.

Brauer, M., Hoek, G., Vliet, V. P., Meliefste, K., Fischer, P. H., Wijga, A., Koopman, L. P., Neijens, H. J., Gerritsen, J., Kerkhof, M., Heinrich, J., Bellander, T., and Brunekreef, B.: Air pollution from traffic and the development of respiratory infections and asthmatic and allergic symptoms in children. *Am. J. Respir. Crit. Care Med.*, **166**, 1092-1098, https://doi.org/10.1146/rccm.200108-007OC, 2002.

Brown, S. S., and Stutz, J.: Nighttime radical observation and chemistry. *Chem. Soc. Rev.*, **41**, 6405-6447, https://doi.org/10.1039/c2cs35181a, 2012.

Calvert, J. G., and Stockwell, W. R.: Acid generation in the troposphere by gas-phase chemistry. *Environ. Sci. Technol.*, **17**, 428-443, https://doi.org/10.1021/es00115a727, 1983.

Chan, C. K., and Yao, X.: Air pollution in mega cities in China. *Atmos. Enviro.,* **42**, 1-

42, https://doi.org/10.1016/j.atmosenv.2007.09.003, 2008.

Chang, W. L., Bhave, P. V., Brown, S. S., Riemer, N., Stutz, J., and Dabdub, D.: Heterogeneous atmospheric chemistry, ambient measurements, and model calculations of N_2O_5: a review. *Aerosol Sc. Technol.*, **45**, 655 - 685, https://doi.org/10.1080/02786826.2010.551672, 2011.

Defino, R. J., Siotuas, C., and Malik, S.: Potential role of ultrafine particles in associations between airborne particle mass and cardiovascular health. *Environ. Health Perspect.*, **113**, 934-938, https://doi.org/10.1289/ehp.7938, 2005.

Fountoukis, C., and Nenes, A.: ISORROPIA II: a computationally efficient thermodynamic equilibrium model for K^+-Ca^{2+}-Mg^{2+}-NH_4^+-Na^+-SO_4^{2-}-NO_3^--Cl^--H_2O. *Atmos. Chem. Phys.*, **7**, 4639-4659, https://doi.org/10.5194/acp-7-4639-2007, 2007.

Ge, X., Li, L., Chen, Y., Chen, H., Wu, D., Wang, J., Xie, X., Ge, S., Ye, Z., Xu, J., and Chen, M.: Aerosol characteristics and sources in Yangzhou, China resolved by offline aerosol mass spectrometry and other techniques. *Environ. Pollut.*, **225**, 74-85, https://doi.org/10.1016/j.encpol.2017.03.044, 2017.

Goodman, A. L., Underwood, G. M., and Grassian, V. H.: A laboratory study of the heterogeneous reaction of nitric acid on calcium carbonate particles. *J. Geophys. Res. Atmos.,* **105**, 29053-29064, https://doi.org/10.1029/2000JD900396, 2000.

Griffith, S. M., Huang, X. H. H., Louie, P. K. K., and Yu, J. Z.: Characterizing the thermodynamic and chemical composition factors controlling $PM_{2.5}$ nitrate: Insights from two years of online measurements in Hong Kong. *Atmos. Environ.*, **122**, 864-875, https://doi.org/10.1016/ j.atmosenv.2015.02.009, 2015.

Guo, H., Xu, L., Bougiatioti, A., Cerully, K. M. , Capps, S. L., Heti Jr., J. R., Carton, A. G., Lee, S.-H., Bergin, M. H., Ng, N. L., Nenes, A., and Weber, R. J.: Fine particle water and pH in the southeastern United States. *Atmos. Chem. Phys.*, **15**, 5221-5228. https://doi.org/10.5194/acp-15-5211-2015, 2015.

Guo, H., Otjes, R., Schlag, P., Kiendler-Schar, A., Nenes, A., and Weber, R. J.: Effectiveness of ammonia reduction of control of fine particulate nitrate. *Atmos. Chem. Phys.*, **18**, 12241-12256. https://doi.org/10.5194/acp-18-12241, 2018, 2018.

He, K., Zhao, Q., Ma, Y., Duan, F., Yang, F., Shi, Z., and Chen, G.: Spatial and seasonal variability of $PM_{2.5}$ acidity at two Chinese megacities: insights into the formation of secondary inorganic aerosols. *Atmos. Chem. Phys.*, **12**, 1377-1395. https://doi.org/10.5194/acp-12-1377-2012, 2012.

Huang, R.-J., Zhang, Y., Bozzetti, C., Ho, K.-F., Cao, J.-J., Han, Y., Daellenbach, R., Slowik, J. G., Platt, S. M., Canonaco, F., Zotter, P., Wolf, R., Pieber, S. M., Bruns, E. A., Crippa, M., Ciarelli, G., Piazzalunga, A., Schwikkowski, M., Abbaszade, G., Schnelle-Kreis, J., Zimmerman, R., An, Z., Szidat, S., Baltensperger, U., Haddad, I. E., and Prévôt, A. H.: High secondary aerosol contribution to particulate pollution during haze events in China. *Nature*, **514**, 218-222, https://doi.org/10.1038/nature13774, 2014a.

Huang, R. J., Chen, R., Jing, M., Yang, L., Li, Y., Chen, Q., Chen, Y., Yan, J., Lin, C., Wu, Y., Zhang, R., Haddad, J. E., Prevot, A. S. H., O'Dowd, C. D., and Cao, J.: Source-specific health risk analysis on particulate trace elements: coal combustion and traffic emission as major contributors in wintertime Beijing. *Environ. Sci. Technol. 52,* 10967-10974, https://doi.org/10.1021/acs.est.8b02091.

Huang, Y., Shen, H., Chen, H., Wang, R., Zhang, Y., Su, S., Chen, Y., Lin, N., Zhong, Q., Wang, X., Liu, J., Li, B., Liu, W., and Tao, S.: Quantification of global primary emissions of $PM_{2.5}$, PM_{10} and TSP from combustion and industrial process sources. *Environ. Sci. Technol.,* **48**, 13834-13843, https://doi.org/10.1021/es503696k, 2014b.

Hui, L., Liu, X., Tan, Q., Feng, M., An. J., Qu, Y., Zhang, Y., and Jiang, M.: Characteristics, source apportionment and contribution of VOCs to ozone formation in Wuhan, Central China. *Atmos. Environ.,* **192**, 55-71, https://doi.org/10.1016/j.atmosenv.2018.08.0642, 2018.

Khoder, M. I.: Atmospheric conversion of sulfur dioxide to particulate sulfate and nitrogen dioxide to particulate nitrate and gaseous nitric acid in an urban area. *Chemosphere*, **49**, 675-684, https://doi.org/10.1016/S0045-6535(02)00391-0, 2002.

Kong, L., Yang, Y., Zhang, S., Zhao, X., Du, H., Fu, H., Zhang, S., Cheng, T., Yang, X., Chen, J., Wu, D., Sheng, J., Hong, S., and Jiao, L.: Observation of linear dependence between sulfate and nitrate in atmospheric particles. *J. Geophys. Res. Atmos.,* **119**, 341-361, https://doi.org/10.1002/2013JD020222, 2014.

Lin, Y.-C., and Cheng, M.-T.: Evaluation of formation rates of NO_2 to gaseous and particulate nitrate in the urban atmosphere. *Atmos. Environ.,* **41**, 1903-1910, https://doi.org/10.1016/j.atmosenv.2006.10.065, 2007.

Lin, Y.-C., Cheng, M.-T., Ting, W.-Y., and Yeh, C.-R.: Characteristics of gaseous HNO_2, HNO_3, NH_3 and particulate ammonium nitrate in an urban city of central Taiwan. *Atmos. Environ.,* **40**(25), 4725-4733, https://doi.org/10.1016/j.atmosenv.2006.04.037, 2006.

Liu, M., Song, Y., Zhou, T., Xu, Z., Yan, C., Zheng, M., Wu, Z., Hu, M., Wu, Y., and Zhu, T.: Fine particle pH during severe haze episodes in northern China. *Geophys. Res. Lett.,* **44**, 5213-5222, https://doi.org/10.1002/2017GL073210, 2017.

Mental, T. F., Sohn, M., and Wahner, A.: Nitrate effect in the heterogeneous hydrolysis of dinitrogen pentoxide on aqueous aerosols. *Phys. Chem. Chem. Phys.*, **1**, 5451-5457, https://doi.org/10.1039/a905338g, 1999.

Nel, A.: Air pollution-related illness: effects of particles. *Science*, **308**, 804-806, https://doi.org/10.1126/science.1108752, 2005.

Pan, Y., Tian, S., Zhao, Y., Zhang, L., Zhu, X., Gao, J., Huang, W., Zhou, Y., Song, Y., Zhang, Q., and Wang, Y.: Identifying ammonia hotspots in China using a national observation work. *Environ. Sci. and Technol.*, **52**, 3926-3934. https://doi.org/10.1021.acs/est.7b05235, 2018.

Pathak, R. K., Wu, W. S., and Wang, T.: Summertime $PM_{2.5}$ ionic species in four major cities of China: nitrate formation in an ammonia-deficient atmosphere. *Atmos. Chem. and Phys.*, **9**, 1711-1722, https://doi.org/10.5194/acp-9-1711-2009, 2009.

Pathak, R. K., Wang, T., and Wu, W. H.: Nighttime enhancement of $PM_{2.5}$ in ammonia-poor atmospheric conditions in Beijing and Shanghai: Plausible contributions of heterogeneous hydrolysis of N_2O_5 and HNO_3 partitioning. *Atmos. Environ.,* **45**, 1183-1191, https://doi.org/10.1016/j.atmosenv.2010.09.003, 2011.

Polissar, A. V., Hopke, P. K., Paatero, P., Kaufmann, Y. J., Hall, D. K., Bodhaine, B. A., Dutton, E. G., and Harris, J. M.: The aerosol at Barrow, Alaska: long-term trends and source locations. Atmos. Environ., **33**, 2441-2458, https://doi.org/10.1016/j.atmosenv.2018.08.0642, 2018.

Prabhakar, G., Parworth, C. L., Zhang, X., Kim, H., Young, D. E., Beyersdorf, A. J., Ziemba, L. D., Nowak, J. B., Bertram, T. H., Faloona, I. C., Zhang, Q., and Cappa, C. D.: Observational assessment of the role of nocturnal residual-layer chemistry in determining daytime surface particulate nitrate concentrations. *Atmos. Chem. Phys.*, **17**, 14747-14770, https://doi.org/10.5194/acp-17-14747-2017, 2017.

Squizzato, S., Masiol, M., Brunelli, A., Pistollato, S., Tarabotti, Z., Rampazzo, G., and

Pavoni, B.: Factors determining the formation of secondary inorganic aerosol: a case study in the Po Valley (Italy). *Atmos. Chem. and Phys.,* **13**, 1927-1339, https://doi.org/10.5194/acp-13-1927-2013, 2013.

Tang, X., Zhang, X., Ci, Z., Guo, J., and Wang, J.: Speciation of the major inorganic salts in atmospheric aerosols of Beijing: China: measurements and comparison with model. *Atmos. Environ.,* **133**, 123-134, https://doi.org/10.1016/j.atmosenv. 2016.03.013.

Tao, Y., Ye, X., Ma, Z., Xie, Y., Wang, R., Chen, J., Yang, X., and Jiang, S.: Insights into different nitrate formation mechanisms from seasonal variations of secondary inorganic aerosols in Shanghai. *Atmos. Environ.,* **145**, 1-9, https://doi.org/10.1016/j.atmosenv.2016.09.012, 2016.

ten Brink, H., Otjes, R., Jongejan, P., and Slanina, S.: An instrument for semi-continuous monitoring of the size-distribution of nitrate, ammonium, sulfate and chloride in aerosols. *Atmos. Environ.,* **41**, 2768-2779, https://doi.org/10.1016/j.atmosenv.2006.11.041, 2007.

Wahner, A., Mental, T. F., Sohn, M., and Stier, J.: Heterogenous reaction of N_2O_5 on sodium nitrate aerosol. *J. Geophys. Res. Atmos.*, **103**, 31103-31112, https://doi.org/10.1029/1998JD100022, 1998.

Wang, G., Wang, H., Yu, Y., Gao, S., Feng, J., Gao, S., & Wang, L.: Chemical characterization of water-soluble components of PM_{10} and $PM_{2.5}$ atmospheric aerosols in five locations of Nanjing, China. *Atmos. Environ.*, **37**., 2893-2902. https://doi.org/10.1016/j.atmosenv.S1352-2310(03)00271-1, 2003.

Wang, G., Zhang, R., Geomez, M. E., Yang, L., Zamora, M. L., Hu, M., Lin, Y., Peng, J., Guo, S., Meng, J., Li, J., Cheng, C., Hu, T., Ren, Y., Wang, Y., Gao, J., An, Z., Zhou, W., Li, G., Wang, J., Tian, P., Marrero-Ortiz, W., Secrest, J., Du, Z., Zheng, J., Shang, D., Zheng, L., Shao, M., Wang, W., Huang, Y., Wang, Y., Zhu, Y., Li, Y., Hu, J., Pan, B., Cai, L., Cheng, Y., Ji, Y., Zhang, F., Rosenfeld, D., Liss, P. S., Duce, R. A., Kolb, C. E., and Molina, M. J.: Persistent sulfate formation from London fog to Chinese haze. *Proc. Natl. Acad. Sci.*, **113**, 13630-13635, https://doi.org/ 10.1073/pnas.1616540113, 2016.

Wang, H., Lu, K., Chen, X., Zhu, Q., Chen, Q., Guo, S., Jiang, M., Li, X., Shang, D., Tang, Z., Wu, Y., Wu, Z., Zou, Q., Zheng, Y., Zheng, L., Zhu, T., Hu, M., and Zhang, Y.: High N_2O_5 concentrations observed in urban Beijing: implications of a large nitrate formation. *Environ. Sci. Technol. Lett.*, **4**, 416-420, https://doi.org/10.1021/acsestlett.7b00341, 2017.

Wang, H., Zhu, B., Shen, L., Xu, H., An, J., Xue, G., and Cao, J.: Water soluble ions in atmospheric aerosols measured in five sites in the Yantze River Delta, China: size-fractionated seasonal variation and sources. *Atmos. Environ.*, **123**(B), 370-379, https://doi.org/10.1016/j.atmosenv.2015.05.070, 2015.

Wang, W., Yu, J., Cui. Y., He, J., Xue, P., Cao, W., Ying, H., Gao, W., YIng, Y., Gao, W., Yan, Y., Hu, B., Xin, J., Wang, L., Liu, Z., Sun, Y., Ji, D., and Wang, Y.: Characteristics of fine particulate matter and its sources in an industrialized coastal city, Ningbo, Yantze River Delta, China. *Atmos. Res.*, **203**, 105-117, https://doi.org/10.1016/j.atmosres.2017.11.033, 2018.

Wang, Y., Zhuang, G., Zhang, X., Xu, C., Tang, A., Chen, J., and An, Z.: The ion chemistry, seasonal cycle, and sources of $PM_{2.5}$ and TSP aerosol in Shanghai. *Atmos. Environ.,* **40**(16), 2935-2952, https://doi.org/10.1016/j.atmosenv.2005.12.051, 2006.

Wei, L., Yue, S., Zhao, W., Yang, W., Zhang, Y., Ren, L., Han, X., Guo, Q., Sun, Y., Wang, Z., and Fu, P.: Stable sulfur isotope ratios and chemical compositions of fine aerosols ($PM_{2.5}$) in Beijing, China. *Sci. Total Environ.*, **633**, 1156-1164, https://doi.org/10.1016/j.scitotenv.2018.03.153, 2018.

Wen, L., Chen, J., Yang, L., Wang, X., Xu, C., Sui, X., Yao, L., Zhu, Y., Zhang, J., Zhu, T., and Wang, W.: Enhanced formation of particulate nitrate at a rural site on the North China Plain in summer: the importance roles of ammonia and ozone. *Atmos. Environ.,* **101**, 294-302, https://doi.org/10.1016/j.atmosenv.2014.11.037, 2015.

Yang, H., Yu, J. Z., Ho, S. S. H., Xu, J., Wu, W.-S., Wan, C. H., Wang, X., Wang, X., and Wang, L.: The chemical composition of inorganic and carbonaceous materials in $PM_{2.5}$ in Nanjing, China. *Atmos. Environ. ,* **39**, 3735-3749, https://doi.org/10.1016/j.atmosenv.2005.03.010, 2005.

Yao, X., Chan, C. K., Fang, M., Cadle, S., Chan, T., Mulawa, P., He, K., and Ye, B.: The water-soluble ionic composition $PM_{2.5}$ in Shanghai and Beijing, China. *Atmos. Environ.,* **36**, 4223-4234, https://doi.org/10.1016/j.atmosenv.2005.12.051, 2002.

Ye, X. N., Ma, Z., Zhang, J. C., Du, H. H., Chen, J. M., Chen, H., Yang, X., Gao, W., and Geng, F. H.: Important role of ammonia on haze formation in Shanghai. *Environ. Res. Lett.*, **6**, 024019, https://doi.org/10.1088/1748-9326/6/2024019, 2011.

Ye, Z., Liu, J., Gu, A., Feng, F., Liu, Y., Bi, C., Xu, J., Li, L., Chen, H., Chen, Y., Dai, L., Zhou, Q., and Ge, X.: Chemical characterization of fine particulate matter in Changzhou, China and source apportionment with offline aerosol mass spectrometry. *Atmos. Chem. .Phys.,* **17**, 2573-2592, https://doi.org/10.5194/acp-17-2573-2017, 2017.

Zhang, R., Jing, J., Tao, J., Hsu, S.-C., Wang, G., Cao, J., Lee, C.S.L., Zhu, L., Chen, Z., Zhao, Y., and Shen, Z., Chemical characterization and source apportionment of $PM_{2.5}$ in Beijing: seasonal perspective. *Atmos. Chem. .Phys.,* **13**, 7053-7074, https://doi.org/10.5194/acp-13-7053-20173, 2013.

Zhang, Y.-L., and Cao, F.: Fine particulate matters ($PM_{2.5}$) in China at a city level. *Sci. Rep.,* **5**, 14884, https://doi.org/10.1038/srep14884, 2015.

Zhao, P. S., Dong, F., He, D., Zhao, X. J., Zhang, X. L., Zhang, W. Z., Yao, Q., and Liu, H. Y.: Characteristics of concentrations and chemical compositions for PM2.5 in the region of Beijing, Tianjin, and Hebei, China. *Atmos. Chem. Phys.,* **13**, 4631-4644, https://doi.org/10.5194/acp-13-4631-2013, 2013.

Zheng, B., Tong, D., Li, M., Liu, F., Hong, C., Geng, G., Li, H., Li, X., Peng, L., Qi, J., Yan, L., Zhang, Y., Zhao, H., Zheng, Y., He, K., and Zhang, Q.: Trends in China's anthropogenic emissions since 2010 as the consequence of clean air actions. *Atmos. Chem. .Phys.,* **18**(19), 14095-14111, https://doi.org/10.5194/acp-18-14095-2018, 2018.

Zou, J., Liu, Z., Hu, B., Huang, X., Wen, T., Ji, D., Liu, J., Yang, Y., Yao, and Wang, Y.: Aerosol chemical compositions in the Northern China Plain and the impact on visibility in Beijing and Tianjin., *Atmos. Res.*, **201**, 235-246, https://doi.org/10.1016/j.atmosres.2017.09.014, 2018.

Table Captions

Table 1 The regression models between NO_3^-/SO_4^{2-} (Y) and NH_4^+/SO_4^{2-} (X) along with the criterion values of NH_4^+/SO_4^{2-} in ammonium-rich regime during the sampling periods.

Figure Captions

Figure 1 Time series of concentrations in (a) $PM_{2.5}$ mass, (b) SIA species, (c) ALWC and (d) Ox along with (e) Fn observed in Nanjing during the sampling periods. The grey shadows represent the high $PM_{2.5}$ periods discussed in the section 3.6.

Figure 2 Abundance of each species in TWSIIs during the (a) entire, (b) haze ($PM_{2.5} \geq 150\ \mu g\ m^{-3}$) and (c) clear ($PM_{2.5} < 35\ \mu g\ m^{-3}$) events. The numbers in the parentheses are standard deviations.

Figure 3 Abundance of each species in TWSIIs during the (a) entire, (b) haze ($PM_{2.5} \geq 150\ \mu g\ m^{-3}$) and (c) clear ($PM_{2.5} < 35\ \mu g\ m^{-3}$) events. The numbers in the parentheses are standard deviations.

Figure 4 The PSCF maps of high nitrate pollution.

Figure 5 Scatter plots of molar ratios of NO_3^-/SO_4^{2-} against NH_4^+/SO_4^{2-} in Nanjing during the different seasons.

Figure 6 Scatter plot of NO_3^- vs. excess-NH_4^+ molar concentrations in Nanjing during the different seasons. The results in Beijing, Shanghai, Guangzhou, Lanzhou and Hong Kong are also shown in this figure.

Figure 7 Scatter plots of (a) Fn against Ox and (b) Fn against ALWC in daytime and nighttime aerosol samples during the high hourly $PM_{2.5}$ concentration conditions (hourly $PM_{2.5} \geqq 150\ \mu g\ m^{-3}$).

Figure 8 Time series of concentrations in (a) $PM_{2.5}$ mass and CO, (b) SIA species

(NO_3^-, SO_4^{2-} and NH_4^+), (c) ALWC, Ox and NO_2 and (d) RH and T in Nanjing City from March 3 to 6, 2016. The grey shadows denote $PM_{2.5}$ episodes. The red numbers represent NO_3^- production rate during the $PM_{2.5}$ episodes.

Figure 9 Nitrate concentrations simulated by ISORROPIA II model dependening on TN and TA concentrations under (a) SO_4^{2-} = 10 μg m^{-3} and (b) SO_4^{2-} = 60 μg m^{-3}. The purple dots denote the observed TN and TA concentrations at the receptor site during the sampling periods.

Table 1 The regression models between NO_3^-/SO_4^{2-} (Y) and NH_4^+/SO_4^{2-} (X) along with the criterion values of NH_4^+/SO_4^{2-} in ammonium-rich regime during the sampling periods.

Sampling periods	Regression models	Criterion values of NH_4^+/SO_4^{2-}
2016 spring	$Y = 0.71\ X – 1.27$; $R^2 = 0.87$	1.8
2016 summer	$Y = 0.67\ X – 1.22$; $R^2 = 0.86$	1.8
2017 winter	$Y = 0.81\ X – 1.50$; $R^2 = 0.91$	1.9
2017 spring	$Y = 0.95\ X – 1.91$; $R^2 = 0.94$	2.0
2017 summer	$Y = 0.79\ X – 1.32$; $R^2 = 0.84$	1.7

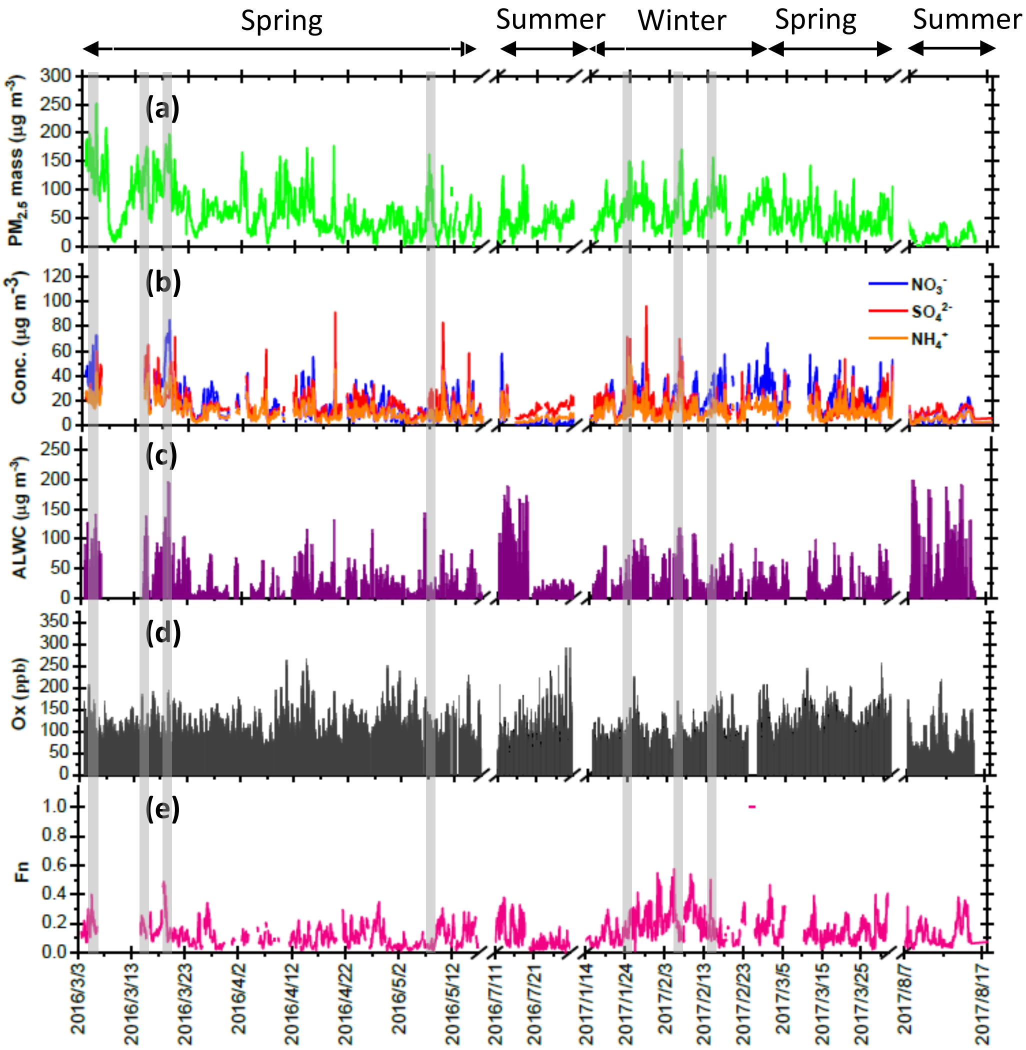

Figure 1 Time series of concentrations in (a) PM$_{2.5}$ mass, (b) SIA species, (c) ALWC and (d) Ox along with (e) Fn observed in Nanjing during the sampling periods. The grey shadows represent the high PM$_{2.5}$ periods discussed in the section 3.6.

(a) Entire days: $PM_{2.5}$ = 58 ± 35 μg m^{-3}

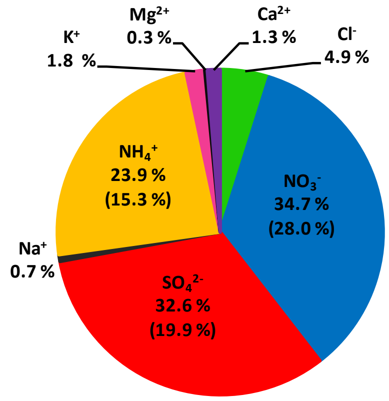

(b) Haze events: $PM_{2.5}$ = 171 ± 18 μg m^{-3}

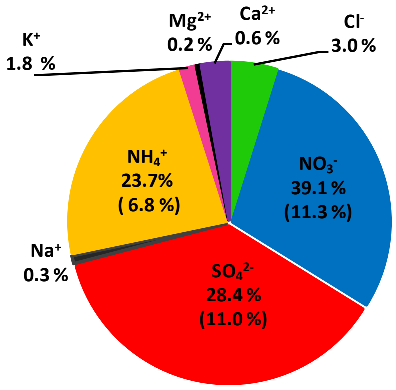

(c) Clear events: $PM_{2.5}$ = 22 ± 9 μg m^{-3}

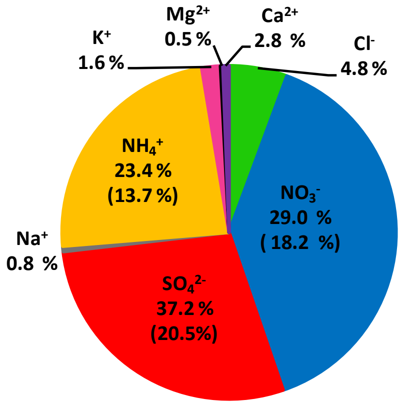

Figurer 2 Abundance of each species in TWSIIs during the (a) entire, (b) haze ($PM_{2.5}$ ≥ 150 μg m^{-3}) and (c) clear ($PM_{2.5} < 35$ μg m^{-3}) events. The numbers in the parentheses are standard deviations.

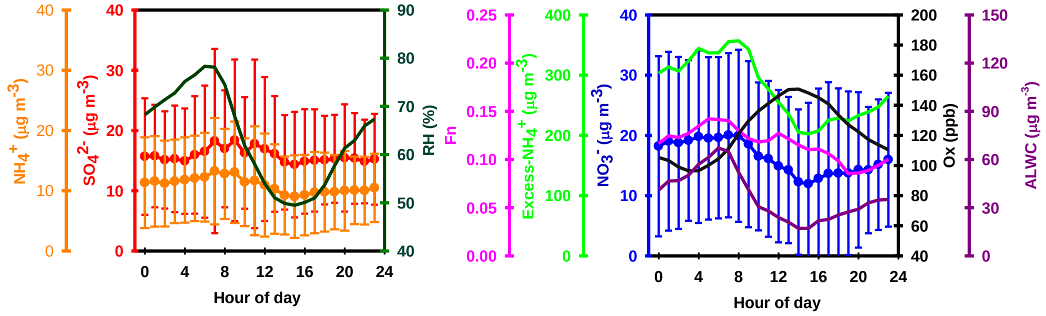

(b) Summer

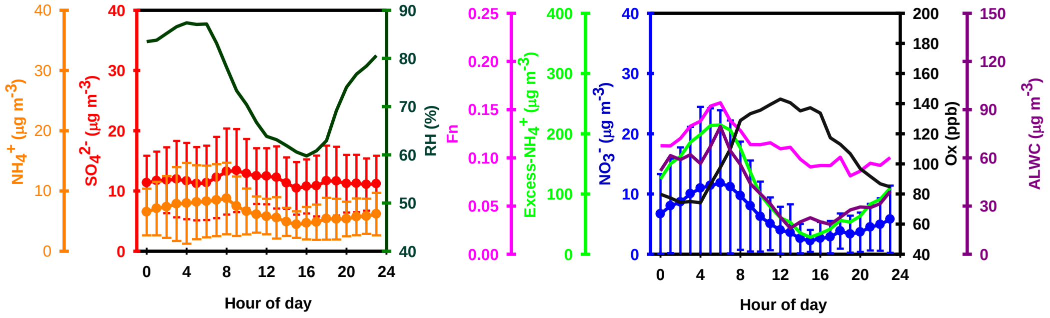

(c) Winter

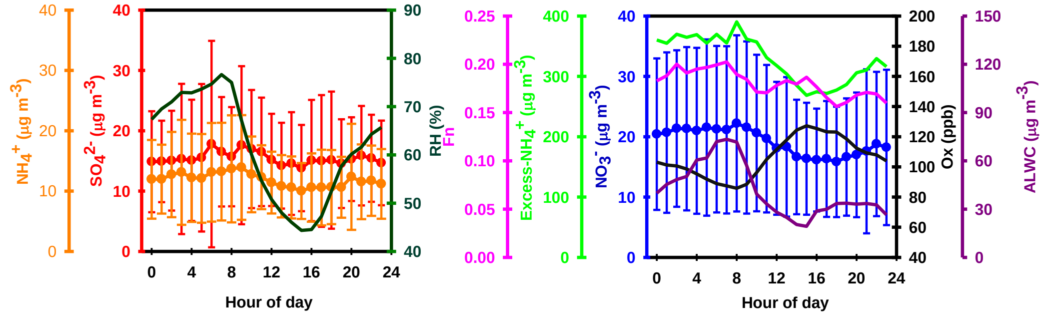

Figure 3 Diurnal variations of the concentrations of NO_3^-, SO_4^{2-} and NH_4^+, excess-NH_4^+, Ox and ALWC, and nitrogen conversion ratio (Fn) as well as ambient relative humidity in Nanjing during the sampling periods. For SO_4^{2-}, NO_3^- and NH_4^+, the mean values (dots) and standard deviations (solid lines) are plotted.

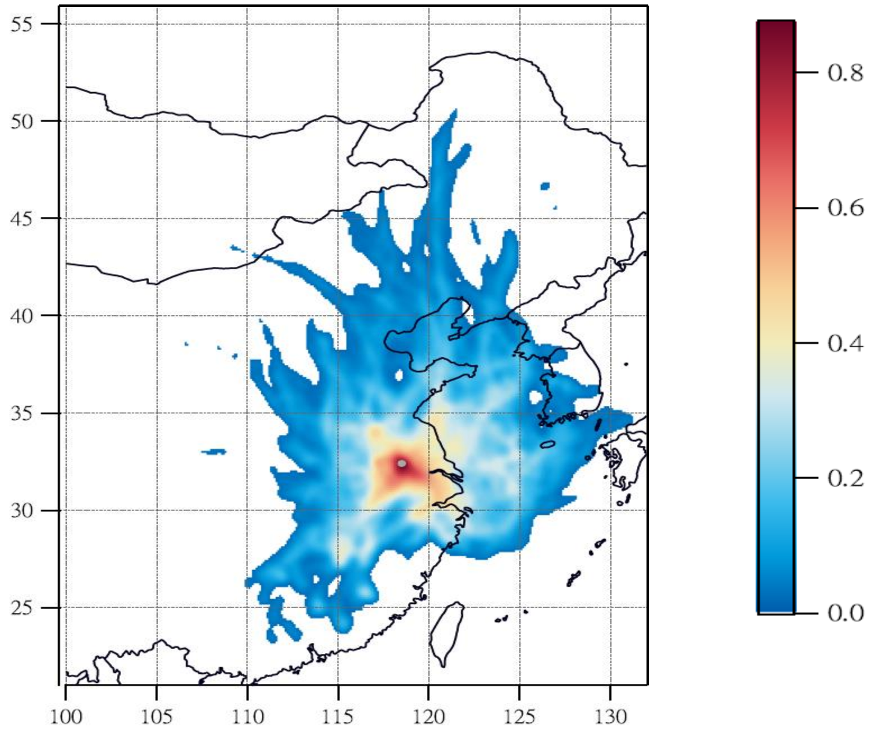

Figure 4 The PSCF maps of high nitrate pollution.

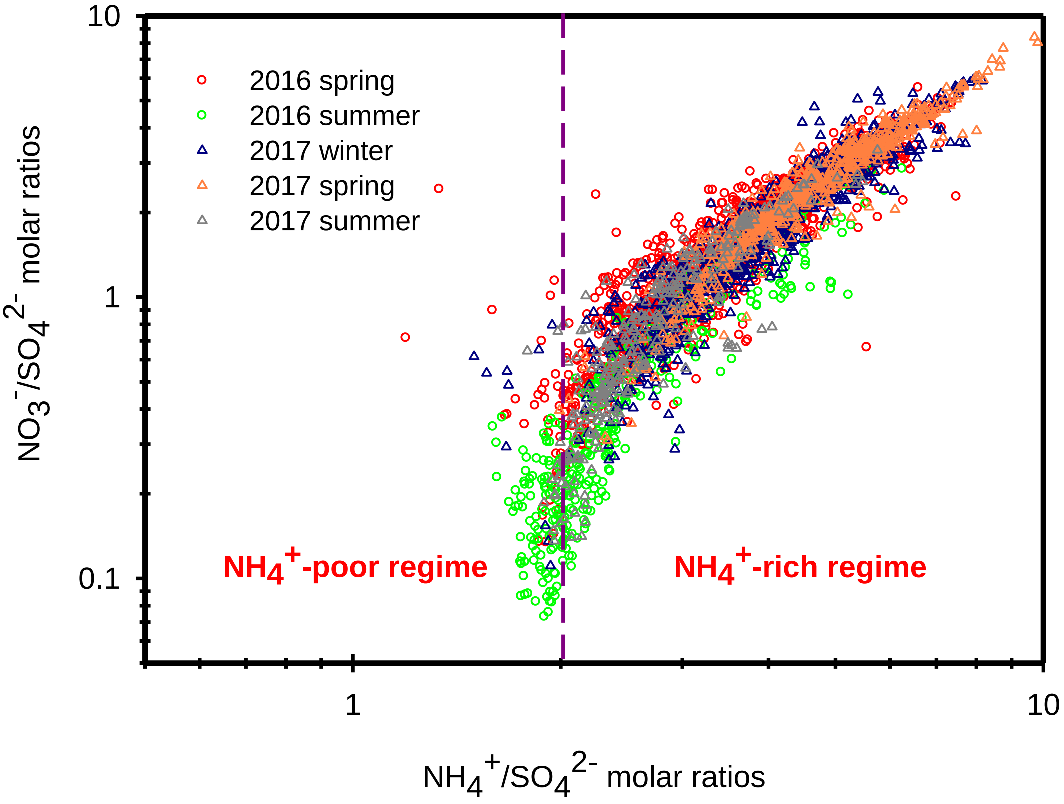

Figure 5 Scatter plots of molar ratios of NO_3^-/SO_4^{2-} against NH_4^+/SO_4^{2-} in Nanjing during the different seasons.

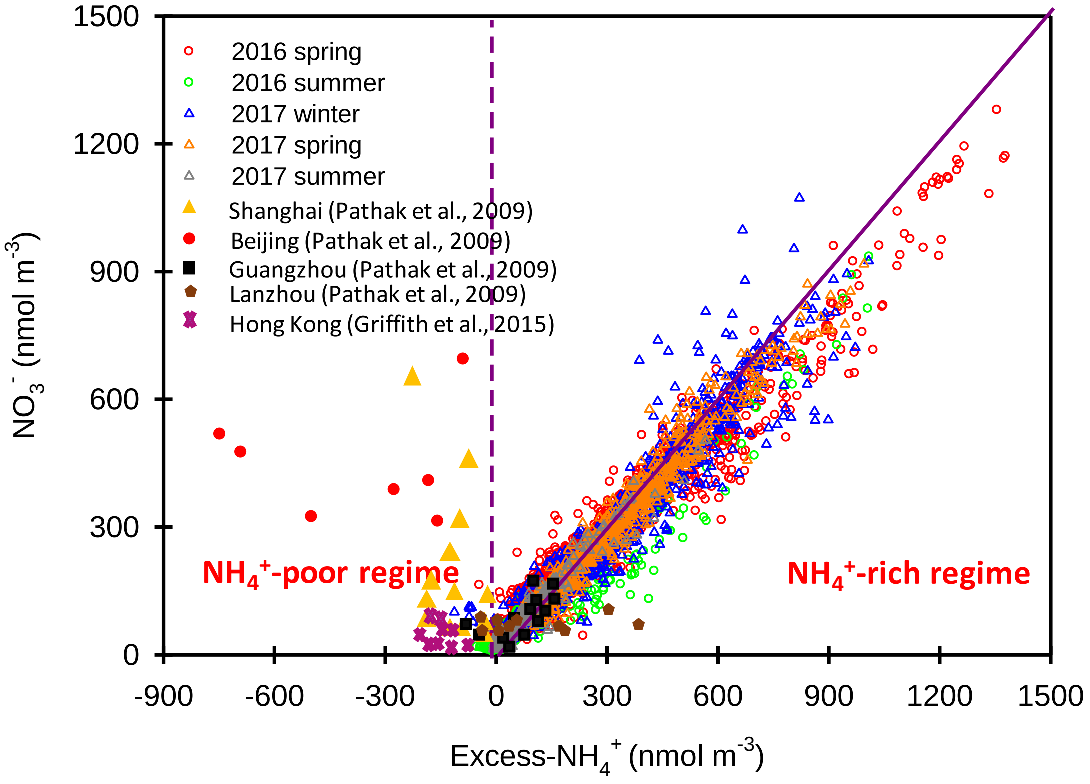

Figure 6 Scatter plot of NO_3^- vs. excess-NH_4^+ molar concentrations in Nanjing during the different seasons. The results in Beijing, Shanghai, Guangzhou, Lanzhou and Hong Kong are also shown in this figure.

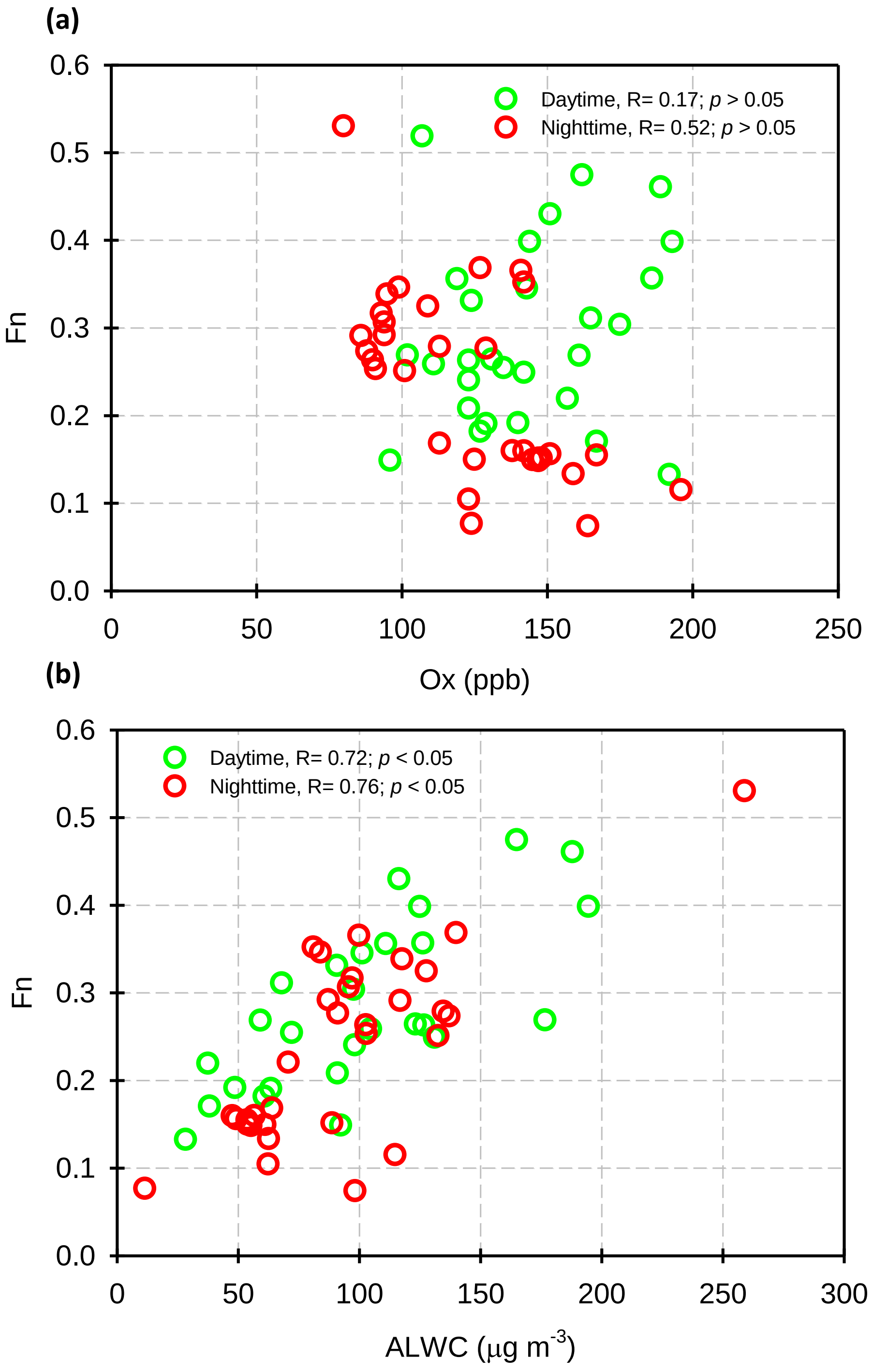

Figure 7 Scatter plots of (a) Fn against Ox and (b) Fn against ALWC in daytime and nighttime aerosol samples during the high hourly $PM_{2.5}$ concentration conditions (hourly $PM_{2.5} \geqq 150\ \mu g\ m^{-3}$).

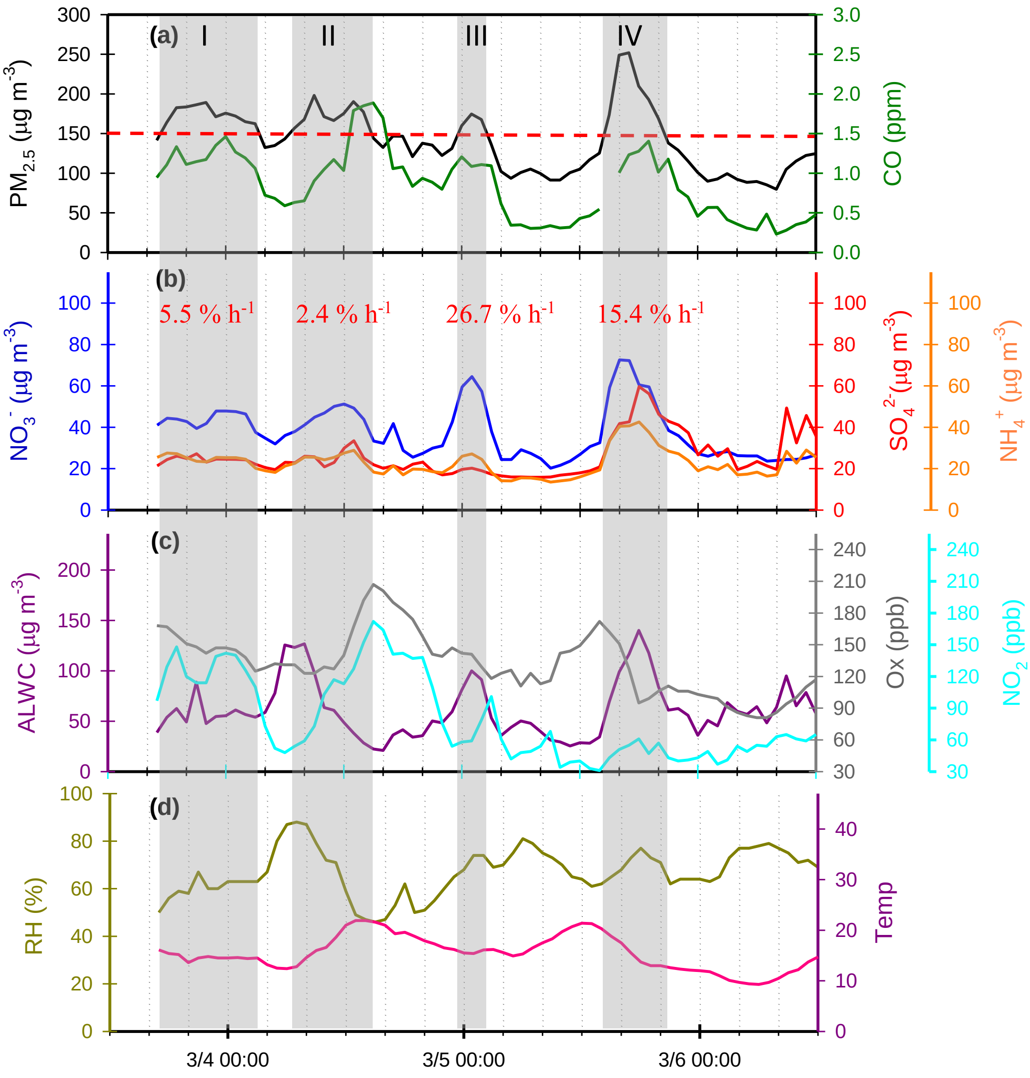

Figure 8 Time series of concentrations in (a) PM$_{2.5}$ mass and CO, (b) SIA species (NO_3^-, SO_4^{2-} and NH_4^+), (c) ALWC, Ox and NO$_2$ and (d) RH and T in Nanjing City from March 3 to 6, 2016. The grey shadows denote PM$_{2.5}$ episodes. The red numbers represent NO_3^- production rate during the PM$_{2.5}$ episodes.

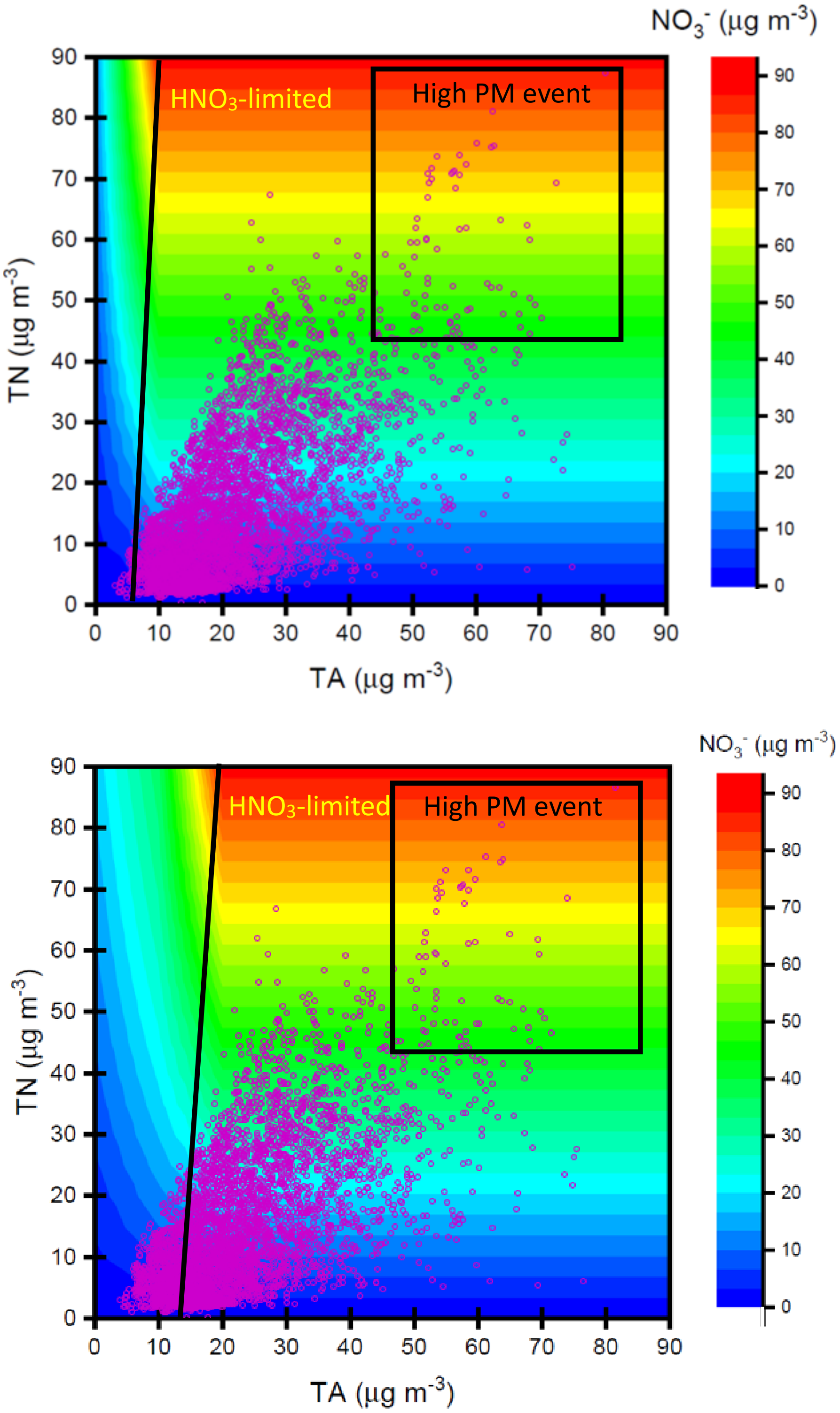

Figure 9 Nitrate concentrations simulated by ISORROPIA II model depending on TN and TA concentrations under (a) SO_4^{2-} = 10 µg m^{-3} and (b) SO_4^{2-} = 60 µg m^{-3}. The purple dots denote the observed TN and TA concentrations at the receptor site during the sampling periods.

Changes are marked in blue color

Heterogeneous Formation of Particulate Nitrate under Ammonium-rich Regime during the High $PM_{2.5}$ Events in Nanjing, China

Yu-Chi Lin[1,2,3], Yan-Lin Zhang[1,2,3*], Mei-Yi Fan[1,2,3], Mengying Bao[1,2,3]

[1]. Yale-NUIST Center on Atmospheric Environment, International Joint Laboratory on Climate and Environment Change, Nanjing University of Information Science and Technology, Nanjing, 210044, China.

[2]. Key Laboratory Meteorological Disaster; Ministry of Education & Collaborative Innovation Center on Forecast and Evaluation of Meteorological Disaster, Nanjing University of Information Science and Technology, Nanjing, 210044, China.

[3]. Jiangsu Provincial Key Laboratory of Agricultural Meteorology, College of Applied Meteorology, Nanjing University of Information Science & Technology, Nanjing 210044, China.

Corresponded to Yan-Lin Zhang (dryanlinzhang@outlook.com; zhangyanlin@nuist.edu.cn)

ABSTRACT

Particulate nitrate (NO_3^-) not only influences regional climates but also contributes to the acidification of terrestrial and aquatic ecosystems. In 2016 and 2017, four intensive online measurements of water-soluble ions in $PM_{2.5}$ were conducted in Nanjing City to investigate the potential formation mechanisms of particulate nitrate. During the sampling periods, NO_3^- was the most predominant species, accounting for 35 % of the total water-soluble inorganic ions, followed by SO_4^{2-} (33 %) and NH_4^+ (24 %). Significant enhancements of nitrate aerosols in terms of both absolute concentrations and relative abundances suggested that NO_3^- was a major contributing species to high-$PM_{2.5}$ events (hourly $PM_{2.5}$ ≧ 150 μg m^{-3}). High NO_3^- concentrations mainly occurred under NH_4^+-rich conditions, implying that the formation of nitrate aerosols in Nanjing involved NH_3. During the high-$PM_{2.5}$ events, the nitrogen conversion ratios (Fn) were positively correlated with the aerosol liquid water content (ALWC, R > 0.72, $p < 0.05$). Meanwhile, increasing NO_3^- concentrations regularly coincided with increasing ALWC and decreasing Ox (Ox = O_3 +NO_2). These results suggested that the heterogeneous reaction was probably a major mechanism of nitrate formation during the high-$PM_{2.5}$ events. Moreover, the average production rate of NO_3^- by heterogeneous processes was estimated to be 12.6 % h^{-1} (4.1 μg m^{-3} h^{-1}), which was much higher than that (2.5 % h^{-1}, 0.8 μg m^{-3} h^{-1}) of gas-phase reactions. This can also explain the abrupt increase of nitrate concentrations during the high $PM_{2.5}$ events. Utilization of ISORROPIA II model, we found that nitrate aerosol formation in Nanjing during the high-$PM_{2.5}$ events was HNO_3-limited. This indicated that the control of NOx emissions will be able to efficiently reduce airborne nitrate concentrations and improve the air quality in this industrial city.

Keywords: Nitrate aerosols, nitrogen conversion ratios, NH_4^+-rich regime, Hydrolysis of N_2O_5, Nitrate production rate

1. Introduction

Due to the rapid growth of industrialization and urbanization, particulate matter (PM) pollution has become a severe problem in China in recent years (Chan and Yao, 2008; Zhang and Cao, 2015). Fine mode particles ($PM_{2.5}$, with aerodynamic diameters less than 2.5 μm) exhibit smaller sizes and contain many toxins emitted from anthropogenic emissions (Huang et al., 2018). $PM_{2.5}$ easily penetrates the upper respiratory tract and is deposited into the human body, causing serious threats to human health. Numerous previous studies have proven that people exposed to high

$PM_{2.5}$ concentrations show increased risks of respiratory illness, cardiovascular diseases and asthma (Brauer et al., 2002; Defino et al., 2005), resulting in an increase of mortality (Nel, 2005).

Secondary inorganic aerosols (SIA), including sulfate (SO_4^{2-}), nitrate (NO_3^-) and ammonium (NH_4^+), are major constituents of $PM_{2.5}$, accounting for 25 - 60 % of the $PM_{2.5}$ mass in urban cities of China (Huang et al.,2014a; Wang et al., 2018; Yang et al., 2005; Ye et al., 2017; Zhao et al., 2013; Zhou et al., 2018). Among these species, SO_4^{2-} and NO_3^- are acidic ions which tend to be neutralized by NH_4^+. Previously, many studies suggested that SO_4^{2-} dominated SIA in urban cities of China (Kong et al., 2014; Tao et al., 2016; Yang et al., 2005; Yao et al., 2002; Zhao et al., 2013). In recent years, the Chinese government reduced its anthropogenic emissions by 62 % and 17 % for SO_2 and NOx, respectively (Zheng et al., 2018). This revealed that the reduction efficiency of SO_2 emissions were much higher than those of NOx. Consequently, nitrate has become the dominant species of SIA, especially during PM haze events (Wang et al., 2018; Wen et al., 2015; Zou et al., 2018).

In the atmosphere, ammonium nitrate (NH_4NO_3) is a major form of nitrate aerosols in fine mode particles. NH_4NO_3 is a semi-volatile species which partitions from the particle phase into the gas phase under high-temperature (T) conditions. It deliquesces when the ambient relative humidity (RH) is higher than its deliquescence relative humidity (DRH, nearly 62 % RH at atmospheric standard condition). To produce NH_4NO_3, nitrogen oxides (NO_x) and ammonia (NH_3) undergo a series of chemical reactions. NO_x mostly emits as fresh NO, which is subsequently oxidized to NO_2 and reacts with hydroxyl (OH) radicals to generate nitric acid (HNO_3), and then HNO_3 reacts with NH_3 to yield NH_4NO_3 particles as listed in R1 and R2 (Calvert and Stockwell, 1983). Particulate NH_4NO_3 formation rate is profoundly dependent on the ambient T and RH since both parameters influence the equilibrium constant of NO_3^-

and NH_4^+ between the particle and gas phases, as listed in R2 (Lin and Cheng, 2007).

$$NO_{2(g)} + OH_{(g)} \rightarrow HNO_{3(g)} \qquad k_1 \qquad (R1)$$

$$HNO_{3(g)} + NH_{3(g)} \rightarrow NH_4NO_{3(s,\ aq)} \qquad k_2 \qquad (R2)$$

Here, k_1 and k_2 are the reaction rate and equilibrium constant of R1 and R2, respectively. The equilibrium constant k_2 can be expressed as the product of HNO_3 and NH_3.

Heterogeneous reactions have been considered an important mechanism of nitrate formation during the nighttime. As listed in R3, liquid HNO_3 is produced by the hydrolysis of dinitrogen pentoxide (N_2O_5) on aerosol surfaces (Brown & Stutz, 2012; Chang et al., 2011; Mental et al., 1999; Wahner et al., 1998). Liquid HNO_3 can be neutralized by NH_4^+, which is produced from the conversion of gaseous NH_3. Nitrate aerosols yielded from both R2 and R3 require NH_3, and we can therefore consider these processes of NO_3^- formation to occur under NH_4 -rich conditions. Sometimes, there is not enough NH_3 (NH_4^+) to react (to be neutralized) with HNO_3 (NO_3^-) after complete neutralization by H_2SO_4. Under this condition, HNO_3 tends to react (or to be neutralized) with other alkaline species such as Ca-rich dust ($CaCO_3$), and subsequently, nitrate aerosol is produced under a NH_4^+-poor regime (Goodman et al., 2000).

$$N_2O_{5(g)} + H_2O_{(l)} \rightarrow 2HNO_{3(aq)} \qquad (R3)$$

The Yangtze River Delta (YRD) region is one of the well-known polluted areas in China (Zhang and Cao, 2015). Different from the case of dramatic elevated sulfate aerosol levels in Beijing (Wang et al., 2016), nitrate aerosols seemed to be a major contributing species during haze days in the YRD region (Wang et al., 2015; Wang et al., 2018). The formation mechanisms of nitrate in Nanjing have not yet been well understood, especially during high PM events. In this study, four intensive online measurements of water-soluble ions in $PM_{2.5}$ were conducted in Nanjing City in 2016 and 2017. The data provided information on the hourly evolution of water-soluble inorganic ions (WSIIs) in the industrial city. The NO_3^- distributions under different NH_4^+ regimes (NH_4^+-poor and NH_4^+-rich conditions) were also discussed. Finally, we investigated the potential formation mechanisms of nitrate aerosols and their production rates during high-$PM_{2.5}$ events based on the online measurements.

2. Methodology

2.1 Sampling site

Particulate WSIIs and inorganic gases were continuously monitored at Nanjing University of Information Science and Technology (NUIST) located in the northern part of Nanjing City (see Figure S1). In addition to the contributions from vehicle emissions, petroleum chemical refineries and steel manufacturing plants are situated in the northeast and east direction at a distance of approximately 5 km. Four intensive campaigns were conducted from March 2016 to August 2017. During each experiment, the hourly concentrations of WSIIs in $PM_{2.5}$ and inorganic gases were continuously observed. Meanwhile, the hourly $PM_{2.5}$, NO_2 and O_3 concentrations along with the ambient T and RH were acquired from the Pukou air quality monitoring station which is located to the southwest of the receptor site.

2.2 Instruments

To monitor the hourly concentrations of WSIIs (Cl^-, NO_3^-, SO_4^{2-}, Na^+, NH_4^+, K^+, Mg^{2+} and Ca^{2+}), an online Monitor for Aerosols and Gases (MAGAR, Applikon-ENC, The Netherlands) instrument with a $PM_{2.5}$ inlet was employed. Using this instrument, the WSIIs in $PM_{2.5}$ were collected by a stream jet aerosol collector, while acidic (HCl, HONO, HNO_3 and SO_2) and basic gases (NH_3) were dissolved in a hydrogen peroxide solution on a wet rotation denuder (ten Brink et al., 2007; Griffith, et al., 2015). The liquid samples were then collected with syringe pumps and analyzed by ion chromatography (IC). Before each campaign, a seven-point calibration curve of each species was made, and an internal standard solution (LiBr) was used to check instrumental drifts. The method detection limits (MDLs) of Cl^-, NO_3^-, SO_4^{2-}, Na^+, NH_4^+, K^+, Mg^{2+} and Ca^{2+} were, 0.01, 0.04, 0.06, 0.05, 0.05, 0.07, 0.05 and 0.11 μg m^{-3}, respectively. For gases, the MDLs were 0.07, 0.09, 0.06, 0.02 and 0.08 μg m^{-3} for HCl, HONO, HNO_3, SO_2 and NH_3, respectively.

2.3 ISORROPIA-II model

In this work, we used the ISORROPIA-II model to calculate the aerosol liquid water content (ALWC). ISORROPIA II is a thermodynamic equilibrium model which is built based on the Na^+ - Cl^- - Ca^{2+} - K^+ - Mg^{2+} - SO_4^{2-} - NH_4^+ - NO_3^- - H_2O aerosol system (Fountoukis & Nenes, 2007). This model has been successfully used to estimate the liquid water content in aerosols with uncertainty of ~ 20 % compared to the observed ALWC (Bian et al., 2014; Guo et al., 2015; Liu et al., 2017). This underestimation might be due to the missed species in ISORROPIA II, organic aerosols, , which contributed approximately 27 % of the total ALWC (Bougiatioti et al., 2007). Here, the model was computed as a “forward problem”, in which the quantities of aerosol- and gas-phase compositions along with the T and RH were well known. Additionally, the modeled values were determined using the “metastable” mode, which indicated that the aerosol compositions were assumed to be composed of an aqueous solution (Liu et al., 2017). The details of this model can be found elsewhere (Fountoukis and Nenes, 2007). In this work, the observed concentrations of total nitrate (HNO_3+NO_3^-), total ammonium (NH_3 + NH_4^+), total chloride (HCl + Cl-), SO_4^{2-}, Na^+, K^+, Mg^{2+} and Ca^{2+} along with measured ambient T and RH served as input of ISORROPIA II model.

2.4 Potential source contribution function

Potential source contribution function (PSCF) is a method to identify the potential source regions of air pollutants. It has also been widely used to differentiate local emission from long-range transported pollution (Zhang et al., 2013; Hui et al., 2018) based on the trajectory analysis calculated from GDAS (Global Data Assimilation System), which processed by the National Centers for Environmental Prediction (NCEP). The zone of concern is divided into $i \times j$ small equal grid cells and then PSCF in the *i-jth* cell ($PSCF_{ij}$) can be defined as (Polissar et al., 1999):

$$PSCF_{ij} = \frac{m_{ij}}{n_{ij}} \tag{1}$$

where m_{ij} is the number of “high nitrate pollution” trajectory endpoints in the *i-jth* cell and n_{ij} is the total number of trajectory endpoints fallen into the *i-jth* cell. In this study, the 80th percentile value of nitrate concentration was treated as “high nitrate pollution” threshold. To reduce the uncertainty caused by the small values of n_{ij}, the weighting function of W_{ij} has to be considered (Polissar et al., 1999):

$$Wij = \left\{ \begin{array}{l} 1.00;\ 80 < n_{ij} \\ 0.70;\ 20 < n_{ij} \leqq 80 \\ 0.42;\ 10 < n_{ij} \leqq 20 \\ 0.05;\ n_{ij} \leqq 10 \end{array} \right\}$$

In this study, the domain of the study area was in a range of 20-55 °N and 105-135 °E; the resolution of grid cell was 0.5°×0.5°.

3. Results and discussion

3.1 Overview of water-soluble inorganic ions

Four intensive online measurements of WSIIs in $PM_{2.5}$ were carried out in Nanjing City from March 2016 to August 2017. Figure 1a plots the time series of the hourly $PM_{2.5}$ mass concentrations during the sampling periods. As seen, the hourly $PM_{2.5}$ mass concentrations varied from 5 to 252 μg m^{-3} with a mean value of 58 ± 35 μg m^{-3}. Compared with the 24-hour guideline (25 μg m^{-3}) suggested by the World Health Organization (WHO), our average $PM_{2.5}$ concentration (58 μg m^{-3}) was 2.3 times higher. This indicated that PM pollution in Nanjing City was a serious problem. During the campaigns, several high-$PM_{2.5}$ events with hourly $PM_{2.5}$ concentrations of higher than 150 μg m^{-3} were observed in the springtime and wintertime. These high $PM_{2.5}$ levels lasted for more than 3 hours, with obviously elevated NO_3^-. The details of nitrate formation during the high-$PM_{2.5}$ hours will be discussed in the following sections.

Figure 1b shows the time series of the hourly concentrations of SIA species, including SO_4^{2-}, NO_3^- and NH_4^+. The lack of data from March 7 to 14, 2016 was due to a malfunction of the MARGA instrument. During the sampling periods, the NO_3^- concentrations varied from 0.1 to 85.1 μg m^{-3} with a mean value of 16.7 ± 12.8 μg m^{-3}. The SO_4^{2-} concentrations ranged from 1.7 to 96.2 μg m^{-3} and averaged 14.9 ± 9.1 μg m^{-3}. The NH_4^+ concentrations fluctuated between 0.8 and 44.9 μg m^{-3} with a mean value of 10.7 ± 6.7 μg m^{-3}. On average, SIA accounted for 91 % of the total water-soluble inorganic ions (TWSIIs) during the entirety of the sampling periods (see Figure 2a). Among these species, NO_3^- accounted for 35 % of the TWSIIs, followed by SO_4^{2-} (33 %) and NH_4^+ (24 %). The abundances of other ions, including Cl^-, K^+, Ca^{2+}, Na^+ and Mg^{2+}, were 5, 2, 1, 0.7 and 0.3 %, respectively. Figure S2 shows the scatter plot of the equivalent concentrations of the cations (Na^+, NH_4^+, K^+, Mg^{2+} and

Ca^{2+}) and anions (Cl^-, SO_4^{2-} and NH_4^+). As seen, good correlations (R = 0.98 -0.99, with a significance level $p<0.05$) between cations and anions were found during the various sampling periods. The ratio of cation-to-anion was very close to 1.0 during each season, reflecting an ionic balance. This also indicated that our data exhibited good quality and was able to be used for the further analysis of scientific issues.

All SIA species exhibited similar seasonal patterns, with lower concentrations in the summer, especially for NO_3^-. The average concentrations of nitrate were 6.7 and 5.7 μg m^{-3} in the summertime of 2016 and 2017, respectively (see Figure S3). These values were much lower than those observed during other seasons. The local meteorological conditions, which were favorable for the dilution of air pollution, were one of the reasons for the declined NO_3^- concentrations during the hot seasons (Zhang and Cao, 2015). Another important reason for this effect was attributed to the formation process of $PM_{2.5}$ nitrate, which is very sensitive to the ambient T and RH (Lin and Cheng, 2007). Figure S4a depicts the theoretical equilibrium constants of partitioned NO_3^- and NH_4^+ between the particle and gas phase ($HNO_{3(g)} + NH_{3(g)} \rightarrow NH_4NO_{3(s,\ aq)}$ as seen in R2) under different T and RH conditions. The details of calculation approach of the theoretical equilibrium constants are described in *Supplementary S1*. Note that the *Y-axis* is presented on a log scale. The theoretical equilibrium constants increased exponentially with increasing ambient temperature but decreased with increasing RH. This indicated that NH_4NO_3 would be partitioned into the gas phase due to high equilibrium constants under high-temperature and low-RH conditions. Figure S4b illustrates the time series of the theoretical and observed equilibrium constants during the sampling periods. As can be seen, most of the observed equilibrium constants were higher than the theoretical ones, suggesting that NH_4NO_3 aerosols were produced in Nanjing during the sampling periods. Obviously, higher theoretical and lower observed equilibrium constants were found during the summer. This suggested that more NO_3^- and NH_4^+ would tend to be partitioned into the gas phase, resulting in lower particulate nitrate concentrations during hot seasons (Lin and Cheng, 2007).

Apart from seasonal variations, pronounced diurnal patterns were also found for SIA species (see Figure 3). NO_3^- exhibited similar diel cycles during different seasons, with higher concentrations in the early morning (3 a.m. - 7 a.m.) and lower levels between 2 p.m. and 5 p.m. The high nitrate concentrations in the early morning might be caused by the nitrate formation via heterogeneous reaction in the dark, and gas-phase oxidation after sunrise and the subsequent condensation on pre-existing particles before the temperature increased and RH decreased afterwards. Moreover, the lower planet boundary layer (PBL) might be another reason for enhanced nitrate in the early morning. However, the lower concentrations of nitrate during the daytime might be attributed to the higher PBL, and high temperatures, which inhibited the build-up of nitrate, especially during the summertime. In terms of sulfate, higher concentrations were observed between 6 am. and 1 p.m., indicating that the formation rate of sulfate was higher than the removal/dilution rate, leading to an increase of the sulfate concentration during the daytime. The diurnal patterns of NH_4^+ mimicked those of NO_3^-, showing lower concentrations during the daytime. This was explained by the drastic decrease of particulate NH_4NO_3 concentrations under high temperatures and low relative humidity, resulting in lower NH_4^+ levels during the daytime.

3.2 Enhancements of nitrate at high $PM_{2.5}$ levels

Figure S5 shows the scatter plots of NO_3^-, SO_4^{2-} and NH_4^+ against $PM_{2.5}$. As seen, the slopes of NO_3^- (NO_3^- vs. $PM_{2.5}$ mass), SO_4^{2-} and NH_4^+ were 0.30, 0.24 and 0.19, respectively. This suggested that the increasing rate of NO_3^- during the high-$PM_{2.5}$ events was higher than those of other SIA species. At high $PM_{2.5}$ levels ($PM_{2.5} \geq$

150 μg/m^3), NO_3^-, SO_4^{2-} and NH_4^+ contributed 39, 28 and 24 % of the TWSIIs, respectively (Figure 2b). However, the relative abundances of NO_3^-, SO_4^{2-} and NH_4^+ during low $PM_{2.5}$ concentrations (hourly $PM_{2.5}$ < 35 μg/m^3, see Figure 2c) were 29, 37 and 23 %, respectively. In recent years, dramatically enhanced amounts of nitrate aerosols during high-PM events have been observed at many urban sites in China (Wen et al., 2015; Wang et al., 2017; 2018; Zou et al., 2018). For instance, Zou et al. (2018) found that the nitrate concentrations during the occurrence of polluted air in Beijing and Tianjin were almost 14 times higher than those on relatively clean days ($PM_{2.5}$ < 75 μg/m^3), and the enhancement ratio of nitrate was much higher than that (5.3) of sulfate. Wang et al. (2018) noted that the enhancement ratio of NO_3^- (~6) between haze and clear days in Ningbo of the YRD region was much higher than that of SO_4^{2-} (~3). These findings suggested that NO_3^- was a major contributing species to fine particles during haze days since its increasing ratio between haze and non-haze days was much higher than those of other SIA species, such as sulfate and ammonium.

3.3 PSCF result of high nitrate pollution

During the high $PM_{2.5}$ pollution, significant enhanced nitrate aerosols in terms of both absolute concentration and relative abundance to TWSIIs were found. Next, we tried to use PSCF analysis to identify whether local emission or long-range transported pollution was the major source of high nitrate concentrations at the receptor site. In this work, the 80th percentile values of nitrate concentration was selected as "high nitrate pollution" threshold for PSCF analysis. Figure 4 plots the PSCF result of high nitrate pollution in Nanjing during the sampling periods. The region corresponding to high PSCF value grid is a potential source region of nitrate aerosols. As can be seen, the areas with high PSCF value (>0.8) were regularly local areas surrounding by Nanjing while PSCF values from other long-distance areas were lower than 0.2. This suggested that NO_3^- aerosols in Nanjing during the high nitrate pollution were likely from local emissions rather than long-range transported sources.

3.4 Nitrate formation under different ammonium regimes

Ammonium is a major species that neutralizes particulate SO_4^{2-} and NO_3^-. In the atmosphere, SO_4^{2-} competes with NO_3^- for NH_4^+ during their formation processes, and therefore, the relationship between the molar ratios of NO_3^-/SO_4^{2-} and NH_4^+/SO_4^{2-} can give us a hint for understanding the formation of NO_3^- under different ammonium regimes (Pathak et al., 2009; He et al., 2012; Tao et al., 2016). In an ammonium-rich regime, the HNO_3 produced by both gas oxidation and heterogeneous process reacts (or neutralizes) with "excess-ammonium" (excess-NH_4^+) at a NH_4^+/SO_4^{2-} molar ratio > 2 (theoretical value in an NH_4^+-rich regime) when sulfate is completely neutralized by NH_4^+ to form $(NH_4)_2SO_4$ (Squizzato et al., 2013; Ye et al., 2011). In contrast, nitrate can be found under ammonium-poor conditions with a theoretical NH_4^+/SO_4^{2-} value that should be less than 2 (Pathak et al., 2009). Under NH_4^+-poor conditions, HNO_3 reacts with other cations, such as the calcium carbonate frequently found in natural dust.

Figure 5 shows the scatter plot of the molar ratios of NO_3^-/SO_4^{2-} against NH_4^+/SO_4^{2-}. It is found that good correlations exist between NO_3^-/SO_4^{2-} and NH_4^+/SO_4^{2-} under NH_4^+-rich regimes, with a coefficient of determination (R^2) of 0.84 - 0.94 in the different seasons (see in Table 1). Utilizing the linear regression model, we suggested that nitrate aerosols (in NH_4^+-rich regimes) began to form when the NH_4^+/SO_4^{2-} molar ratios exceeded the criterion values of 1.7-2.0 during the different seasons (Table 1). The criterion value can be calculated as absolute value of "intercept" dividing by slope in each linear regression model (He et al., 2012). The criterion values below 2 suggested that part of the sulfate might have existed in other forms, such as ammonium bisulfate. On the other hand, under ammonium-rich conditions, nitrate concentrations should be positively proportional to "excess-NH_4^+" concentrations, a relationship which was defined as [excess-NH_4^+] = (NH_4^+/SO_4^{2-} - criterion value) × [SO_4-$^{2-}$] (Pathak et al., 2009) (sulfate is in the units of nmol m^{-3} here). The criterion values were acquired from the regression models, as listed in Table 1. The results revealed that the excess-NH_4^+ concentrations varied from -283 to 1422 nmol m^{-3} (see Figure 6), and only 1 % of data showed deficit-NH_4^+ conditions, reflecting that NO_3^- formation in Nanjing occurred primarily under the NH_4^+-rich conditions. Moreover, the excess-NH_4^+ had apparent diurnal cycles, with higher concentrations in the early morning and lower concentrations at midday and in the early afternoon (see Figure 3, where we converted the units from nmol m^{-3} to µg m^{-3}). The diurnal patterns of NO_3^- mimicked those of the excess-NH_4^+. This also suggested that particulate NO_3^- formation occurred mainly under NH_4^+-rich conditions. Figure 6 illustrates the relationship between the nitrate and excess-NH_4^+ molar concentrations during the sampling periods. The nitrate molar concentrations correlated linearly with the excess-NH_4^+ molar concentrations with a slope of approximately 1.0, which was consistent with the molar ratio of reaction between HNO_3 and NH_3. Interestingly, some scattered points were found in high ammonium concentrations (excess-NH_4^+ ≧ 900 nmol m^{-3} ~ 16.2 µg m^{-3}), implying that residual NH_4^+ might be presented in another form such as NH_4Cl under high-NH_4^+ conditions. On the contrary, NO_3^- aerosols can be produced without involving NH_3; therefore, NO_3^- did not correlate well with the excess NH_4^+ under a NH_4^+-poor regime.

In this study, high nitrate concentrations were always found under NH_4^+-rich regimes, elucidating that nitrate production during high PM levels in Nanjing had to be involved with NH_3 or NH_4^+. Figure 6 also shows the nitrate concentrations against the excess-NH_4^+ observed in various cities of China during the summertime (Pathak et al., 2009; Griffith et al., 2015). In Beijing and Shanghai, high nitrate concentrations during the summertime were found under NH_4^+-deficient conditions, which was very different from the findings of this work. In these studies (Pathak et al., 2009; Griffith et al., 2015), the high nitrate concentrations associated with NH_4^+-poor conditions might be due to the lower excess-NH_4^+ concentrations under high-SO_4^{2-} conditions at that time since the strict control of SO_2 emissions by the Chinese government started in 2010 (Zheng et al., 2018). In recent years, the reduction of anthropogenic SO_2 emissions decreased the airborne SO_4^{2-} concentrations, resulting in more excess-NH_4^+ and leading to nitrate aerosol formation under NH_4^+-rich regimes. This argument can be supported by the recent results shown in Figure S6, in which high nitrate concentrations in Beijing were always found under NH_4^+-rich regimes.

3.5 Nitrate formation mechanism during high-$PM_{2.5}$ episodes

In this section, we attempted to explore the formation mechanisms of nitrate aerosols during high $PM_{2.5}$ levels. Here, nitrogen conversion ratio (Fn) was used to evaluate the conversion capability of NO_2 to total nitrate (TN, TN=HNO_3 + NO_3^-), and it can be defined as (Khoder, 2002; Lin et al., 2006):

$$F_n = \frac{GNO_3^- + PNO_3^-}{GNO_3^- + PNO_3 + NO_2} \qquad (1)$$

where GNO_3^- and PNO_3^- represent the NO_2 concentrations in nitric acid and particulate nitrate, respectively, with the units of μg m^{-3}. The results showed that the Fn values during the sampling periods varied from 0.01 to 0.57 with a mean value of 0.14 ± 0.09 (see Figure 1e). This value was comparable to that (0.17) in Taichung, Taiwan, where both gas-oxidation and heterogeneous reaction were the dominant formation mechanisms of atmospheric HNO_3 (or NO_3^-) (Lin et al., 2006). However, our Fn value was 2.3 time higher than that (0.06) in Dokki, Egypt (Khoder, 2002). The reason of significant discrepancy of Fn between this work and that in Dokki was not clearly understood, but it might be attributed to different formation processes of HNO_3. In Dokki, gas-phase oxidation was the dominant pathway of HNO_3 production while heterogeneous process (R3) played an important role in HNO_3 formation in addition to gas-phase oxidation in Nanjing, especially during the high-$PM_{2.5}$ events (discussed later). The reaction rate of HNO_3 by heterogeneous process was much higher than that by gas-phase oxidation (Calvert and Stockwell, 1983) and therefore, the Fn value was much higher in this study. On the other hand, Fn displayed significant diurnal cycles, with the highest value in the early morning (see in Figure 3). This elevated Fn coincided with increasing ALWC, suggesting heterogeneous reaction since ALWC is one of the key parameters which favors the transformation of N_2O_5 to liquid HNO_3 in this process (also indicated that nitrate formation was associated with heterogeneous process). On the contrary, a second peak of Fn was found in the early afternoon when Ox ($Ox = NO_2 + O_3$, an index of the oxidation capacity) concentrations increased, but ALWC decreased. This suggested that the HNO_3 formation might be mainly associated with the gas-phase reaction of NO_2 + OH during the daytime; also reflected that nitrate formation was via gas-phase oxidation.

Assuming that long-range transported nitrate can be neglected in this study (in section 3.3), we attempted to analyze the correlations of Fn vs. OH and Fn vs. ALWC to investigate whether gas-phase oxidation or heterogeneous reactions might be the dominant mechanism of nitrate production. In this work, the OH radical concentrations were not measured; hence, we used O_X as a proxy of OH. The ALWC was acquired by computing the ISOPROPIA II model as described in section 2.3. Figure 7 illustrates the scatter plots of Fn against Ox and ALWC in both daytime and nighttime aerosol samples during the high-$PM_{2.5}$ events. Fn correlated well with the ALWC, with a correlation coefficient (R) of 0.72 and 0.76 ($p < 0.05$) at daytime and nighttime samples, respectively. However, a poor correlation was found between Fn and Ox (R was 0.17 and 0.52 for the daytime and nighttime samples, $p>0.05$). This implied that nitrate formation during the high-$PM_{2.5}$ events in Nanjing was likely attributed to heterogeneous reactions. This result was consistent with recent conclusions reached by oxygen isotope techniques, in which the hydrolysis of N_2O_5 in preexisting aerosols was found to be a major mechanism of NO_3^- formation (Chang et al., 2018).

3.6 Case study and production rate of NO_3^- during $PM_{2.5}$ episodes

Figure 8 shows several high-$PM_{2.5}$ events observed from March 3 to 6 in 2016. In case I, the high $PM_{2.5}$ concentrations started at 6 p.m. on March 3 and ended at 3 a.m. on March 4. During this event, the SO_4^{2-} and NH_4^+ concentrations remained at almost constant levels, but the NO_3^- concentrations revealed a slight enhancement. In the early morning of March 4, the NO_3^- concentrations increased from 39.4 to 47.8 μg m^{-3} within 4 hours, resulting in a nitrate production rate of 2.3 μg m^{-3} h^{-1} (~5.5 % h^{-1}, the calculation of NO_3^- production rate can be seen in the *Supplementary S2*). In case II, high $PM_{2.5}$ concentrations were observed from 8. a.m. to 2. p.m. on March 4. The NO_3^- concentrations were much higher than those of SO_4^{2-}, indicating nitrate-dominated aerosols. In this case, the NO_3^- concentrations increased from 38.1 to 51.2 μg m^{-3} within 6 hours, suggesting that the increasing rate of NO_3^- was 1.0 μg m^{-3} h^{-1} (2.4 % h^{-1}). Since the high NO_3^- concentrations occurred under high-Ox and low-ALWC conditions, this suggested that the gas-phase reaction of NO_2 + OH might be the dominant source of NO_3^- production in this event. In case III, a rapid growth of the $PM_{2.5}$ mass was found around midnight, along with a dramatic increase of NO_3^-

concentrations from 11 p.m. on March 4 (31.0 μg m^{-3}) and maximizing at 1 a.m. the next day (64.5 μg m^{-3}). The increasing rate of NO_3^- was estimated to be 11.4 μg m^{-3} h^{-1} (~19.5 % h^{-1}), which was much higher than those in case I and II. The high-nitrate event was found under increasing ALWC and decreasing Ox concentration conditions, suggesting that nitrate production occurred through heterogeneous processes. In case IV, the enhancements of all SIA species coincided with increasing ALWC and declining Ox concentrations. Again, the enhancement of nitrate was likely attributed to heterogeneous reactions rather than to gas-phase processes. In these events, the NO_3^- production rate was estimated to be 5.0 μg m^{-3} h^{-1} (~ 15.4 % h^{-1}).

Through the sampling periods, a total of twelve high $PM_{2.5}$ events were found, and the NO_3^- concentrations increased significantly during all the episodes (see in Table S1). Seven episodes suggested that heterogeneous processes ($N_2O_5 + H_2O$) might be a major pathway for nitrate formation since elevated NO_3^- levels coincided with increasing AWLC and decreasing Ox (or Ox remaining at a constant level). Among these heterogeneous process events, five cases (Case III, Case IX, Case X, Case XI and Case XII in Table S1) were observed during the nighttime (5 p.m. – 6 a.m. on the next day). This suggested that approximately 70 % heterogeneous reaction of nitrate production was observed in the dark. In these events, the average NO_3^- growth rate was 12.6 ± 7.3 % h^{-1} (4.1 ± 3.6 μg m^{-3} h^{-1}). This value was in agreement with those in the literatures which the production rate of nitrate via heterogeneous reaction were 14.3 % h^{-1} by both field measurements and laboratory works (Calvert and Stockwell, 1983; Pathak et al., 2011). On the contrary, NO_3^- concentrations rose with increasing Ox and decreasing ALWC in two $PM_{2.5}$ episodes, indicating gas-phase processes (NO_2 + OH). As listed in Table S1, these gas-phase reaction cases occurred mainly during the daytime. The average production rate of NO_3^- in the gas-oxidation reaction cases averaged 2.5 ± 0.1 % h^{-1} (0.8 ± 0.3 μg m^{-3} h^{-1}), which was in line with that (2.4

% h^{-1}) in the subtropical polluted urban site that nitrate aerosols were mainly from gas-oxidation process (Lin et al., 2007). Moreover, we also found some cases in which the elevated NO_3^- might have been from both gas-phase and heterogeneous reactions, and the corresponding NO_3^- growth rate was approximately 7.5 ± 3.0 % h^{-1}(2.5 ± 0.2 μg m^{-3} h^{-1}). In conclusion, enhancements of NO_3^- in Nanjing usually occurred under increased ALWC and decreased Ox conditions, indicating that heterogeneous reactions provided the dominant pathway of nitrate formation during the $PM_{2.5}$ episodes. Moreover, the average growth rate of NO_3^- (12.6 % h^{-1}) by heterogeneous processes was 5 times higher than that (2.5 % h^{-1}) of gas-phase reactions. This might explain the abrupt increase of nitrate concentrations during the high $PM_{2.5}$ events.

3.7 HNO_3/NH_3 limitation of nitrate aerosol formation

In Nanjing, high nitrate concentrations occurred mainly under NH_4^+-rich regimes, indicating the involvement of atmospheric NH_3. This also demonstrated that both HNO_3 and NH_3 were crucial precursors for particulate nitrate formation. In this section, we attempted to discuss whether HNO_3 or NH_3 was the limited factor for nitrate formation in Nanjing during the high-$PM_{2.5}$ events. ISORROIPA II model is capable of predicting concentrations of particulate ions in addition to ALWC under thermodynamic equilibrium between gas- and aerosol-phase of these ions (Tang et al., 2016). In section 3.5, we used this model to estimate ALWC. Indeed, the output data also included concentrations of ionic species. Figure S7 illustrates the scatter plots of modeled results against observations of NO_3^-, SO_4^{2-} and NH_4^+ in Nanjing during the sampling periods. Good correlations were found between modeled results and observations (R^2=0.97-0.99 with all slopes of approximately 1.0), suggesting that ISORROPIA II had a good performance in prediction of SIA species. As a result, we can use ISORROPIA II model to test sensitivity of HNO_3 and NH_3 to particulate nitrate concentrations (Guo et al., 2018).

Figure 7 shows the contour plot of the simulated nitrate concentrations depending on the various total nitrate (TN) and total ammonium (TA, TA=NH_3 + NH_4^+) levels under thermodynamic equilibrium conditions computed by ISORROPIA II model. The details of considered chemical reactions in ISORROPIA II model can be seen elsewhere (Fountoukis & Nenes, 2007). Here, sulfate concentrations were assumed to be 10 and 60 μg m^{-3} for the tests of different sulfate conditions. The average concentrations of total chloride (HCl + Cl^-, 1.3 μg m^{-3}), Na^+ (0.2 μg m^{-3}), K^+ (0.8 μg m^{-3}), Mg^{2+} (0.1 μg m^{-3}) and Ca^{2+} (0.5 μg m^{-3}) along with ambient T (20 °C) and RH (62 %) at the receptor site during the sampling period served as input data in this model. The results showed that the lower simulated NO_3^- concentrations was found in the higher SO_4^{2-} case. This was attributed to less NH_4NO_3 formation under higher SO_4^{2-} conditions since SO_4^{2-} would compete with NO_3^- for NH_4^+.

According to the simulated results, we can roughly split the plots into two parts: one is HNO_3-limited area (right), and another is NH_3-limited region (left). The observed TN and TA concentrations (pink circles) in Nanjing are also plotted in this figure. Most of the observed data sets were mainly affected by TN under a low-SO_4^{2-} case. Under a high-SO_4^{2-} condition, the observed data fell into TA-limited under a low-TN and -TA regime, but fell into TN-limited in high-TA and-TN regimes. During the sampling period, high nitrate concentrations always accompanied with high TN and TA levels, highlighting that nitrate aerosol production in Nanjing during the high $PM_{2.5}$ levels was mainly control by HNO_3. Therefore, control of NOx emissions, which reduced HNO_3 concentrations, might be an important way to decrease airborne nitrate concentrations and ameliorate the air quality in Nanjing.

4. Conclusion and remarks

Four intensive online measurements of water-soluble ions in $PM_{2.5}$ were carried out in Nanjing City in 2016 and 2017 to realize the evolutions of SIA and the potential formation mechanisms of particulate nitrate. During the sampling periods, the average concentrations of NO_3^-, SO_4^{2-} and NH_4^+ were 16.7, 14.9 and 10.7 μg m^{-3}, respectively. This indicated that NO_3^- dominated the SIA. Significant seasonal variations and diurnal cycles were found for all SIA species. The low NO_3^- concentrations observed during the summer daytime could be attributed to the enhanced theoretical and declined observed equilibrium constants of NO_3^- and NH_4^+ between gas- and particle-phase. Obvious enhancements of NO_3^- were found in terms of both absolute concentrations and relative abundances during the $PM_{2.5}$ episodes, indicating that NO_3^- was a major contributing species to $PM_{2.5}$. Different from the results obtained in Beijing and Shanghai, high nitrate concentrations always occurred under NH_4^+-rich regimes. The nitrogen conversion ratio, Fn, correlated well with the ALWC but not with Ox during high-$PM_{2.5}$ episodes. These findings indicated that NO_3^- aerosols at the receptor site were mainly produced by heterogeneous reactions (N_2O_5 + H_2O) with the involvement of NH_3. The average production rate of NO_3^- from heterogeneous reactions was estimated to be 12.6 % h^{-1}, which was 5 time higher than that of gas-phase reactions. According to the observations and ISORROPIA II simulated results, particulate nitrate formation in Nanjing was HNO_3-limited, suggesting that the control of NOx emissions will be able to decrease the nitrate concentration and improve the air quality in this industrial city.

During the last decade, the mass ratios of nitrate-to-sulfate in $PM_{2.5}$ in the YRD region have been found to range from 0.3 to 0.7 (Lai et al., 2007; Wang et al., 2003; 2006; Yang et al., 2005; Yao et al., 2002), reflecting that the SO_4^{2-} concentration was much higher than the NO_3^- concentration. In the current study, the average mass ratio of nitrate-to-sulfate was 1.1. Indeed, high nitrate-to-sulfate mass ratios of > 1 were also observed in other mega-cities of China recently (Ge et al., 2017; Wei et al., 2018; Ye et al., 2017; Zou et al., 2018). The elevated nitrate-to-sulfate ratio should be due to the dramatic reduction of SO_2 emissions. The enhanced ratio also suggests that we should pay more attention to and develop some strategies for the reduction of NOx emissions, leading to declined nitrate concentrations in the atmosphere and improvement of the air quality in China.

Data availability

All the data used in this paper are available from the corresponding author upon request (dryanlinzhang@outlook.com or zhangyanlin@nuist.edu.cn).

Author contributions

YLZ conceived and designed the study. YCL analyzed the data and wrote the manuscript with YLZ. FM and MB performed aerosol sampling and data analyses with YCL.

Competing interests

The authors declare that they have no conflict of interest.

Acknowledgements

This study was financially supported by the National Key R&D Program of China (Grant No. 2017YFC0212700), the Natural Scientific Foundation of China (Nos. 41761144056, 91644103 and 41977185) and Jiangsu Innovation & Entrepreneurship Team.

References

Baasandorj, M., Hoch, S. W., Bares, R., Lin, J. C., Brown, S. S., Millet, D. B., Martin, R., Kelly, K., Zarzana, K. J., Whiteman, C. D., Bube, W. P., Tonnesen, G., Jaramillo, J. C. and Sohl, J.: Coupling between chemical and meteorological processes under persistent coal-air poor conditions: evolution of wintertime $PM_{2.5}$ events and N_2O_5 observation in Utah's Salt Lake Valley. *Environ. Sci. Technol.*, **51**, 5941-5950, https://doi.org/10.1021/acs.est.6b06603, 2017.

Bian, Y. X., Zhao, C. S., Ma, N., Chen, J., and Xu, W. Y.: A study of aerosol liquid water content based on hygroscopicity measurements at high relative humidity in the Northern China Plain. *Atmos. Chem. Phys.,* **14**, 6417-6426, https://doi.org/10.5194/acp-14-6417-2014, 2014.

Bougiatioti, A., Nikolaou, P., Stavroulas, I., Kouvarakis, G., Weber, A., Nenes, R., Kanakidou, M., and Mihalopoulos, N.: Particle water and pH in the eastern Mediterranean: source variability and implication of nutrient availability. *Atmos. Chem. Phys.,* **16**, 4579-4591, https://doi.org/10.5194/acp-7-4639-2007, 2007.

Brauer, M., Hoek, G., Vliet, V. P., Meliefste, K., Fischer, P. H., Wijga, A., Koopman, L. P., Neijens, H. J., Gerritsen, J., Kerkhof, M., Heinrich, J., Bellander, T., and Brunekreef, B.: Air pollution from traffic and the development of respiratory infections and asthmatic and allergic symptoms in children. *Am. J. Respir. Crit. Care Med.*, **166**, 1092-1098, https://doi.org/10.1146/rccm.200108-007OC, 2002.

Brown, S. S., and Stutz, J.: Nighttime radical observation and chemistry. *Chem. Soc. Rev.*, **41**, 6405-6447, https://doi.org/10.1039/c2cs35181a, 2012.

Calvert, J. G., and Stockwell, W. R.: Acid generation in the troposphere by gas-phase chemistry. *Environ. Sci. Technol.*, **17**, 428-443, https://doi.org/10.1021/es00115a727, 1983.

Chan, C. K., and Yao, X.: Air pollution in mega cities in China. *Atmos. Enviro.,* **42**, 1-

42, https://doi.org/10.1016/j.atmosenv.2007.09.003, 2008.

Chang, W. L., Bhave, P. V., Brown, S. S., Riemer, N., Stutz, J., and Dabdub, D.: Heterogeneous atmospheric chemistry, ambient measurements, and model calculations of N_2O_5: a review. *Aerosol Sc. Technol.*, **45**, 655 - 685, https://doi.org/10.1080/02786826.2010.551672, 2011.

Defino, R. J., Siotuas, C., and Malik, S.: Potential role of ultrafine particles in associations between airborne particle mass and cardiovascular health. *Environ. Health Perspect.*, **113**, 934-938, https://doi.org/10.1289/ehp.7938, 2005.

Fountoukis, C., and Nenes, A.: ISORROPIA II: a computationally efficient thermodynamic equilibrium model for K^+-Ca^{2+}-Mg^{2+}-NH_4^+-Na^+-SO_4^{2-}-NO_3^--Cl^--H_2O. *Atmos. Chem. Phys.*, **7**, 4639-4659, https://doi.org/10.5194/acp-7-4639-2007, 2007.

Ge, X., Li, L., Chen, Y., Chen, H., Wu, D., Wang, J., Xie, X., Ge, S., Ye, Z., Xu, J., and Chen, M.: Aerosol characteristics and sources in Yangzhou, China resolved by offline aerosol mass spectrometry and other techniques. *Environ. Pollut.*, **225**, 74-85, https://doi.org/10.1016/j.encpol.2017.03.044, 2017.

Goodman, A. L., Underwood, G. M., and Grassian, V. H.: A laboratory study of the heterogeneous reaction of nitric acid on calcium carbonate particles. *J. Geophys. Res. Atmos.,* **105**, 29053-29064, https://doi.org/10.1029/2000JD900396, 2000.

Griffith, S. M., Huang, X. H. H., Louie, P. K. K., and Yu, J. Z.: Characterizing the thermodynamic and chemical composition factors controlling $PM_{2.5}$ nitrate: Insights from two years of online measurements in Hong Kong. *Atmos. Environ.*, **122**, 864-875, https://doi.org/10.1016/ j.atmosenv.2015.02.009, 2015.

Guo, H., Xu, L., Bougiatioti, A., Cerully, K. M. , Capps, S. L., Heti Jr., J. R., Carton, A. G., Lee, S.-H., Bergin, M. H., Ng, N. L., Nenes, A., and Weber, R. J.: Fine particle water and pH in the southeastern United States. *Atmos. Chem. Phys.*, **15**, 5221-5228. https://doi.org/10.5194/acp-15-5211-2015, 2015.

Guo, H., Otjes, R., Schlag, P., Kiendler-Schar, A., Nenes, A., and Weber, R. J.: Effectiveness of ammonia reduction of control of fine particulate nitrate. *Atmos. Chem. Phys.*, **18**, 12241-12256. https://doi.org/10.5194/acp-18-12241, 2018, 2018.

He, K., Zhao, Q., Ma, Y., Duan, F., Yang, F., Shi, Z., and Chen, G.: Spatial and seasonal variability of $PM_{2.5}$ acidity at two Chinese megacities: insights into the formation of secondary inorganic aerosols. *Atmos. Chem. Phys.*, **12**, 1377-1395. https://doi.org/10.5194/acp-12-1377-2012, 2012.

Huang, R.-J., Zhang, Y., Bozzetti, C., Ho, K.-F., Cao, J.-J., Han, Y., Daellenbach, R., Slowik, J. G., Platt, S. M., Canonaco, F., Zotter, P., Wolf, R., Pieber, S. M., Bruns, E. A., Crippa, M., Ciarelli, G., Piazzalunga, A., Schwikkowski, M., Abbaszade, G., Schnelle-Kreis, J., Zimmerman, R., An, Z., Szidat, S., Baltensperger, U., Haddad, I. E., and Prévôt, A. H.: High secondary aerosol contribution to particulate pollution during haze events in China. *Nature*, **514**, 218-222, https://doi.org/10.1038/nature13774, 2014a.

Huang, R. J., Chen, R., Jing, M., Yang, L., Li, Y., Chen, Q., Chen, Y., Yan, J., Lin, C., Wu, Y., Zhang, R., Haddad, J. E., Prevot, A. S. H., O'Dowd, C. D., and Cao, J.: Source-specific health risk analysis on particulate trace elements: coal combustion and traffic emission as major contributors in wintertime Beijing. *Environ. Sci. Technol. 52,* 10967-10974, https://doi.org/10.1021/acs.est.8b02091.

Huang, Y., Shen, H., Chen, H., Wang, R., Zhang, Y., Su, S., Chen, Y., Lin, N., Zhong, Q., Wang, X., Liu, J., Li, B., Liu, W., and Tao, S.: Quantification of global primary emissions of $PM_{2.5}$, PM_{10} and TSP from combustion and industrial process sources. *Environ. Sci. Technol.,* **48**, 13834-13843, https://doi.org/10.1021/es503696k, 2014b.

Hui, L., Liu, X., Tan, Q., Feng, M., An. J., Qu, Y., Zhang, Y., and Jiang, M.: Characteristics, source apportionment and contribution of VOCs to ozone formation in Wuhan, Central China. *Atmos. Environ.,* **192**, 55-71, https://doi.org/10.1016/j.atmosenv.2018.08.0642, 2018.

Khoder, M. I.: Atmospheric conversion of sulfur dioxide to particulate sulfate and nitrogen dioxide to particulate nitrate and gaseous nitric acid in an urban area. *Chemosphere*, **49**, 675-684, https://doi.org/10.1016/S0045-6535(02)00391-0, 2002.

Kong, L., Yang, Y., Zhang, S., Zhao, X., Du, H., Fu, H., Zhang, S., Cheng, T., Yang, X., Chen, J., Wu, D., Sheng, J., Hong, S., and Jiao, L.: Observation of linear dependence between sulfate and nitrate in atmospheric particles. *J. Geophys. Res. Atmos.,* **119**, 341-361, https://doi.org/10.1002/2013JD020222, 2014.

Lin, Y.-C., and Cheng, M.-T.: Evaluation of formation rates of NO_2 to gaseous and particulate nitrate in the urban atmosphere. *Atmos. Environ.,* **41**, 1903-1910, https://doi.org/10.1016/j.atmosenv.2006.10.065, 2007.

Lin, Y.-C., Cheng, M.-T., Ting, W.-Y., and Yeh, C.-R.: Characteristics of gaseous HNO_2, HNO_3, NH_3 and particulate ammonium nitrate in an urban city of central Taiwan. *Atmos. Environ.,* **40**(25), 4725-4733, https://doi.org/10.1016/j.atmosenv.2006.04.037, 2006.

Liu, M., Song, Y., Zhou, T., Xu, Z., Yan, C., Zheng, M., Wu, Z., Hu, M., Wu, Y., and Zhu, T.: Fine particle pH during severe haze episodes in northern China. *Geophys. Res. Lett.,* **44**, 5213-5222, https://doi.org/10.1002/2017GL073210, 2017.

Mental, T. F., Sohn, M., and Wahner, A.: Nitrate effect in the heterogeneous hydrolysis of dinitrogen pentoxide on aqueous aerosols. *Phys. Chem. Chem. Phys.*, **1**, 5451-5457, https://doi.org/10.1039/a905338g, 1999.

Nel, A.: Air pollution-related illness: effects of particles. *Science*, **308**, 804-806, https://doi.org/10.1126/science.1108752, 2005.

Pan, Y., Tian, S., Zhao, Y., Zhang, L., Zhu, X., Gao, J., Huang, W., Zhou, Y., Song, Y., Zhang, Q., and Wang, Y.: Identifying ammonia hotspots in China using a national observation work. *Environ. Sci. and Technol.*, **52**, 3926-3934. https://doi.org/10.1021.acs/est.7b05235, 2018.

Pathak, R. K., Wu, W. S., and Wang, T.: Summertime $PM_{2.5}$ ionic species in four major cities of China: nitrate formation in an ammonia-deficient atmosphere. *Atmos. Chem. and Phys.*, **9**, 1711-1722, https://doi.org/10.5194/acp-9-1711-2009, 2009.

Pathak, R. K., Wang, T., and Wu, W. H.: Nighttime enhancement of $PM_{2.5}$ in ammonia-poor atmospheric conditions in Beijing and Shanghai: Plausible contributions of heterogeneous hydrolysis of N_2O_5 and HNO_3 partitioning. *Atmos. Environ.*, **45**, 1183-1191, https://doi.org/10.1016/j.atmosenv.2010.09.003, 2011.

Polissar, A. V., Hopke, P. K., Paatero, P., Kaufmann, Y. J., Hall, D. K., Bodhaine, B. A., Dutton, E. G., and Harris, J. M.: The aerosol at Barrow, Alaska: long-term trends and source locations. Atmos. Environ., **33**, 2441-2458, https://doi.org/10.1016/j.atmosenv.2018.08.0642, 2018.

Prabhakar, G., Parworth, C. L., Zhang, X., Kim, H., Young, D. E., Beyersdorf, A. J., Ziemba, L. D., Nowak, J. B., Bertram, T. H., Faloona, I. C., Zhang, Q., and Cappa, C. D.: Observational assessment of the role of nocturnal residual-layer chemistry in determining daytime surface particulate nitrate concentrations. *Atmos. Chem. Phys.*, **17**, 14747-14770, https://doi.org/10.5194/acp-17-14747-2017, 2017.

Squizzato, S., Masiol, M., Brunelli, A., Pistollato, S., Tarabotti, Z., Rampazzo, G., and

Pavoni, B.: Factors determining the formation of secondary inorganic aerosol: a case study in the Po Valley (Italy). *Atmos. Chem. and Phys.,* **13**, 1927-1339, https://doi.org/10.5194/acp-13-1927-2013, 2013.

Tang, X., Zhang, X., Ci, Z., Guo, J., and Wang, J.: Speciation of the major inorganic salts in atmospheric aerosols of Beijing: China: measurements and comparison with model. *Atmos. Environ.,* **133**, 123-134, https://doi.org/10.1016/j.atmosenv.2016.03.013.

Tao, Y., Ye, X., Ma, Z., Xie, Y., Wang, R., Chen, J., Yang, X., and Jiang, S.: Insights into different nitrate formation mechanisms from seasonal variations of secondary inorganic aerosols in Shanghai. *Atmos. Environ.,* **145**, 1-9, https://doi.org/10.1016/j.atmosenv.2016.09.012, 2016.

ten Brink, H., Otjes, R., Jongejan, P., and Slanina, S.: An instrument for semi-continuous monitoring of the size-distribution of nitrate, ammonium, sulfate and chloride in aerosols. *Atmos. Environ.,* **41**, 2768-2779, https://doi.org/10.1016/j.atmosenv.2006.11.041, 2007.

Wahner, A., Mental, T. F., Sohn, M., and Stier, J.: Heterogenous reaction of N_2O_5 on sodium nitrate aerosol. *J. Geophys. Res. Atmos.*, **103**, 31103-31112, https://doi.org/10.1029/1998JD100022, 1998.

Wang, G., Wang, H., Yu, Y., Gao, S., Feng, J., Gao, S., & Wang, L.: Chemical characterization of water-soluble components of PM_{10} and $PM_{2.5}$ atmospheric aerosols in five locations of Nanjing, China. *Atmos. Environ.*, **37**., 2893-2902. https://doi.org/10.1016/j.atmosenv.S1352-2310(03)00271-1, 2003.

Wang, G., Zhang, R., Geomez, M. E., Yang, L., Zamora, M. L., Hu, M., Lin, Y., Peng, J., Guo, S., Meng, J., Li, J., Cheng, C., Hu, T., Ren, Y., Wang, Y., Gao, J., An, Z., Zhou, W., Li, G., Wang, J., Tian, P., Marrero-Ortiz, W., Secrest, J., Du, Z., Zheng, J., Shang, D., Zheng, L., Shao, M., Wang, W., Huang, Y., Wang, Y., Zhu, Y., Li, Y., Hu, J., Pan, B., Cai, L., Cheng, Y., Ji, Y., Zhang, F., Rosenfeld, D., Liss, P. S., Duce, R. A., Kolb, C. E., and Molina, M. J.: Persistent sulfate formation from London fog to Chinese haze. *Proc. Natl. Acad. Sci.*, **113**, 13630-13635, https://doi.org/ 10.1073/pnas.1616540113, 2016.

Wang, H., Lu, K., Chen, X., Zhu, Q., Chen, Q., Guo, S., Jiang, M., Li, X., Shang, D., Tang, Z., Wu, Y., Wu, Z., Zou, Q., Zheng, Y., Zheng, L., Zhu, T., Hu, M., and Zhang, Y.: High N_2O_5 concentrations observed in urban Beijing: implications of a large nitrate formation. *Environ. Sci. Technol. Lett.*, **4**, 416-420, https://doi.org/10.1021/acsestlett.7b00341, 2017.

Wang, H., Zhu, B., Shen, L., Xu, H., An, J., Xue, G., and Cao, J.: Water soluble ions in atmospheric aerosols measured in five sites in the Yantze River Delta, China: size-fractionated seasonal variation and sources. *Atmos. Environ.*, **123**(B), 370-379, https://doi.org/10.1016/j.atmosenv.2015.05.070, 2015.

Wang, W., Yu, J., Cui. Y., He, J., Xue, P., Cao, W., Ying, H., Gao, W., YIng, Y., Gao, W., Yan, Y., Hu, B., Xin, J., Wang, L., Liu, Z., Sun, Y., Ji, D., and Wang, Y.: Characteristics of fine particulate matter and its sources in an industrialized coastal city, Ningbo, Yantze River Delta, China. *Atmos. Res.*, **203**, 105-117, https://doi.org/10.1016/j.atmosres.2017.11.033, 2018.

Wang, Y., Zhuang, G., Zhang, X., Xu, C., Tang, A., Chen, J., and An, Z.: The ion chemistry, seasonal cycle, and sources of $PM_{2.5}$ and TSP aerosol in Shanghai. *Atmos. Environ.,* **40**(16), 2935-2952, https://doi.org/10.1016/j.atmosenv.2005.12.051, 2006.

Wei, L., Yue, S., Zhao, W., Yang, W., Zhang, Y., Ren, L., Han, X., Guo, Q., Sun, Y., Wang, Z., and Fu, P.: Stable sulfur isotope ratios and chemical compositions of fine aerosols ($PM_{2.5}$) in Beijing, China. *Sci. Total Environ.*, **633**, 1156-1164, https://doi.org/10.1016/j.scitotenv.2018.03.153, 2018.

Wen, L., Chen, J., Yang, L., Wang, X., Xu, C., Sui, X., Yao, L., Zhu, Y., Zhang, J., Zhu, T., and Wang, W.: Enhanced formation of particulate nitrate at a rural site on the North China Plain in summer: the importance roles of ammonia and ozone. *Atmos. Environ.,* **101**, 294-302, https://doi.org/10.1016/j.atmosenv.2014.11.037, 2015.

Yang, H., Yu, J. Z., Ho, S. S. H., Xu, J., Wu, W.-S., Wan, C. H., Wang, X., Wang, X., and Wang, L.: The chemical composition of inorganic and carbonaceous materials in $PM_{2.5}$ in Nanjing, China. *Atmos. Environ. ,* **39**, 3735-3749, https://doi.org/10.1016/j.atmosenv.2005.03.010, 2005.

Yao, X., Chan, C. K., Fang, M., Cadle, S., Chan, T., Mulawa, P., He, K., and Ye, B.: The water-soluble ionic composition $PM_{2.5}$ in Shanghai and Beijing, China. *Atmos. Environ.,* **36**, 4223-4234, https://doi.org/10.1016/j.atmosenv.2005.12.051, 2002.

Ye, X. N., Ma, Z., Zhang, J. C., Du, H. H., Chen, J. M., Chen, H., Yang, X., Gao, W., and Geng, F. H.: Important role of ammonia on haze formation in Shanghai. *Environ. Res. Lett.*, **6**, 024019, https://doi.org/10.1088/1748-9326/6/2024019, 2011.

Ye, Z., Liu, J., Gu, A., Feng, F., Liu, Y., Bi, C., Xu, J., Li, L., Chen, H., Chen, Y., Dai, L., Zhou, Q., and Ge, X.: Chemical characterization of fine particulate matter in Changzhou, China and source apportionment with offline aerosol mass spectrometry. *Atmos. Chem. .Phys.,* **17**, 2573-2592, https://doi.org/10.5194/acp-17-2573-2017, 2017.

Zhang, R., Jing, J., Tao, J., Hsu, S.-C., Wang, G., Cao, J., Lee, C.S.L., Zhu, L., Chen, Z., Zhao, Y., and Shen, Z., Chemical characterization and source apportionment of $PM_{2.5}$ in Beijing: seasonal perspective. *Atmos. Chem. .Phys.,* **13**, 7053-7074, https://doi.org/10.5194/acp-13-7053-20173, 2013.

Zhang, Y.-L., and Cao, F.: Fine particulate matters ($PM_{2.5}$) in China at a city level. *Sci. Rep.,* **5**, 14884, https://doi.org/10.1038/srep14884, 2015.

Zhao, P. S., Dong, F., He, D., Zhao, X. J., Zhang, X. L., Zhang, W. Z., Yao, Q., and Liu, H. Y.: Characteristics of concentrations and chemical compositions for PM2.5 in the region of Beijing, Tianjin, and Hebei, China. *Atmos. Chem. Phys.,* **13**, 4631-4644, https://doi.org/10.5194/acp-13-4631-2013, 2013.

Zheng, B., Tong, D., Li, M., Liu, F., Hong, C., Geng, G., Li, H., Li, X., Peng, L., Qi, J., Yan, L., Zhang, Y., Zhao, H., Zheng, Y., He, K., and Zhang, Q.: Trends in China’s anthropogenic emissions since 2010 as the consequence of clean air actions. *Atmos. Chem. .Phys.,* **18**(19), 14095-14111, https://doi.org/10.5194/acp-18-14095-2018, 2018.

Zou, J., Liu, Z., Hu, B., Huang, X., Wen, T., Ji, D., Liu, J., Yang, Y., Yao, and Wang, Y.: Aerosol chemical compositions in the Northern China Plain and the impact on visibility in Beijing and Tianjin., *Atmos. Res.*, **201**, 235-246, https://doi.org/10.1016/j.atmosres.2017.09.014, 2018.

Table Captions

Table 1 The regression models between NO_3^-/SO_4^{2-} (Y) and NH_4^+/SO_4^{2-} (X) along with the criterion values of NH_4^+/SO_4^{2-} in ammonium-rich regime during the sampling periods.

Figure Captions

Figure 1 Time series of concentrations in (a) $PM_{2.5}$ mass, (b) SIA species, (c) ALWC and (d) Ox along with (e) Fn observed in Nanjing during the sampling periods. The grey shadows represent the high $PM_{2.5}$ periods discussed in the section 3.6.

Figure 2 Abundance of each species in TWSIIs during the (a) entire, (b) haze ($PM_{2.5} \geq$ 150 μg m^{-3}) and (c) clear ($PM_{2.5} < 35$ μg m^{-3}) events. The numbers in the parentheses are standard deviations.

Figure 3 Abundance of each species in TWSIIs during the (a) entire, (b) haze ($PM_{2.5} \geq$ 150 μg m^{-3}) and (c) clear ($PM_{2.5} < 35$ μg m^{-3}) events. The numbers in the parentheses are standard deviations.

Figure 4 The PSCF maps of high nitrate pollution.

Figure 5 Scatter plots of molar ratios of NO_3^-/SO_4^{2-} against NH_4^+/SO_4^{2-} in Nanjing during the different seasons.

Figure 6 Scatter plot of NO_3^- vs. excess-NH_4^+ molar concentrations in Nanjing during the different seasons. The results in Beijing, Shanghai, Guangzhou, Lanzhou and Hong Kong are also shown in this figure.

Figure 7 Scatter plots of (a) Fn against Ox and (b) Fn against ALWC in daytime and nighttime aerosol samples during the high hourly $PM_{2.5}$ concentration conditions (hourly $PM_{2.5} \geqq 150$ μg m^{-3}).

Figure 8 Time series of concentrations in (a) $PM_{2.5}$ mass and CO, (b) SIA species

(NO_3^-, SO_4^{2-} and NH_4^+), (c) ALWC, Ox and NO_2 and (d) RH and T in Nanjing City from March 3 to 6, 2016. The grey shadows denote $PM_{2.5}$ episodes. The red numbers represent NO_3^- production rate during the $PM_{2.5}$ episodes.

Figure 9 Nitrate concentrations simulated by ISORROPIA II model dependening on TN and TA concentrations under (a) SO_4^{2-} = 10 μg m^{-3} and (b) SO_4^{2-} = 60 μg m^{-3}. The purple dots denote the observed TN and TA concentrations at the receptor site during the sampling periods.

Table 1 The regression models between NO_3^-/SO_4^{2-} (Y) and NH_4^+/SO_4^{2-} (X) along with the criterion values of NH_4^+/SO_4^{2-} in ammonium-rich regime during the sampling periods.

Sampling periods	Regression models	Criterion values of NH_4^+/SO_4^{2-}
2016 spring	Y = 0.71 X – 1.27; R^2= 0.87	1.8
2016 summer	Y = 0.67 X – 1.22; R^2= 0.86	1.8
2017 winter	Y = 0.81 X – 1.50; R^2= 0.91	1.9
2017 spring	Y = 0.95 X – 1.91; R^2= 0.94	2.0
2017 summer	Y = 0.79 X – 1.32; R^2=0.84	1.7

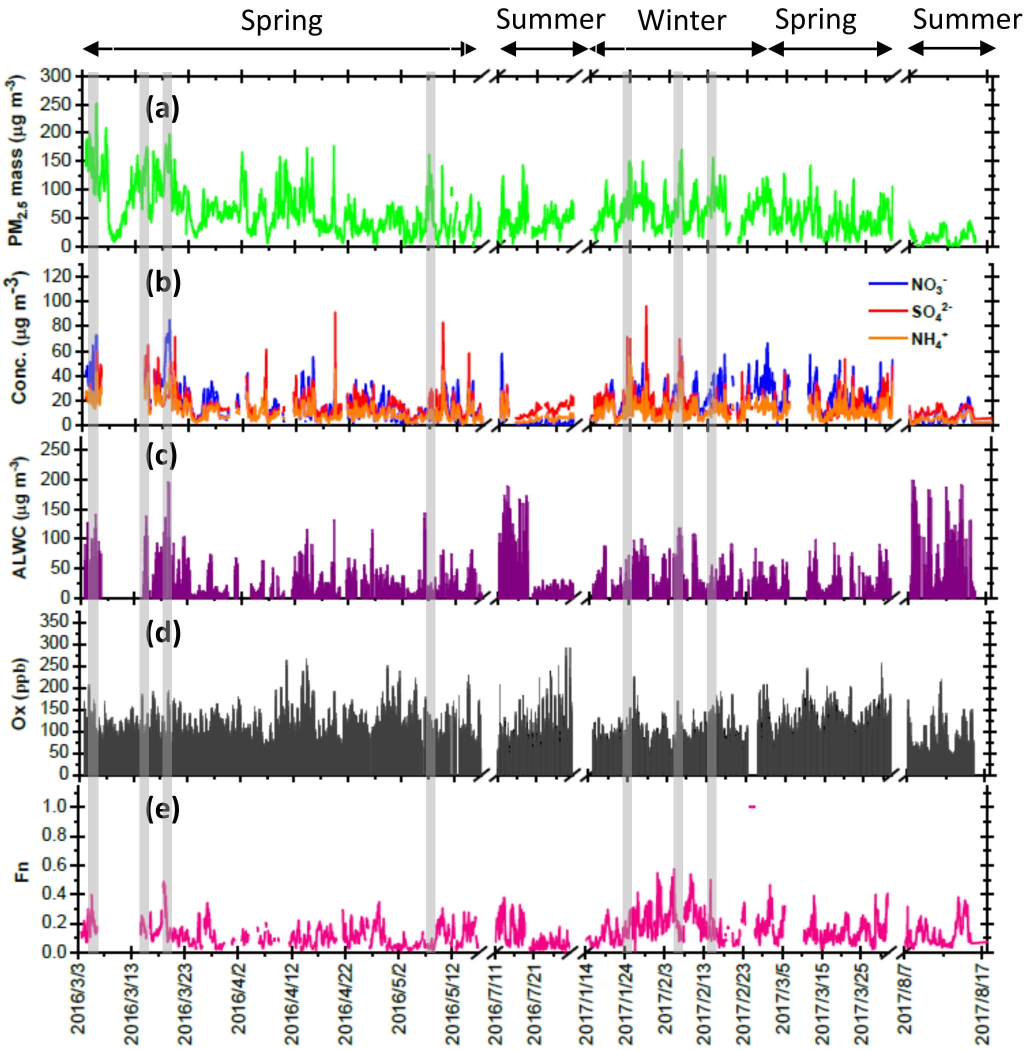

Figure 1 Time series of concentrations in (a) PM$_{2.5}$ mass, (b) SIA species, (c) ALWC and (d) Ox along with (e) Fn observed in Nanjing during the sampling periods. The grey shadows represent the high PM$_{2.5}$ periods discussed in the section 3.6.

(a) Entire days: $PM_{2.5}$ = 58 ± 35 μg m^{-3}

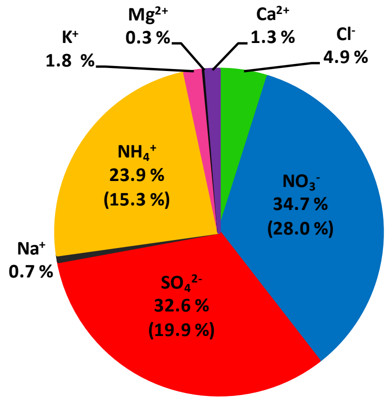

(b) Haze events: $PM_{2.5}$ = 171 ± 18 μg m^{-3}

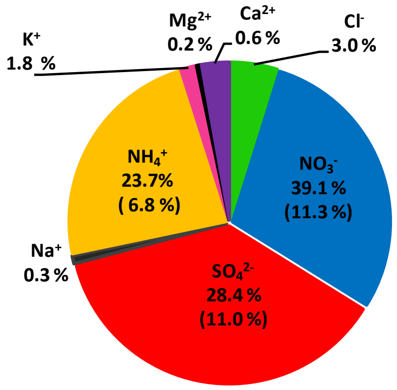

(c) Clear events: $PM_{2.5}$ = 22 ± 9 μg m^{-3}

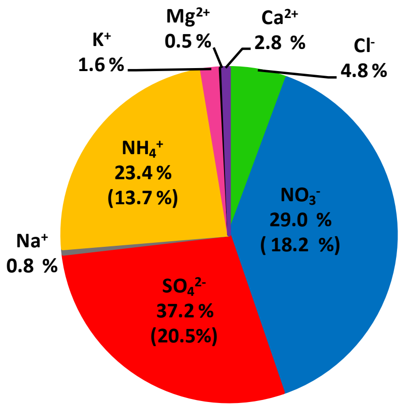

Figurer 2 Abundance of each species in TWSIIs during the (a) entire, (b) haze ($PM_{2.5}$ ≥ 150 μg m^{-3}) and (c) clear ($PM_{2.5}$ < 35 μg m^{-3}) events. The numbers in the parentheses are standard deviations.

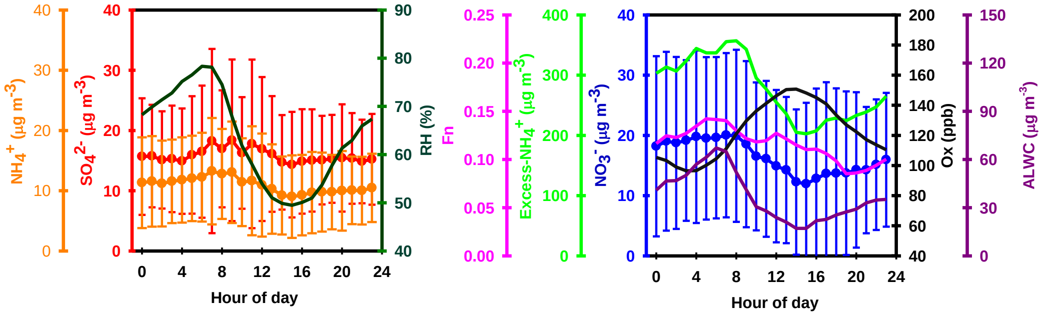

(b) Summer

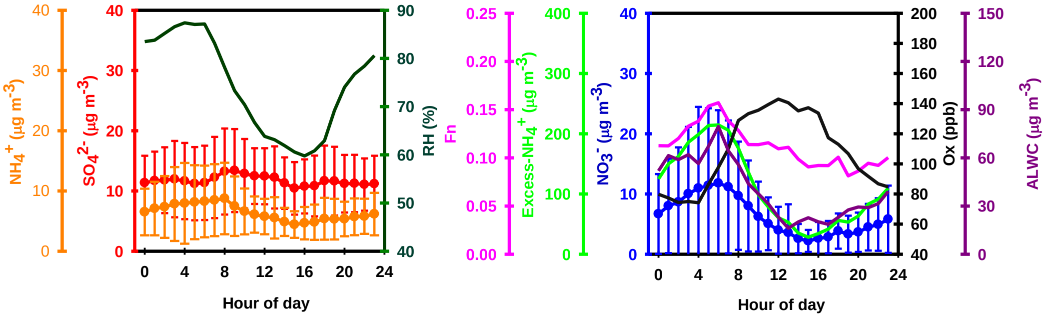

(c) Winter

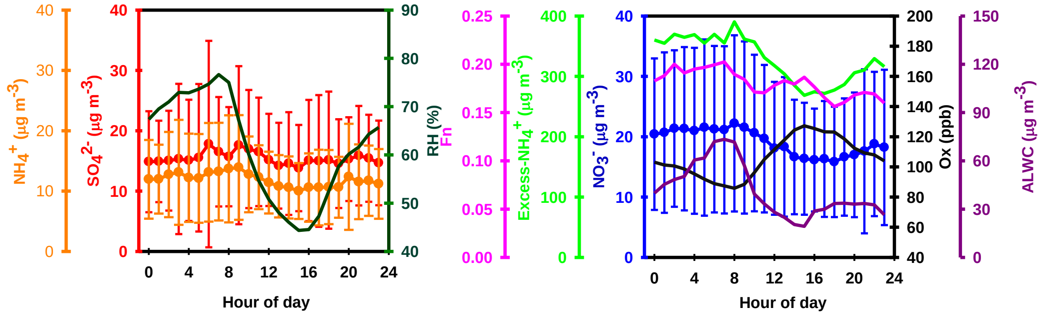

Figure 3 Diurnal variations of the concentrations of NO_3^-, SO_4^{2-} and NH_4^+, excess-NH_4^+, Ox and ALWC, and nitrogen conversion ratio (Fn) as well as ambient relative humidity in Nanjing during the sampling periods. For SO_4^{2-}, NO_3^- and NH_4^+, the mean values (dots) and standard deviations (solid lines) are plotted.

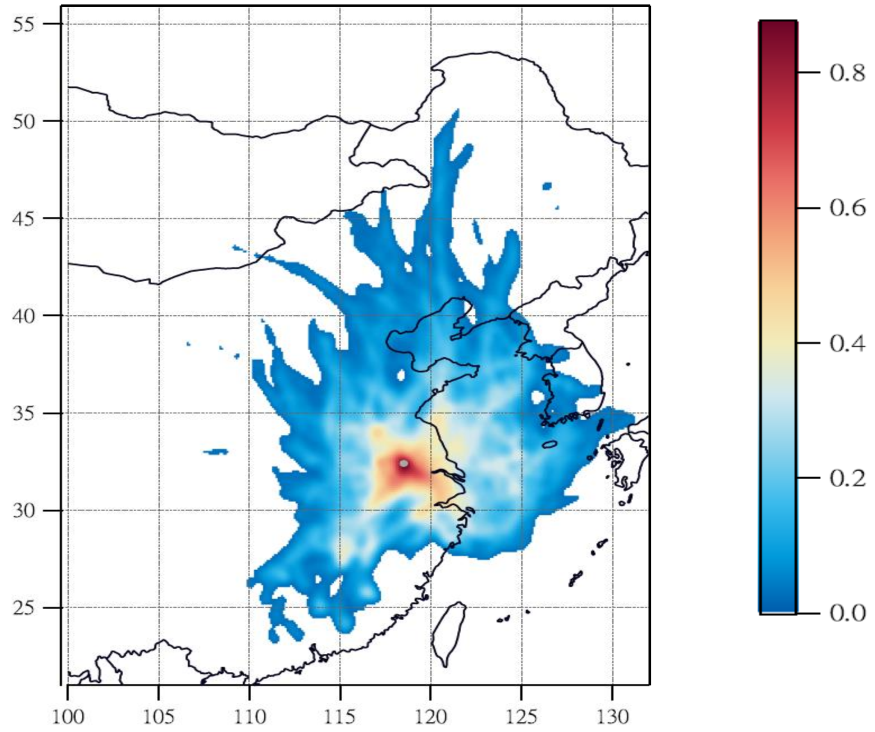

Figure 4 The PSCF maps of high nitrate pollution.

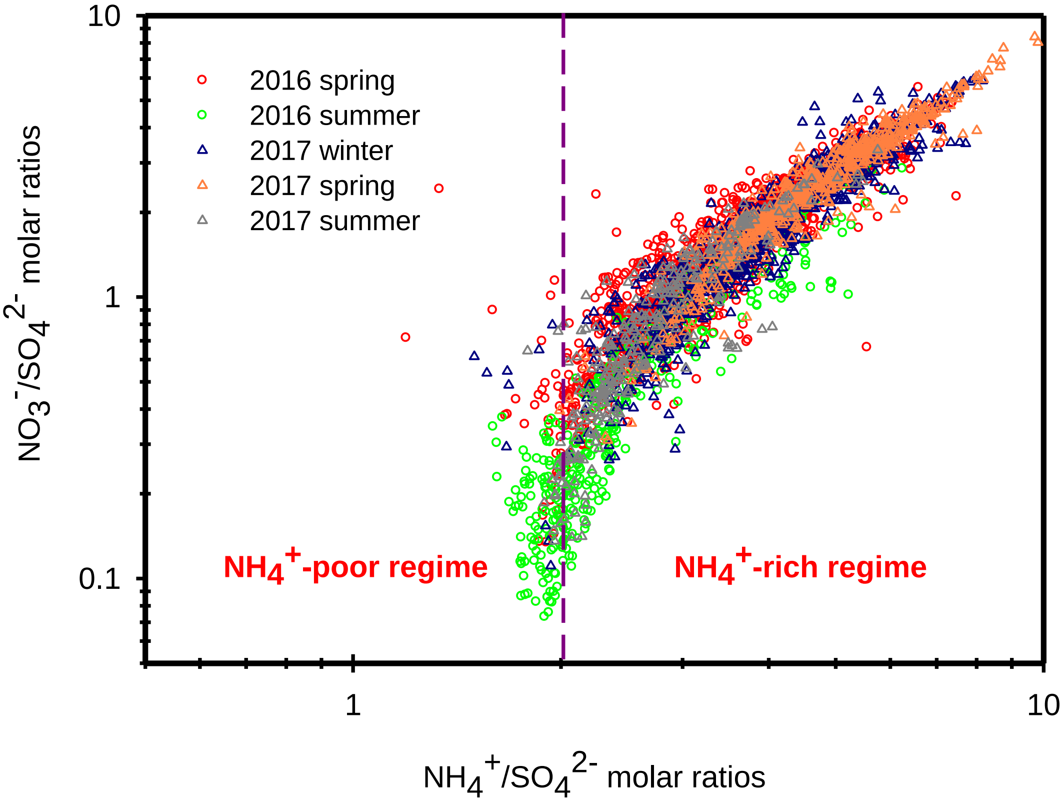

Figure 5 Scatter plots of molar ratios of NO_3^-/SO_4^{2-} against NH_4^+/SO_4^{2-} in Nanjing during the different seasons.

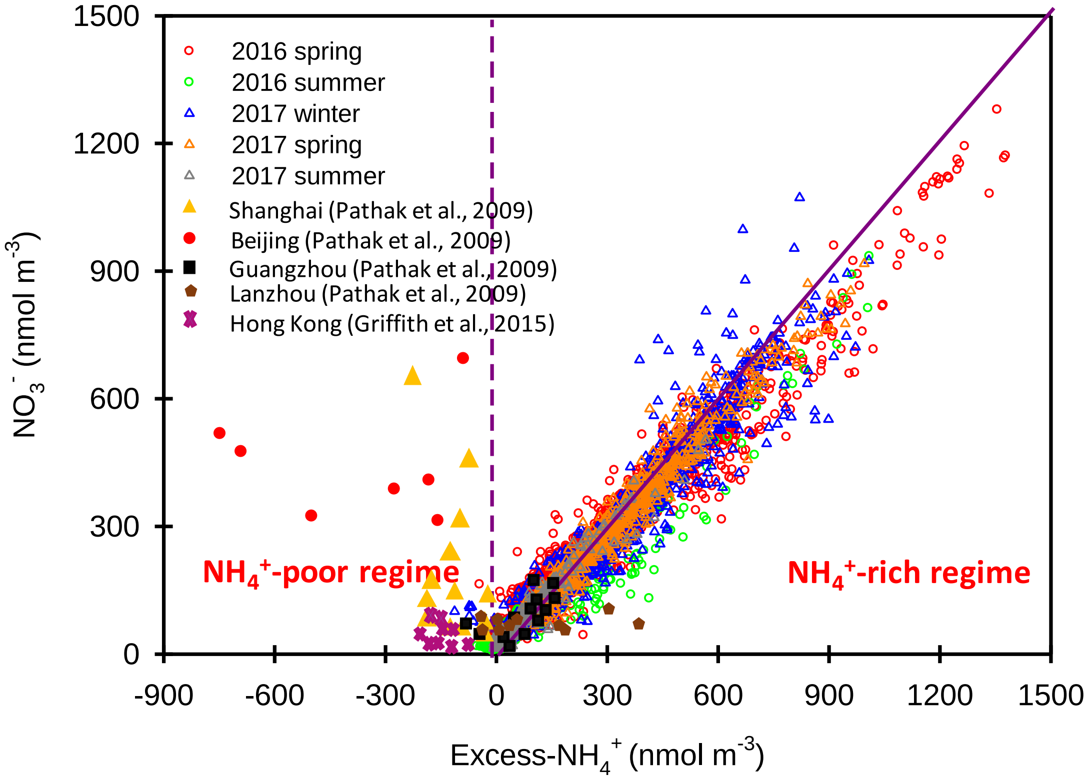

Figure 6 Scatter plot of NO_3^- vs. excess-NH_4^+ molar concentrations in Nanjing during the different seasons. The results in Beijing, Shanghai, Guangzhou, Lanzhou and Hong Kong are also shown in this figure.

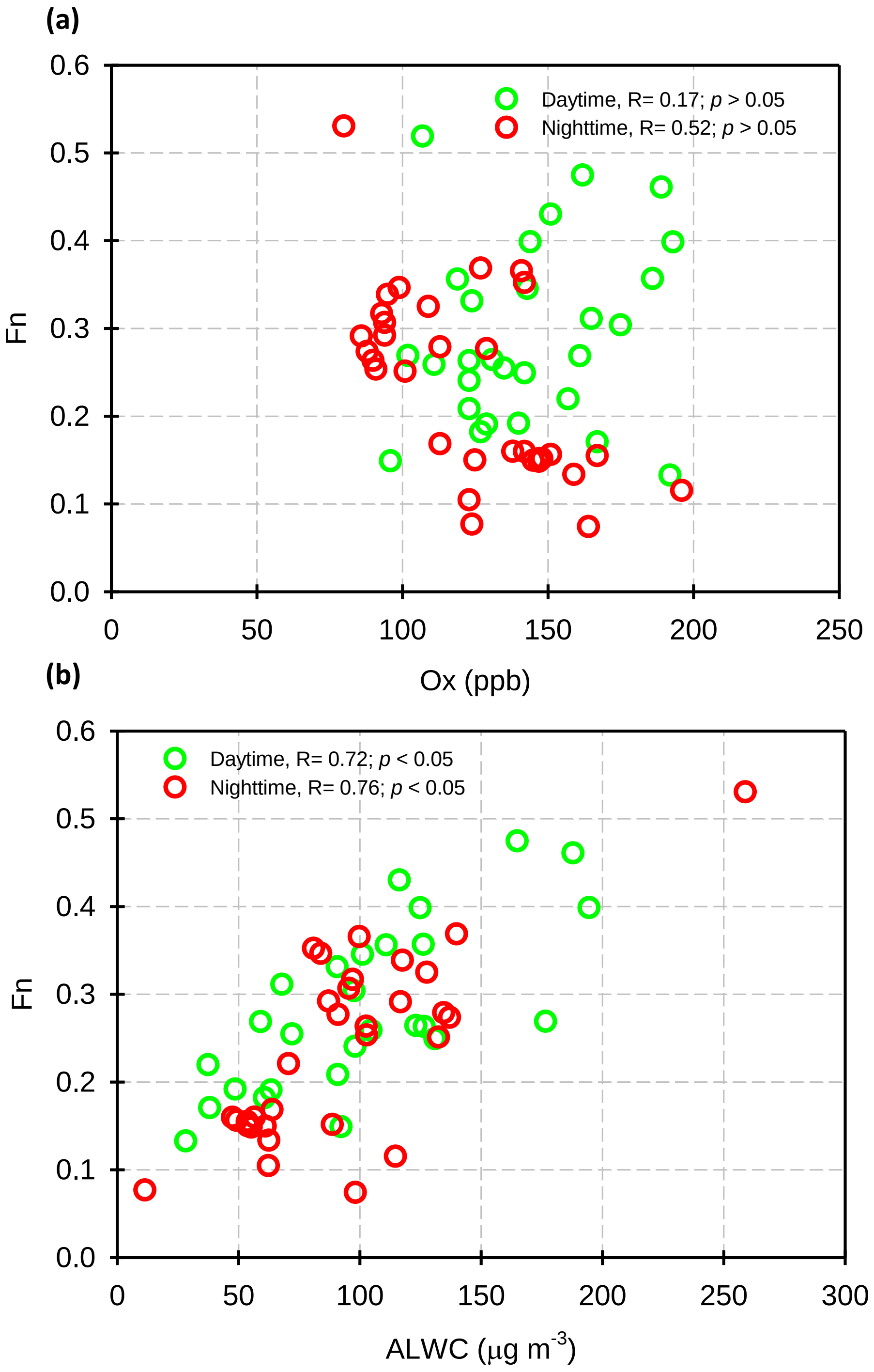

Figure 7 Scatter plots of (a) Fn against Ox and (b) Fn against ALWC in daytime and nighttime aerosol samples during the high hourly $PM_{2.5}$ concentration conditions (hourly $PM_{2.5} \geqq 150$ μg m^{-3}).

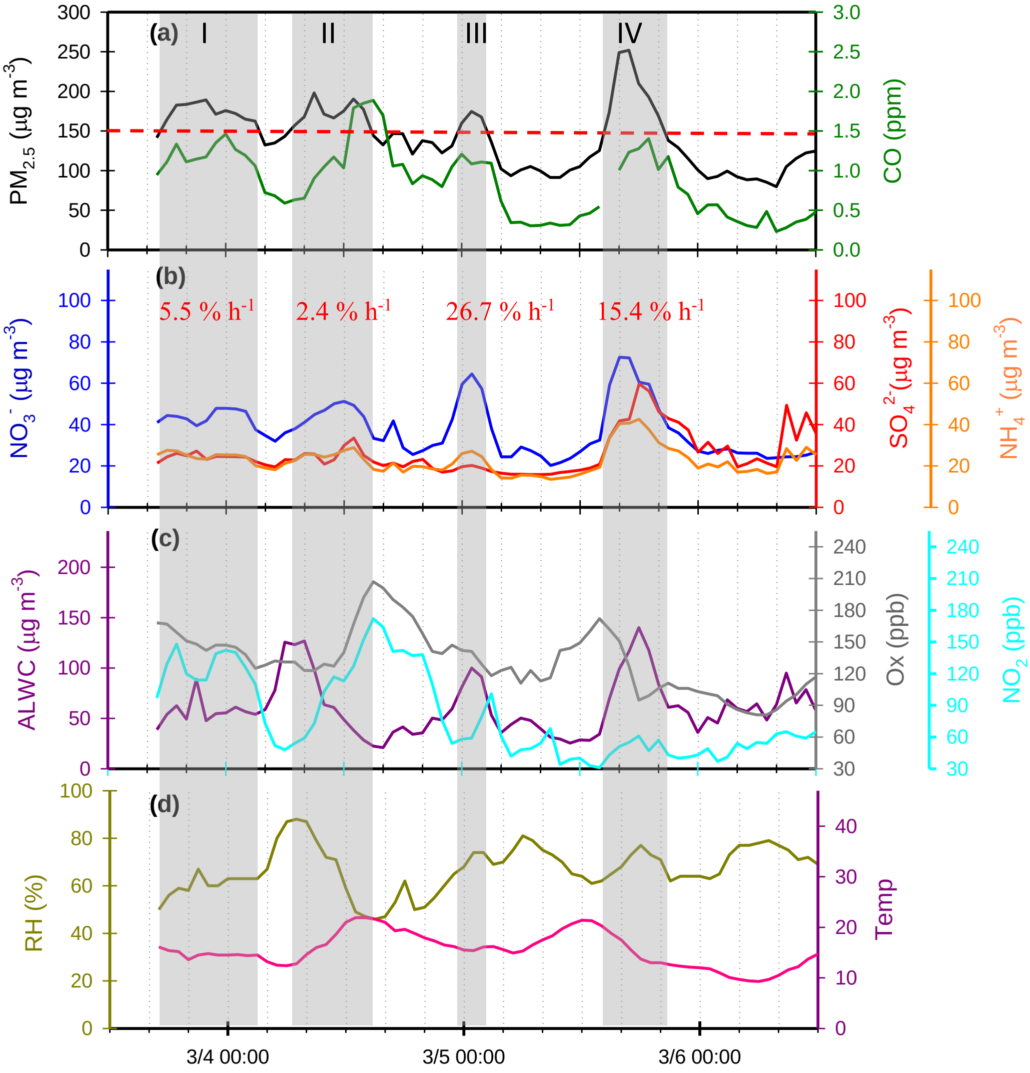

Figure 8 Time series of concentrations in (a) PM$_{2.5}$ mass and CO, (b) SIA species (NO_3^-, SO_4^{2-} and NH_4^+), (c) ALWC, Ox and NO_2 and (d) RH and T in Nanjing City from March 3 to 6, 2016. The grey shadows denote PM$_{2.5}$ episodes. The red numbers represent NO_3^- production rate during the PM$_{2.5}$ episodes.

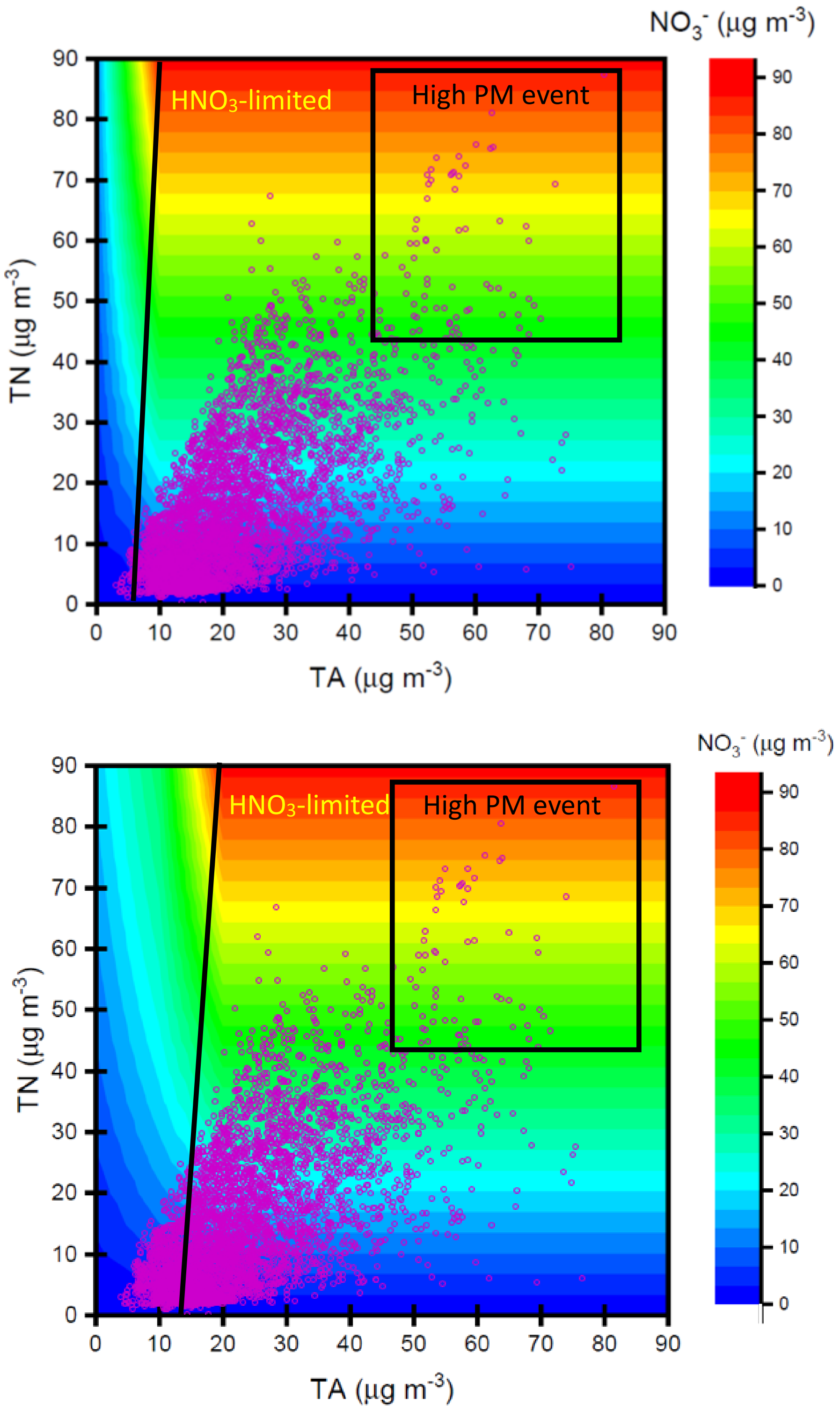

Figure 9 Nitrate concentrations simulated by ISORROPIA II model dependening on TN and TA concentrations under (a) SO_4^{2-} = 10 µg m^{-3} and (b) SO_4^{2-} = 60 µg m^{-3}. The purple dots denote the observed TN and TA concentrations at the receptor site during the sampling periods.